1-1-2013

Liquefaction Potential of South Carolina Coastal Plain Soils Using Dilatometer Data

Joseph Ronald Williamson
University of South Carolina

LIQUEFACTION POTENTIAL OF SOUTH CAROLINA COASTAL PLAIN SOILS USING DILATOMETER DATA

by

Joseph Williamson

Bachelor of Science in Civil Engineering
University of South Carolina, 2010

Submitted in Partial Fulfillment of the Requirements

For the Degree of Master of Science in

Civil Engineering

College of Engineering and Computing

University of South Carolina

2013

Accepted by:

Sarah Gassman, Major Professor

Charles Pierce, Committee Member

Chunyang Liu, Committee Member

Lacy Ford, Vice Provost and Dean of Graduate Studies

ACKNOWLEDGEMENTS

I would like to thank my advisor, Dr. Sarah Gassman, for her guidance, support, and encouragement during the last two years. Even though the progress of this thesis was hindered by my employment obtained during this research, her patience, encouraging support, and prompt response with comments for revising each draft of this work never faltered. The author would also like to thank committee members Dr. Charles Pierce and Dr. Chunyang Liu for their time spent reviewing this thesis and for their comments and recommendations made to improve this work.

Much gratitude is due to Michael Hasek for his work on parallel research in the South Carolina Coastal Plain that combined our efforts to execute the laboratory index testing and for his efforts in performing the cyclic triaxial testing analyzed in this work. Thanks also go out to his wife Ginger for her assistance with Atterberg limit testing. Appreciation is also in store for former USC researchers Ke Hu and Lila Leon whose previous work at the SCCP research sites presented the scope of this thesis

Special thanks go out to Duane Bents of S&ME, Inc. for allowing me to continue my research and coursework during my employment.

Above all I would like to thank my mother, father, brother, and dear friend Courtney Callahan for their unwavering love, support, and encouragement in all my endeavors.

ABSTRACT

In recent years much research has been focused on developing the flat plate dilatometer (DMT) as a tool to estimate the liquefaction potential of soils. Currently the DMT is over shadowed by the more accepted methods of estimating liquefaction potential which utilize test data from either the standard penetration test (SPT), cone penetration test (CPT), or shear wave velocity test (V_s). The SPT, CPT, and V_s tests are all well-developed methods of estimating liquefaction potential and are supported by extensive databases; however, the DMT is believed by many researchers to be the superior alternative. Due to the DMT's minimal amount of soil disturbance the test is able to detect minor changes in soil fabric and thus is sensitive to stress history, cementation, bonding, and aging, all factors which increase liquefaction resistance.

Aging is a critical factor that needs to be considered in liquefaction analysis. The current methods of estimating liquefaction potential were developed based on data from relatively young soil deposits of the Holocene era (<10,000 years); whereas the soil deposits of the South Carolina Coastal Plain (SCCP) range in age from 200,000 to 1.6 million years old. The current SPT and CPT based methods of estimating liquefaction potential, which do not account for the effects of aging, underestimate SCCP soil's resistance to liquefy (e.g. cyclic resistance ratio (CRR)) by as much as 60%.

Given the importance of accounting for aging of soils in liquefaction analysis and the recent developments of the DMT as an in situ tool that is sensitive to aging, this thesis

aims to 1) expand the limited DMT data base by adding data from five research sites in the SCCP and 2) develop new relationships between DMT data and CRR that can be used as first approximations for evaluating the liquefaction potential of soils in the SCCP. The five research sites studied herein are part of a larger study to evaluate the geotechnical properties and liquefaction potential of soils at sites in the SCCP where evidence of paleoliquefaction has been identified through the discovery of sandblows. These sites include Sampit, Gapway, Fort Dorchester, Hollywood, and Four Hole Swamp.

At each site, DMT, SPT, and CPT tests were performed side by side. Laboratory index testing consisting of visual-manual identification, grain size distribution, Atterberg limits, and specific gravity were also performed on SPT samples from each site. The field and laboratory test data was used along with the in situ test parameter upper limits for liquefaction presented in the literature to identify the source sand zones, or the layers that are most prone to liquefy, at each site. The field test data from within the source sand zones was analyzed and correlations between DMT-SPT and DMT-CPT test parameters that are specific to SCCP soils were developed. In analyzing the field test data, the K_D and E_D values of the SCCP soils were found to be higher than the values of Holocene soils of other published data and the K_D upper limit of liquefaction presented in the literature considered the majority of the SCCP soils unliquefiable.

The correlations between DMT-SPT and DMT-CPT test parameters in SCCP soils were used to transform the CRR-SPT and CRR-CPT relations that account for aging into new first approximation CRR-DMT relationships. The first approximation CRR-DMT relations are supported by CRR-DMT relations with CRR obtained from cyclic triaxial tests on high quality undisturbed samples from each site. The first approximation

CRR-DMT relations presented herein are shown to be in good agreement with the SCCP data and serve as appropriate boundaries between unliquefiable soils and soils that are prone to liquefaction.

TABLE OF CONTENTS

LIST OF TABLES

LIST OF FIGURES

CHAPTER ONE
INTRODUCTION

Over the past 40 years a methodology termed the "simplified procedure" has evolved as the standard of practice for evaluating the liquefaction resistance of soils. The method consists of estimating the loading that is induced on the soil by the earthquake (i.e. the cyclic stress ratio (CSR)) and the resistance of the soil to the triggering of liquefaction (i.e. the cyclic resistance ratio (CRR)). Liquefaction is triggered when the induced seismic loading becomes greater than or equal to the soil's resistance to liquefy, (i.e. CSR $\geq$ CRR). CRR is commonly estimated using the results from standard penetration tests (SPT), cone penetration tests (CPT), or shear wave velocity tests (V_s) because of the large supporting databases of paired test results with known CRR data. However, in recent years much effort has been put into the development of the dilatometer (DMT) as another tool for estimating the liquefaction resistance of soils.

The DMT is a flat stainless steel blade with a circular stainless steel membrane mounted flush to one side. The DMT is pushed into the soil to a desired depth, at which point the pressure required to expand the membrane 1.1 mm laterally into the soil is recorded. The DMT's capability to precisely measure horizontal stresses has led many researchers (Monaco et al. (2005), Monaco and Marchetti (2007), and Tsai et al. (2009)) to believe the DMT to be the superior method of estimating CRR. The DMT's sensitivity to horizontal stresses allows it to detect the effects of stress history, prestraining, aging,

cementation, and structure (Marchetti, 2011). Monaco and Schmertmann (2007) concluded that "disregarding aging is equivalent to omitting a primary parameter in the CRR correlations".

Leon et al. (2006) addressed the importance of considering aging, a mechanical or chemical process by which soil strength and stiffness tend to increase over time, and quantified the effects that age has on CRR for soils in the South Carolina Coastal Plain (SCCP). Prior to Leon et al. (2006) methods for estimating CRR (e.g. Idriss and Boulanger (2006) for SPT and Robertson and Wride (1998) for CPT) were applicable only to relatively young, Holocene (<10,000 years) soil deposits. These methods do not consider the increase in CRR over time. The SCCP soils are much older than Holocene soils, ranging from 200,000 to 1,600,000 years old. Leon et al. (2006) found that the methods used to estimate CRR of Holocene soils underestimate CRR of SCCP soils by as much as 60%. New empirical boundary curves to estimate CRR of aged soils were developed as part of the Leon et al. (2006) work.

Given the importance of accounting for aging in liquefaction analysis, this thesis aims to 1) expand the limited DMT data base (which consists of varying soil types throughout the world) by adding data from five research sites in the SCCP and 2) develop new CRR-DMT relationships that can be used as first approximations for evaluating the liquefaction potential of soils in the SCCP. The five research sites studied herein are part of a larger study to evaluate the geotechnical properties and liquefaction potential of soils at sites in the SCCP where evidence of paleoliquefaction has been identified through the discovery of sandblows (Talwani et al. (1999), Talwani and Schaeffer (2001), Hu et al.

(2002a), and Hasek (2013)). These sites include Sampit and Gapway, near Georgetown, Fort Dorchester and Hollywood, near Charleston, and Four Hole Swamp near Dorchester.

At each of the five sites, DMT, SPT, and CPT tests were performed in close proximity to one another and the results are used herein to develop correlations between the different test results so that the existing SPT and CPT based methods of estimating liquefaction resistance could be transformed into new DMT based methods. Index tests on samples from the Sampit, Fort Dorchester, Hollywood, and Four Hole Swamp sites were performed as part of this thesis, while index tests for Gapway were performed and provided by Hu et al., 2002.

The correlations between DMT, SPT, and CPT test parameters for SCCP soils derived herein are used to transform the Idriss and Boulanger (2006) CRR-SPT relation and the Robertson and Wride (1998) CRR-CPT relation into first approximation CRR-DMT relations following the recommendations made by Marchetti (2011). The Leon et al. (2006) methodology is also applied to account for the effects of aging. The newly acquired first approximation CRR-DMT relations are then compared to CRR-DMT relations developed using CRR obtained from cyclic triaxial testing of high quality undisturbed samples from each site performed by Hasek (2013).

This thesis is organized as follows. Chapter 2 presents the descriptions of the five research sites studied in this thesis, test procedures of the DMT, SPT, and CPT tests, and the current simplified methods for estimating liquefaction potential. Chapter 3 presents the field and laboratory tests performed at each site, and addresses the methodologies used to analyze the test data and identify the source sand layer. Chapter 4 presents the

data from the field and laboratory testing, correlations between DMT-SPT and DMT-CPT test parameters, the results of the simplified procedure, recommends new CRR-K_D and CRR-E_D boundary curves for estimating the liquefaction potential of SCCP soils, and validates these curves with site specific CRR-K_D and CRR-E_D relations derived from cyclic triaxial testing. Conclusions are drawn in Chapter 5.

CHAPTER TWO
BACKGROUND

2.1 Introduction

This chapter presents and describes the five sites in the South Carolina Coastal Plain where geotechnical testing was performed. The procedures of the in situ tests and the procedures and assumptions used in reducing the experimental data are also presented. The in-situ tests performed at the sites include dilatometer tests, standard penetration tests, and cone penetration tests. The advantages and disadvantages of each test and the existing correlations between the different test parameters are also highlighted. Lastly, the current methods used to evaluate the liquefaction potential of soils are summarized.

2.2 Site Descriptions

2.2.1 Introduction

In the past thirty years much effort has been put forth to locate and study paleoliquefaction features in the South Carolina Coastal Plain. Today more than 50 sandblows have been discovered that are associated with earthquakes that date back as far as 6,000 years (see Talwani et al., 1999 and Talwani and Schaeffer, 2001). As shown in Figure 2.1, these features are centered around the Charleston area, the Georgetown and Myrtle Beach area, and the Bluffton and Hilton Head area.

Hu et al. (2002a) studied the geotechnical data (SPT blow count $(N_1)_{60cs}$, CPT tip resistance (q_{c1}), Shear Wave Velocity, and index properties) and analyzed the liquefaction potential at Sampit (SAM) and Gapway (GAP) in Georgetown County and Ten Mile Hill (TMHA and TMHB) near the Charleston Air Force Base. More recently, Hasek (2013) studied three additional sites: Four Hole Swamp (FHS), Hollywood (HOL), and Fort Dorchester (FD) which is approximately 5 miles south of Summerville. Flat Plate Dilatometer (DMT) tests were performed at SAM, GAP, FHS, HOL and FD and are the focus of this work.

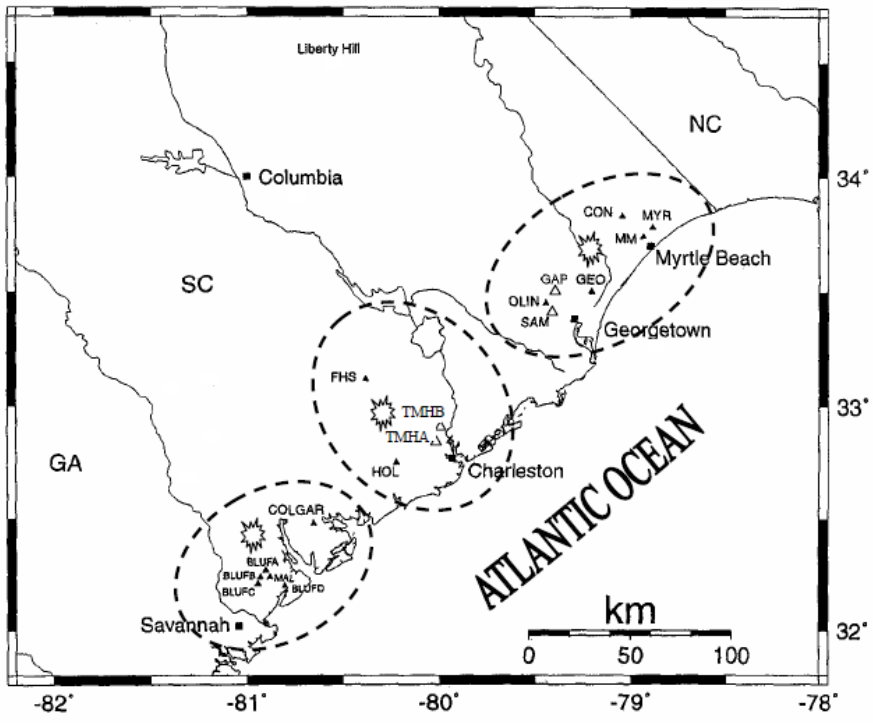

Figure 2.1 Locations of Paleoliquefaction Features in the South Carolina Coastal Plain (Reproduced from Hu et al. 2002a)

2.2.2 Sampit Site Description

The Sampit site is located about 9.2 miles (14.8 km) west-northwest of Georgetown, South Carolina. This site consists of a NW-SE trending drainage ditch approximately 1500 ft (500 m) long and ranging in depth from 6 to 10 ft (2 to 3 m). Three sandblows were discovered along the ditch (Talwani and Schaffer, 2001). Their locations (labeled SBN (north), SBM (middle), and SBS (south)) are shown in Figure 2.2, along with the locations of all geotechnical exploration points studied by USC researchers to date. The topography gently slopes to the northwest with ground surface elevations ranging from 37 to 43 ft (11.3 to 13.2 m) above MSL.

Hu et al. (2002a) analyzed data from six SCPT and six SPT tests (SAM-01 through 06) and Hasek (2013) studied three additional SCPT tests (SAM-SCPT-1 through 3), two SPTE tests (SAM-SPTE-1 and 2), and a DMT test (SAM-DMT). A piezometer (SAM-PZ) was installed (Hasek, 2013) to monitor ground water levels at the site. The work presented herein uses the DMT test and the CPT and SPT tests closest to the DMT (SAM-SCPT-1 and SAM-SPTE-1, respectively). Index tests were performed on samples obtained from SAM-SPTE-1. The site consists of 9 ft (2.7 m) of sand underlain by 13 ft (4.0 m) of source sand, 9 ft (2.7 m) of clay, and silt beginning at a depth of 31 ft below the ground surface. The ground water table was approximately 6.5 ft (2.0 m) below the ground surface. The source sand, which extends from 9 to 22 ft (2.7 to 6.7 m) deep, is estimated to be 450,000 years old (Weems and Lemon, 1984)). The three sandblows are estimated to range from 500 to 2,500 years old (Talwani et al., 1999; Amick, 1990).

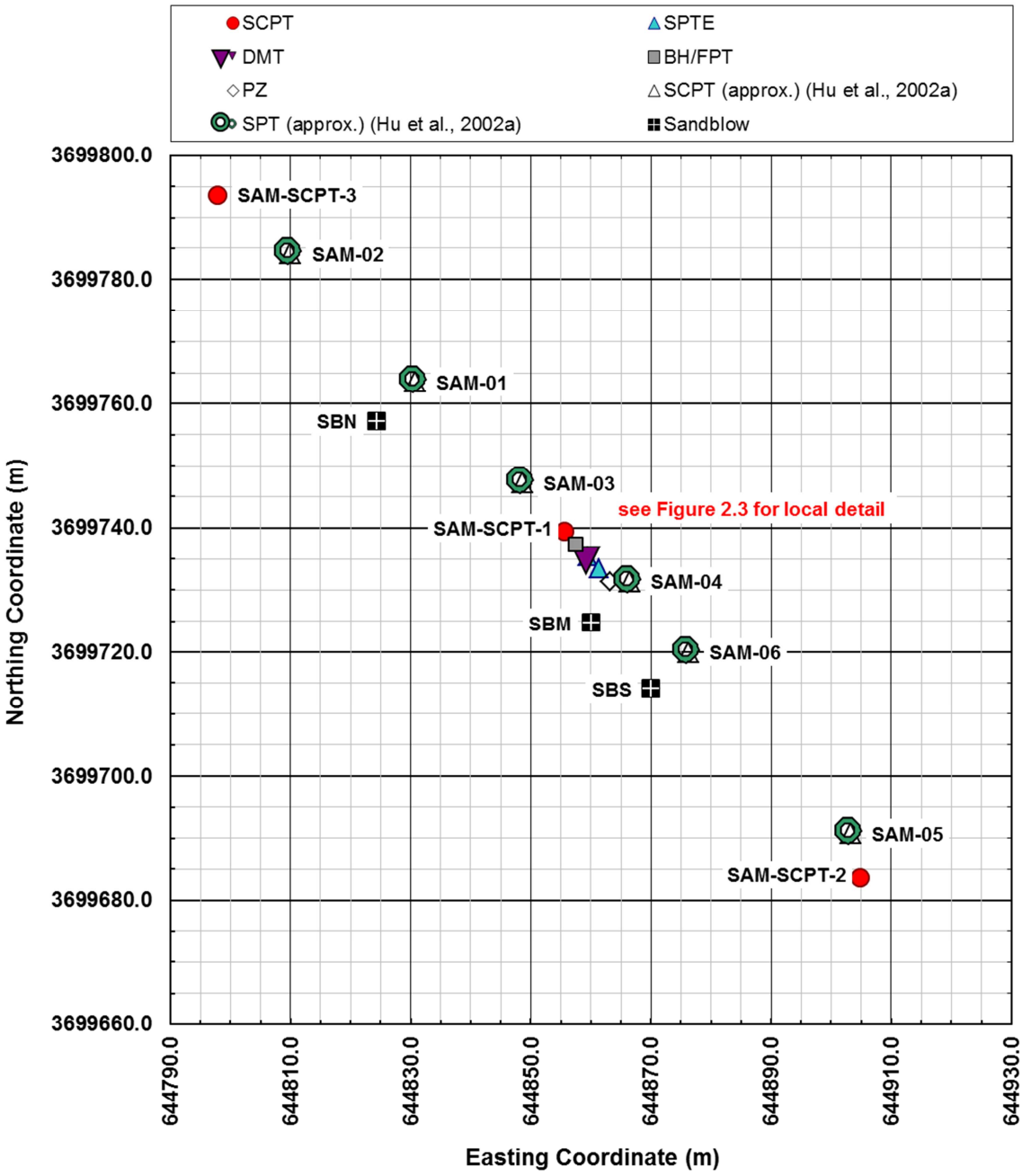

Figure 2.2 Exploration and Test Locations at the Sampit Research Site
(Modified from Hasek, 2013)

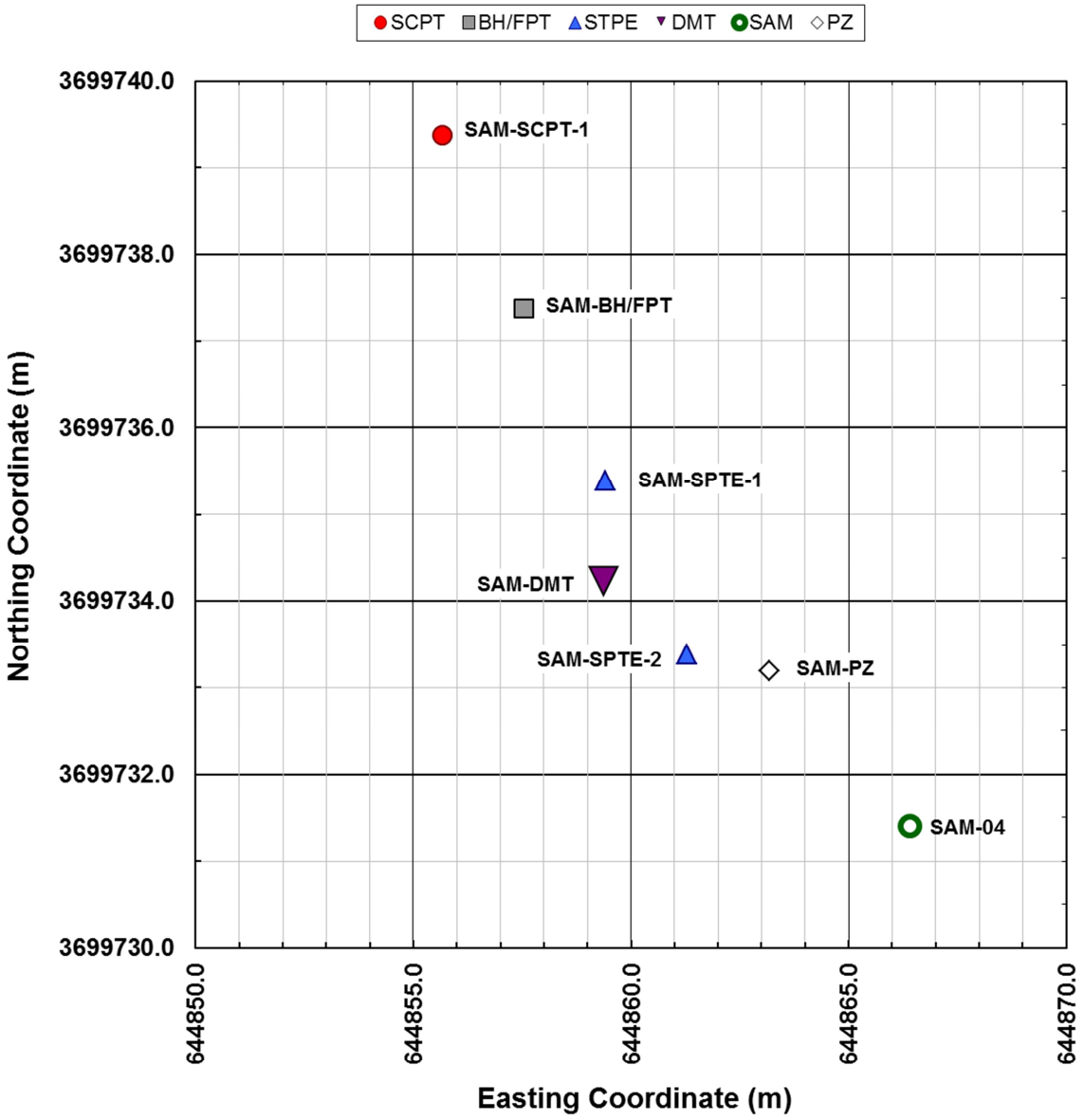

Figure 2.3 Exploration and Test Locations at the Sampit Research Site
(Modified from Hasek, 2013)

2.2.3 Gapway Site Description

The Gapway site is located about 9 mi (14.5 km) west-northwest of Georgetown and approximately 1.2 miles (1.9 km) northeast of the Sampit site. This site consists of a NE-SW trending drainage ditch approximately 2,600 ft (800 m) long and 6-9 ft (2-3 m) deep (Hu et al, 2002a). Four sandblows were discovered in the drainage ditch and are identified as A, B, C, and D in Figure 2.4 (Talwani et al. 1999). The figure also shows the locations of all geotechnical exploration points studied by USC researchers to date. The site is relatively flat with ground surface elevations ranging from 13 to 16 ft (4.0 to 4.8 m) above MSL.

Hu et al. (2002a) studied the results from 5 CPT tests with shear wave velocity measurements and 4 SPT tests, which are labeled GAP-01 through 05 in Figure 2.4. (An SPT test was not performed at GAP-04). Hasek (2012) studied an additional 3 CPT tests (labeled GAP-SCPT-1 through -3) and a DMT test (labeled GAP-DMT). This study focuses on the DMT, GAP-CPT-1 because of its relative proximity to the DMT, and the SPT test GAP-03. GAP-03 was selected because Hu (2001) deemed this profile the most indicative of the overall site conditions, and as such, was the most thoroughly tested for grain size distribution by sieve analyses.

The site stratigraphy, as reported by Hu (2001), consists of 3 ft (1 m) of mixed sands at the surface overlaying a 1 ft (0.3 m) clay layer that acts as a confining cap to the source sand which is 3 ft (1 m) thick. Beneath the source sand layer lies an 8 ft (2.7 m) clay layer that overlies coarse sand starting at approximately 15 ft (4.6 m) below the ground surface. The ground water table was approximately 4.5 ft (1.4 m) below the ground surface. The source sand at Gapway, which extends from 4 to 7 ft (1.2 to 2.1 m),

is estimated to be 450,000 years old (Weems and Lemon, 1984). Organic material collected from the sandblows was used to date the liquefaction events and estimated the three sandblows to have formed between 1,500 and 5,300 years ago (Talwani et al. 1999).

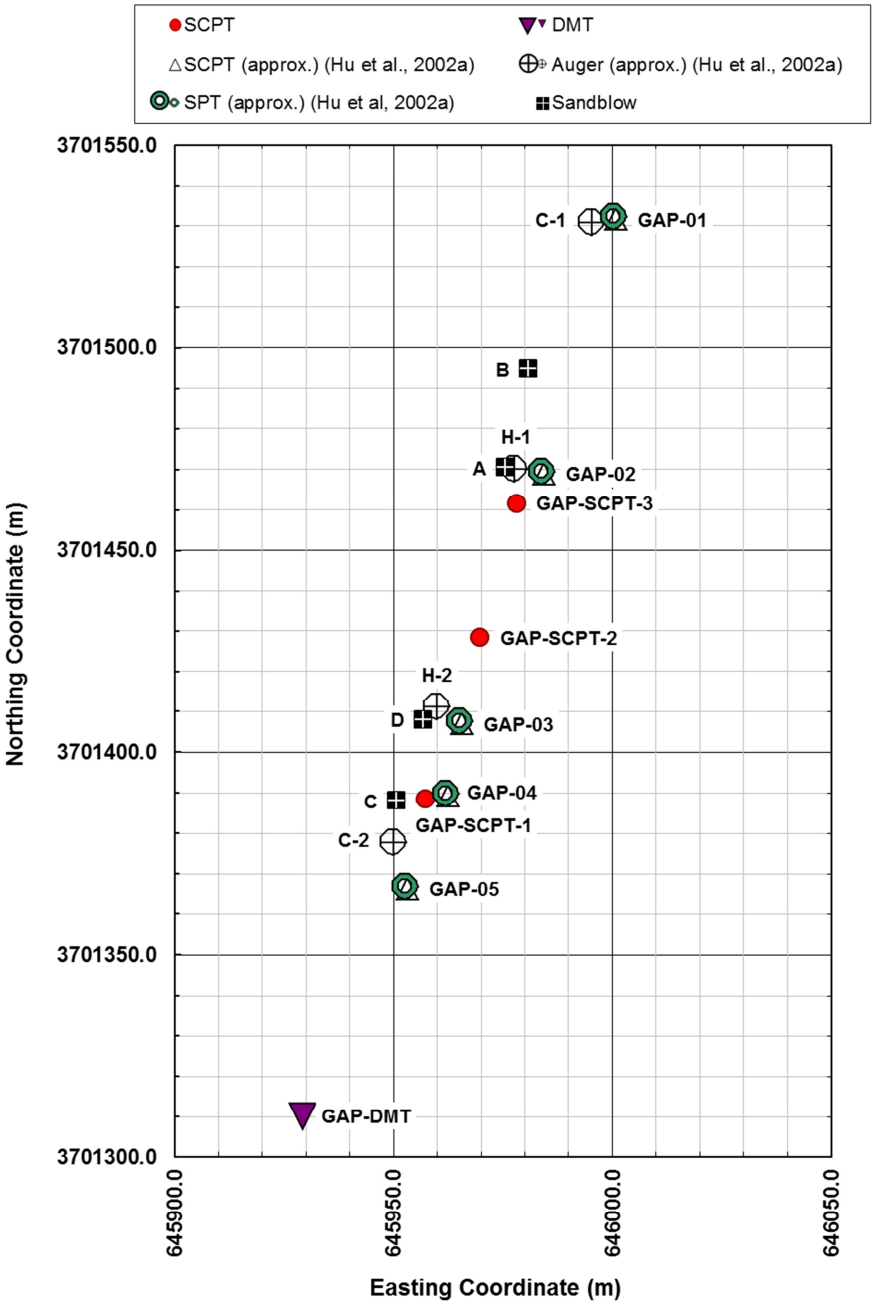

Figure 2.4 Exploration and Test Locations at the Gapway Research Site (Reproduced from Hasek, 2013)

2.2.4 Fort Dorchester Site Description

The Fort Dorchester site is located at Colonial Dorchester State historic Site in Summerville, South Carolina and overlooks the Ashley River. As reported by Hasek (2012), the topography gently slopes to the west and south towards the Ashley River with ground surface elevations ranging from river level (mean tide elevation of 3 ft. (1 m)) to about 27 ft (9 m) above mean sea level. Geotechnical field testing was performed at the locations shown in Figure 2.5 and laboratory testing was performed on soils obtained from three vibracores.

The work by Hasek (2012) entails 3 CPT tests (FD-CPT-4, FD-CPT-5, and FD-CPT-7a), 5 SCPT tests (FD-SCPT-1, FD-SCPT-2, FD-SCPT-3, FD-SCPT-6, and FD-SCPT-7b), 3 vibracores (FD-VC-1 through 3), two DMT tests (FD-DMT-NS and FD-DMT-EW) and 1 piezometer (FD-PZ). The two DMT tests are in close proximity to one another to study the effects of the dilatometer plate orientation. One test was performed with the plate oriented north and south (FD-DMT-NS) and one oriented east and west (FD-DMT-EW). There is also a test pit that was excavated by Talwani et al. (2011) to examine the soil fabric within the sandblow and to obtain samples for carbon dating. This study addresses the two DMT tests and CPT tests FD-SCPT-1 and FD-SCPT-2 which are closest to the E-W and N-S oriented DMT, respectively. Samples taken from vibracore FD-VC-1 were used for index testing.

The source sand at this site was identified to be approximately 8 ft (2.4 m) thick, ranging from 8 to 16 ft (2.4 to 4.9 m) below ground surface and is overlaid by a mixture of clayey sand and silty clay (Talwani et al. (2011)). Underneath the source sand lays a 2 ft (0.6 m) layer of silty sand which transitions to sandy silt at 18 ft (5.5 m). The ground

water table was measured at 17 ft (5.2 m) below the ground surface during testing but it is assumed that the ground water was much higher at the time of the paleoliquefaction events. The source sand is estimated to be about 200,000 years old, while the sandblow was estimated to be more than 5,000 years old (Weems and Lemon, 1984).

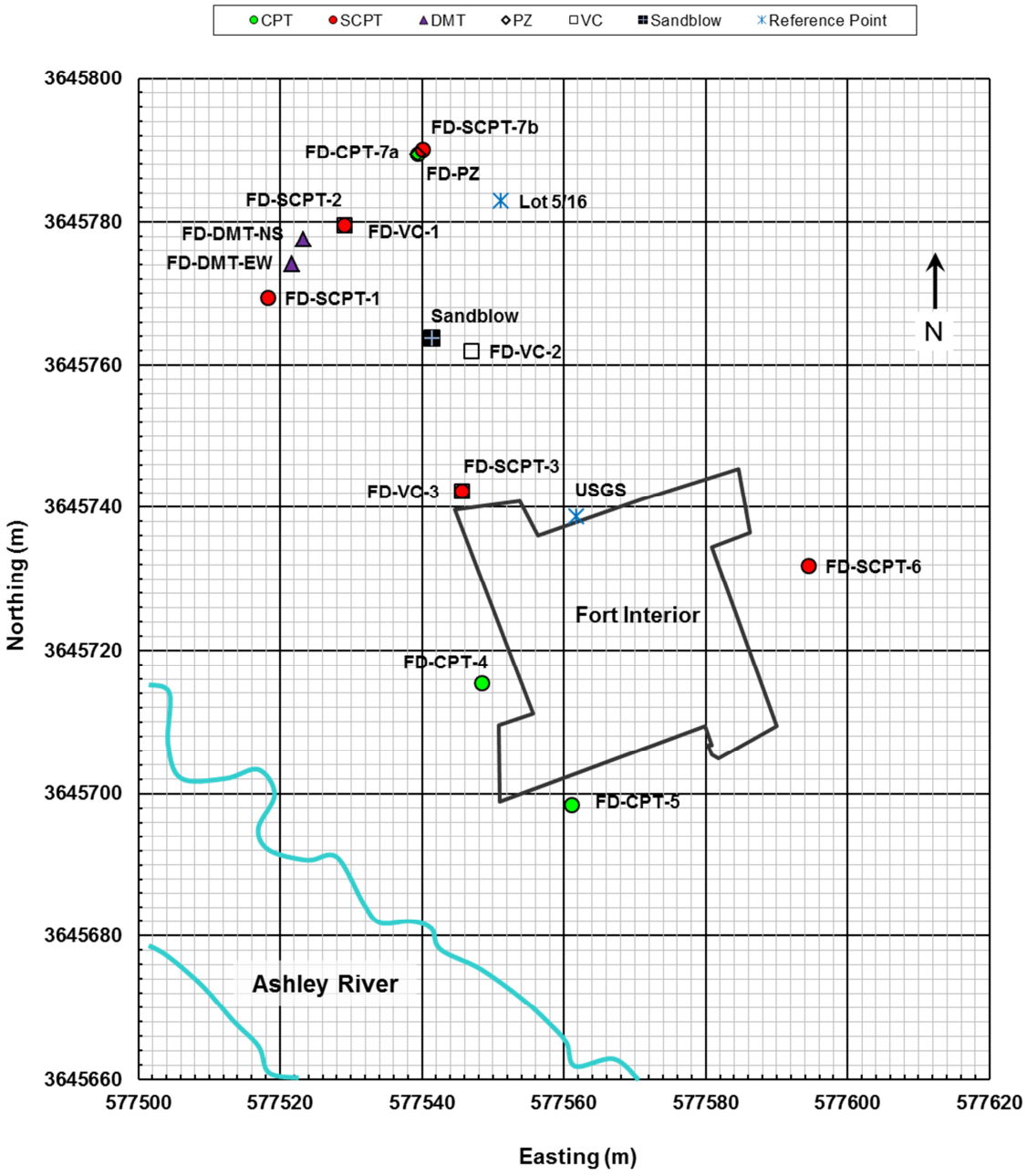

Figure 2.5 Exploration and Test Locations at the Fort Dorchester Research Site (Modified from Hasek, 2013)

2.2.5 Hollywood Site Description

The Hollywood site is located about 0.5 miles (0.8 km) northeast of the town of Hollywood, South Carolina (see Martin, 1990 and Hasek, 2013). The site consists of two drainage ditches that contain some of the most prolific evidence of paleoliquefaction ever observed. Obermeir (1985, 1986, and 1987) identified 162 liquefaction features that date back to five separate earthquakes. Twenty-four of these features were associated with the 1886 earthquake, while the others were formed during prehistoric earthquakes. Talwani and Cox (1985) estimated the sandblows along the channel to range from 500 to 4,200 years old.

Geotechnical field testing was performed at the locations shown in Figure 2.6. The topography gently slopes from east to west with ground surface elevations ranging from 28 to 35 ft (8.4 to 10.6 m) MSL. Hasek (2013) studied the results from 3 CPT tests (HWD-CPT-4 through -6), 3 SCPT tests (HWD-SCPT-1 through -3), 2 SPT tests (HWD-SPTE-1 and -2), and 1 DMT test (HWD-DMT). This study examines the results from the DMT, HWD-CPT-4, and HWD-SPTE-1 because of their proximity to the DMT. Samples obtained from HWD-SPTE-1 were used for index property testing.

The site stratigraphy consists of 9 ft (2.7 m) of silty sand underlain by the 5 ft (1.5 m) source sand layer, with silty, clayey sand starting at 14 ft (4.3 m) below the ground surface. The ground water table was approximately 9 ft (2.7 m) below the ground surface. Weems et al. (1986) estimated the source sand layer, which extends from 9 to 14 ft (2.7 to 4.3 m) below the ground surface, to be 120,000-130,000 years old.

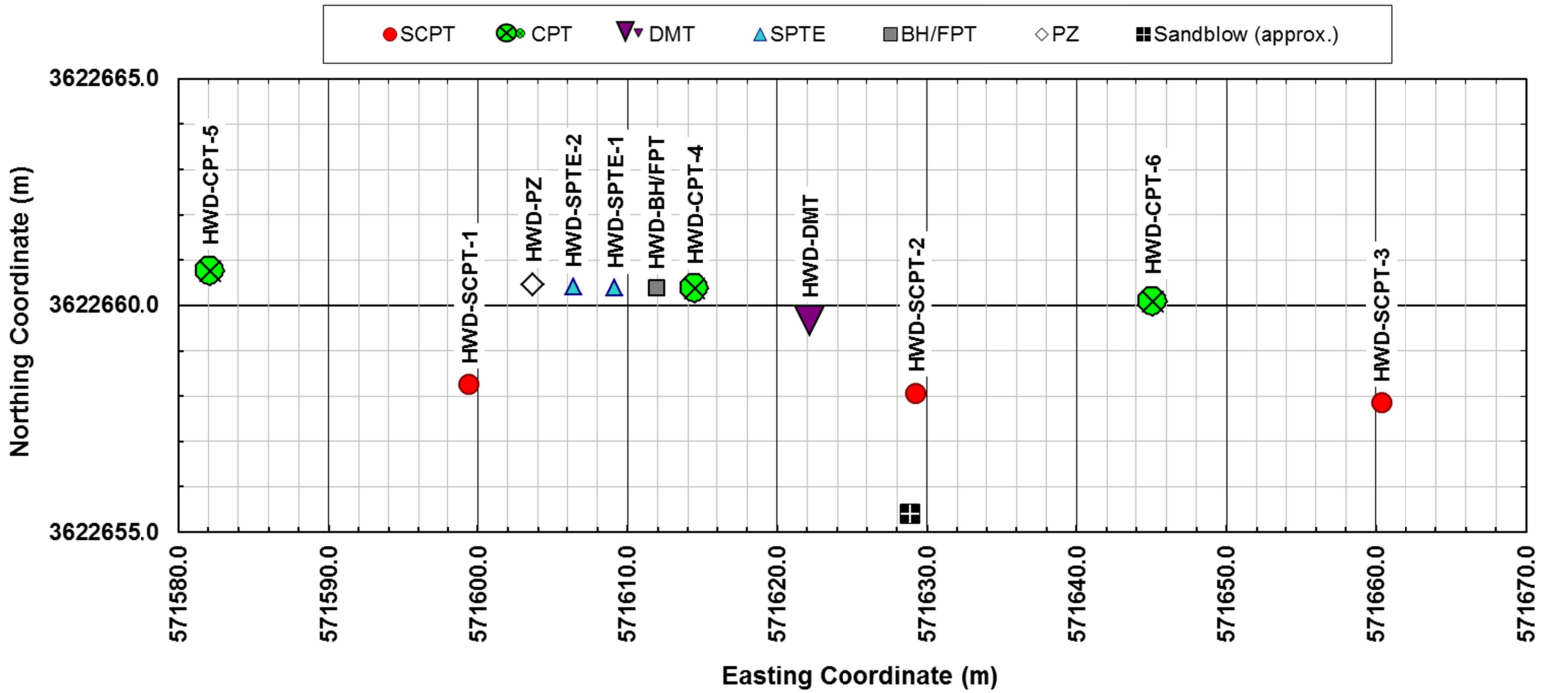

Figure 2.6 Exploration Layout and Field Test Locations at the Hollywood Research Site (Reproduced from Hasek, 2013)

2.2.6 Four Hole Swamp Site Description

The Four Hole Swamp site is located near the intersection of State Highways 78 and 178, approximately 2.6 miles east of Dorchester, SC. As reported by Hasek (2012), the site is located at the easternmost boundary of Waste Management's Oakridge Landfill within a wooded area. The surrounding topography gently slopes towards the formal Four Hole Swamp to the northeast with ground surface elevations ranging from 57 to 72 ft (17.4 to 22 m).

Hasek (2012) analyzed data from three SCPT tests (FHS-SCPT-1 through 3), two SPT tests (FHS-SPTE-1 and 2), a DMT test (FHS-DMT), and a piezometer (FHS-PZ). The work presented herein uses FHS-SCPTE-1 and FHS-SCPT-1 due to their proximity to the DMT. Index tests were performed on samples obtained from FHS-SPTE-1.The locations of all geotechnical tests are shown in Figure 2.7.

The site stratigraphy consists of 9 ft (2.7 m) of silty, clayey sand underlain by 6 ft (1.8 m) of source sand, with clayey sand beginning at a depth of 15 ft (4.6 m) below the ground surface. The ground water table was approximately 9 ft (2.7 m) below the ground surface. The source sand, which extends from 9 to 15 ft. (2.7 m to 4.6 m) deep, is estimated to be 1.4 to 1.6 million years old (Weems et al. 1997). The sandblow is estimated to be 1,660 years old (Rajendran and Talwani, 1993)

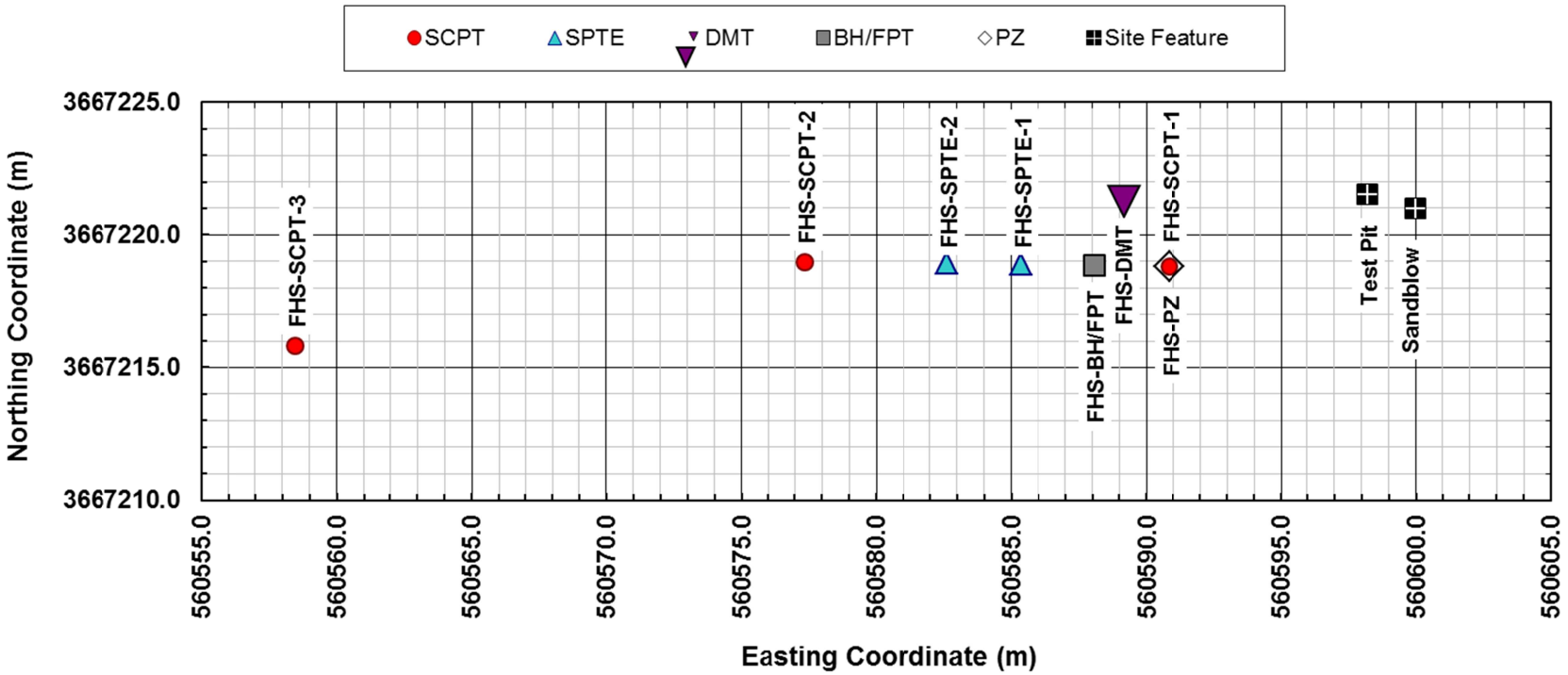

Figure 2.7 Exploration Layout and Field Test Locations at the Four Hole Swamp Research Site (Reproduced from Hasek, 2013)

2.3 Methods for In situ testing

2.3.1 Dilatometer Test

The dilatometer test was developed by Silvano Marchetti in Italy during the 1970's. Marchetti (1975) performed tests at over 40 well geotechnically defined sites and used the results of the DMT to draw empirical relationships to many common geotechnical parameters used in design. In the past forty years DMT research has expanded to include many different soil deposits from all over the world (Marchetti, 1980). The extensive study and calibration of the DMT has given geotechnical engineers another option for subsurface exploration (in addition to the more commonly used SPT and CPT tests). The DMT can be used to evaluate settlement analysis, estimate the stresses acting on axially and laterally loaded piles, detect slip surfaces, monitor the change in stress as the relative density of the soil varies (either as an increase in D_r by means of compaction or as a decrease in D_r caused by the installation of various types of piles), and to evaluate the liquefaction potential of a given soil (Marchetti et al., 2001).

The significance of the DMT in liquefaction analysis has increased greatly in recent years. Many authors (e.g. Monaco and Schmertmann (2007) and Marchetti (2010)) have suggested that the DMT is superior to the SPT and CPT for estimating liquefaction resistance. This is due to the fact that the DMT is capable of precisely measuring horizontal stresses. The DMT's sensitivity to horizontal stresses allows it to detect the effects of stress history, prestraining, aging, cementation, and structure. Monaco and Schmertmann (2007) concluded that "disregarding aging is equivalent to omitting a primary parameter in the CRR correlations". This theory is supported by the work of Leon et al. (2006) where it was shown that ignoring the effects of aging overestimated CRR by as much as 60%. This overestimation leads to overly conservative

designs which can inflate the cost of the projects and in extreme cases can bring about the cancelation of a project.

With the significance of the DMT noted, there lies a need to develop DMT-based methods for liquefaction analysis which would provide a more accurate approximation than the existing CRR-SPT and CRR-CPT relationships. The issue that hinders the development of new methods is the lack of CRR-DMT data.

2.3.1.1 DMT Test Procedure

The dilatometer is a flat stainless steel blade with a circular stainless steel membrane mounted flush to one side (Figure 2.8 (a)), which is inflated using nitrogen gas. The test consists of monitoring the pressure necessary to inflate the membrane a distance of 1.1 mm into the soil at different depths (Figure 2.9) (Marchetti et al., 2001). Using pneumatic tubes, the dilatometer is attached to a nitrogen gas tank and a control box (Figure 2.8 (b)), which is equipped with a pressure regulator, pressure gauges, an audio-visual signal, and vent valves.

The test begins with the dilatometer being pushed vertically into the soil to a desired depth at a rate of 2 cm/s with a penetrometer rig similar to that used in cone penetration tests (Marchetti et al., 2001). When the desired depth is obtained, pushing is stopped and pressure is slowly applied to the dilatometer, causing the membrane to inflate and expand into the soil. As inflation and deformation of the membrane progresses the audio/visual signal is used to indicate when to take pressure readings. Initially, when the membrane is flush, (i.e. no displacement), the signal is on. Once the membrane inflates to the point that it has been displaced 0.05 mm into the soil the signal

is discontinued and the first pressure reading, which is referred to as the “A-pressure” or the “lift-off” pressure is obtained. Pressure continues to be applied until a displacement of 1.1 mm has been reached. At this point the audio/visual signal is reactivated and the corresponding pressure is recorded as the “B-pressure”. After the B-pressure has been recorded the pressure is slowly released and the membrane is allowed to return to its initial position. When the initial position is reached the signal turns back on, indicating the end of the test. An optional closing pressure, C, can be taken at this point as well. When testing is complete the dilatometer is then pushed to the next desired depth (typically 1 ft (0.3 m) intervals) and the process is repeated.

(a)

(b)

Figure 2.8 (a) Front and side views of the flat plate dilatometer (modified after Marchetti et al., 2001); (b) Testing equipment including: the flat plate dilatometer, control unit, pneumatic tubes, and computer for recording data (www.marchetti-dmt.it (2013))

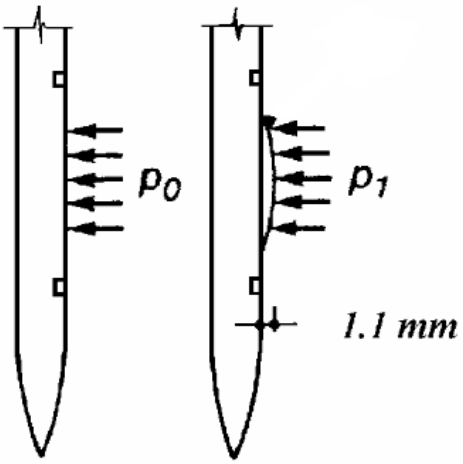

Figure 2.9 Expansion of the Dilatometer Membrane (after Marchetti et al., 2001)

Before testing can begin the dilatometer must first be calibrated so that the readings taken during testing can be corrected to account for the stiffness of the membrane (Marchetti et al., 2001). This can be done by performing the test under atmospheric conditions while a syringe is used to generate a vacuum and apply pressure. It should be noted that while the dilatometer is in its natural state, under atmospheric pressure, the membrane is not truly flush; it has a slight natural outward curvature to it, thus a vacuum pressure must be applied to collapse the membrane and bring it to the A position where it is flush with the plate (See Figure 2.10). The vacuum pulls the membrane inward so that it sits flush with the plate; this causes the audio-visual signal to turn on. Pressure should be slowly released from the vacuum to determine the minimum pressure required to bring the membrane to the A position (indicated by the turning off of the audio-visual signal). This pressure is recorded as ΔA (Marchetti et al., 2001). Then pressure is applied (signal off) using the piston of the syringe until a deformation of 1.1 mm (B position) has been reached, at which point the signal turns on again and the pressure is recorded as ΔB (Marchetti et al. 2001). These values are determined before and after testing to ensure the reliability of the readings. The average of these pre and post readings are taken as the pressure corrections and are applied to every reading taken during testing to account for the stiffness of the membrane.

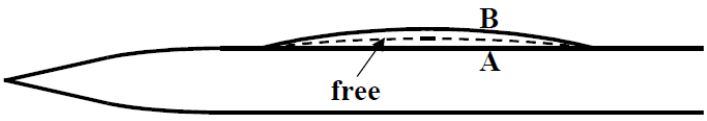

Figure 2.10 Positions of the membrane (free, A and B) (after Marchetti et al., 2001)

2.3.1.2 DMT Data Reduction

Using the pressure corrections ΔA and ΔB, along with the zero correction of the pressure gauge (Z_m), values of p_0 and p_1 can be determined using the following equations presented by Marchetti et al. (2001):

$$p_0 = 1.05(A - Z_m + \Delta A) - 0.05(B - Z_m - \Delta B) \quad 2.1$$

$$p_1 = B - Z_m - \Delta B \quad 2.2$$

The pressure readings p_0 and p_1 obtained from the DMT test can be correlated to many soil parameters and properties. The primary correlations are the material index (I_D), the horizontal stress index (K_D), and the dilatometer modulus (E_D). Equations for these properties were provided by Marchetti (1980) as follows:

$$I_D = \frac{(p_1 - p_0)}{(p_0 - u_0)} \quad 2.3$$

$$K_D = \frac{(p_0 - u_0)}{\sigma'_{v0}} \quad 2.4$$

$$E_D = 34.7\,(p_1 - p_0) \quad 2.5$$

These three primary properties can be correlated to many geotechnical properties, as shown in Table 2.1. Examples of alternate definitions of OCR (Mayne, 1995), Φ' (Campanella and Robertson, 1991), and c_u (Schmertman, 1981) are given below:

$$OCR = 0.509 * \frac{(p_o - u_o)}{\sigma'_{vo}} \quad \text{for } I_D < 1.2 \quad 2.6$$

$$\Phi' = 37.3 * \left(\frac{K_D - 0.8}{K_o + 0.8}\right)^{0.082} \quad \text{for } I_D \geq 1.2 \quad 2.7$$

$$c_u = \left(\frac{p_o - u_o}{10}\right) \quad \text{for } I_D < 1.2 \quad 2.8$$

Table 2.1 Geotechnical parameters that can be derived from DMT data (after, Marchetti et al., 2001).

SYMBOL	DESCRIPTION	BASIC DMT REDUCTION FORMULAE	
p_0	Corrected First Reading	$p_0 = 1.05\ (A - Z_M + \Delta A) - 0.05\ (B - Z_M - \Delta B)$	Z_M = Gage reading when vented to atm. If ΔA & ΔB are measured with the same gage used for current readings A & B, set $Z_M = 0$ (Z_M is compensated)
p_1	Corrected Second Reading	$p_1 = B - Z_M - \Delta B$	
I_D	Material Index	$I_D = (p_1 - p_0) / (p_0 - u_0)$	u_0 = pre-insertion pore pressure
K_D	Horizontal Stress Index	$K_D = (p_0 - u_0) / \sigma'_{v0}$	σ'_{v0} = pre-insertion overburden stress
E_D	Dilatometer Modulus	$E_D = 34.7\ (p_1 - p_0)$	E_D is NOT a Young's modulus E. E_D should be used only AFTER combining it with K_D (Stress History). First obtain $M_{DMT} = R_M E_D$, then e.g. $E \approx 0.8\ M_{DMT}$
K_0	Coeff. Earth Pressure in Situ	$K_{0,DMT} = (K_D / 1.5)^{0.47} - 0.6$	for $I_D < 1.2$
OCR	Overconsolidation Ratio	$OCR_{DMT} = (0.5\ K_D)^{1.56}$	for $I_D < 1.2$
c_u	Undrained Shear Strength	$c_{u,DMT} = 0.22\ \sigma'_{v0}\ (0.5\ K_D)^{1.25}$	for $I_D < 1.2$
Φ	Friction Angle	$\Phi_{safe,DMT} = 28° + 14.6°\ \log K_D - 2.1°\ \log^2 K_D$	for $I_D > 1.8$
c_h	Coefficient of Consolidation	$c_{h,DMTA} \approx 7\ cm^2 / t_{flex}$	t_{flex} from A-log t DMT-A decay curve
k_h	Coefficient of Permeability	$k_h = c_h\ \gamma_w / M_h$ ($M_h \approx K_0\ M_{DMT}$)	
γ	Unit Weight and Description	(see chart in Fig. 16)	
M	Vertical Drained Constrained Modulus	$M_{DMT} = R_M E_D$ if $I_D \leq 0.6$ $R_M = 0.14 + 2.36 \log K_D$ if $I_D \geq 3$ $R_M = 0.5 + 2 \log K_D$ if $0.6 < I_D < 3$ $R_M = R_{M,0} + (2.5 - R_{M,0}) \log K_D$ with $R_{M,0} = 0.14 + 0.15\ (I_D - 0.6)$ if $K_D > 10$ $R_M = 0.32 + 2.18 \log K_D$ if $R_M < 0.85$ set $R_M = 0.85$	
u_0	Equilibrium Pore Pressure	$u_0 = p_2 = C - Z_M + \Delta A$	In free-draining soils

2.3.2 Standard Penetration Test

The standard penetration test (SPT) consist of driving a split spoon sampler into the ground by repeatedly dropping a 140-lb hammer a distance of 30-in. onto an anvil which is connected to the top of the drill rod and the sampler, per ASTM D1586. The number of blows required to penetrate the sampler through three 6-in. intervals is recorded. Due to extensive soil disturbance and soil falling from the borehole wall as the drill rod is raised out of and the sampler is lowered into the borehole, the number of blows recorded in the upper 6-in. is discarded and the blow counts from the two lower 6-in. intervals are added together and referred to as the N value. This N value gives insight to the relative strength, density, and consistency of a soil profile. Once testing is

complete the sampler is removed from the borehole and the recovered soil is visually identified in the field and then placed in glass jars and transported to the laboratory where index tests are performed.

2.3.2.1 SPT Data Reduction

To use the SPT data for liquefaction evaluation some corrections must first be applied to account for energy loss, to normalize the effects of overburden pressure, and to convert the measurement from soil with high fines content to that of clean sand. Youd et al. (2001) provides equations to account for these corrections, the first of which covers both the energy loss and the overburden stress corrections

$$(N_1)_{60} = N_m C_N C_E C_B C_R C_S \quad 2.9$$

where N_m is the measured standard penetration resistance; C_N is a factor to normalize N_m to a common reference effective overburden stress; C_E is a correction for hammer energy ration (ER); C_B is a correction factor for borehole diameter; C_R is a correction factor for rod length; and C_S is a correction for samplers with or without liners.

The C_N correction is necessary to account for the increasing overburden pressure. The overburden pressure skews the SPT data because the N-value increases with the increasing overburden pressure. Kayen et al. (1992) provide the following equation to normalize N_m to an effective overburden pressure (σ'_{vo}) to that of atmospheric pressure, P_a. It should be noted that C_N is limited to a maximum value of 1.7 so that N values at shallow depths (with little overburden pressure) are not incorrectly modified.

$$C_N = \frac{2.2}{\left(1.2 + \frac{\sigma'_{vo}}{P_a}\right)} \quad 2.10$$

C_E is also an important correction factor because energy is lost in the transfer from the drop of the hammer down to the sampler. This can be a result of the rod straying from the vertical position, inconsistent raising and dropping of the hammer, or by many other variables in the testing procedure. This loss of energy can be accounted for by taking ER measurements for each blow. It has been accepted that 60% is a good average ER for standard testing methods in the U.S. and is used as a reference value to compare results from different types of hammers, anvils, and lifting and releasing equipment. Youd et al. (2001) gives the following equation to normalize ER.

$$C_E = \frac{ER}{60} \tag{2.11}$$

The C_E factor was applied to the data by taking the C_E's for each blow in a 6-in. increment and averaging them together so that one C_E could be applied to the whole interval rather than computing different $(N_1)_{60}$'s for every blow.

According to Youd et al (2001), C_R can be taken as equal to one for all depths when evaluating liquefaction potential. This is because the original liquefaction case study history databases did not include this correction, so the correction is implicitly incorporated into the empirical SPT procedure. C_B and C_S were also assumed to equal one for all calculations.

The final correction to apply is that of clean sand equivalence. It was noted by Seed et al. (1985) in their original liquefaction evaluation that CRR appeared to increase with an increase in fines content, suggesting that fines content has a great impact on a soil's likelihood to liquefy. This relationship is so concerning that they produced different CRR curves for soils with varying fines content. Youd et al. (2001) recommend the following equations to account for the influence of fines content (FC) on CRR:

$$(N_1)_{60cs} = \alpha + \beta(N_1)_{60} \quad 2.12$$

where α and β are coefficients determined by the following relationships:

$$\alpha = 0 \qquad \text{for } FC \leq 5\% \quad 2.13$$

$$\alpha = \exp\left[1.76 - \left(\frac{190}{FC^2}\right)\right] \quad \text{for } 5\% < FC < 35\% \quad 2.14$$

$$\alpha = 5.0 \quad \text{for } FC \geq 35\% \quad 2.15$$

$$\beta = 1.0 \quad \text{for } FC \leq 5\% \quad 2.16$$

$$\beta = 0.99 + \left(\frac{FC^{1.5}}{1{,}000}\right) \quad \text{for } 5\% < FC < 35\% \quad 2.17$$

$$\beta = 1.2 \quad \text{for } FC \geq 35\% \quad 2.18$$

With the SPT data corrected for overburden pressure, energy loss, and fines content, CRR of Holocene soils can be calculated using the follow equation provided by Idriss and Boulanger (2006):

$$CRR_{7.5} = \exp\left[\frac{(N_1)_{60cs}}{14.1} + \left(\frac{(N_1)_{60cs}}{126}\right)^2 - \left(\frac{(N_1)_{60cs}}{23.6}\right)^3 + \left(\frac{(N_1)_{60cs}}{25.4}\right)^4 - 2.8\right] \quad 2.19$$

It should be noted that this equation is only valid for $(N_1)_{60cs} < 30$. According to Youd et al. 2001, the soil is considered too dense to liquefy when $(N_1)_{60cs} \geq 30$. Also, the equation is only applicable to magnitude 7.5 earthquakes. To evaluate the liquefaction potential for other magnitudes the following equations, defined by Youd and Idriss (1997), should be applied:

$$CRR_M = CRR_{7.5} * MSF \quad 2.20$$

$$MSF = \frac{10^{2.24}}{M^{2.56}} \quad 2.21$$

where MSF is the "magnitude scaling factor" and M is the earthquake magnitude.

2.3.3 Cone Penetration Test

The cone penetration test (CPT) consists of pushing a 15 cm^2 electric piezocone penetrometer hydraulically into the ground at a rate of 2 cm/s. Load cells located right behind the cone measure tip resistance (q_c) and sleeve friction (f_s) and a pressure transducer determines pore water pressure (u_2).

2.3.3.1 CPT Data Reduction

To use the CPT data for liquefaction evaluation, it must first be normalized and corrected to account for the influence of overburden pressure and fines content. Robertson and Wride (1998) suggest the following equations to normalize q_c into the dimensionless cone penetration resistance, q_{c1N}, where

$$q_{c1N} = C_Q \left(\frac{q_c}{P_a}\right) \quad 2.22$$

$$C_Q = \left(\frac{P_a}{\sigma'_{vo}}\right)^n \quad 2.23$$

and where C_Q is the normalizing factor for cone penetration resistance; P_a = 1 atm of pressure in the same units used for σ'_{vo}; n is an exponent that varies from 0.5-1.0 with soil type; and q_c is the field cone penetration resistance measured at the tip. It should be noted that C_Q becomes quite large near the surface because of low overburden pressures. To account for this occurrence a threshold is set so that the maximum value used does not exceed 1.7. This ensures that soils with low overburden pressures are not incorrectly manipulated.

To determine the proper exponent to use in the above equations the soil type must first be identified. This can be done using a property referred to as the soil behavior type index, I_c, which is defined as:

$$I_c = [(3.47 - \log Q)^2 + (1.22 + \log F)^2]^{0.5} \quad 2.24$$

where

$$Q = \left[\frac{q_c - \sigma_{vo}}{P_a}\right]\left[\left(\frac{P_a}{\sigma'_{vo}}\right)^n\right] \quad 2.25$$

and

$$F = \left(\frac{f_s}{q_c - \sigma_{vo}}\right) \times 100\% \quad 2.26$$

Robertson and Wride (1998) recommend a three step iterative process to determine the proper soil type and exponent used to calculate I_c. In the first step n is assumed to equal one (this is characteristic of clayey soils) when calculating Q. The resulting values of I_c are then examined. If $I_c > 2.6$ then the soil is considered too clay-rich to liquefy and the analysis for these soils is complete. For all values of $I_c < 2.6$ a second iteration is required. These soils are considered to be more granular and an exponent of n=0.5 should be assigned to these soils. Q and I_c are recalculated using n=0.5 and the values of I_c are examined once more. If the new value of I_c is <2.6 the soil is classified as nonplastic and granular; this I_c value should be used in the liquefaction evaluation. However if the recalculated value of I_c is >2.6 then a third iteration is necessary because these soils are likely to be very silty and possibly plastic, so an intermediate exponent of n=0.7 should be applied to the calculations of Q, I_c, C_Q, and q_{c1N}; the resulting I_c should be used in the liquefaction evaluation.

Robertson and Wride (1998) also provide the following equations to correct q_{c1N} to an equivalent clean sand value, $(q_{c1N})_{cs}$:

$$(q_{c1N})_{cs} = K_c q_{c1N} \quad 2.27$$

where K_c is a correction factor for grain characteristics and is defined by:

$$K_c = 1.0 \quad \text{for } I_c \leq 1.64 \quad 2.28$$

$$K_c = -0.403I_c^4 + 5.581I_c^3 - 21.63I_c^2 + 33.75I_c - 17.88 \quad \text{for } I_c > 1.64 \quad 2.29$$

With an appropriate $(q_{c1N})_{cs}$ value, the CRR of Holocene soils can be calculated by the following equations, again provided by Robertson and Wride (1988):

$$\text{If } (q_{c1N})_{cs} < 50 \quad CRR_{7.5} = 0.833\left[\frac{(q_{c1N})_{cs}}{1{,}000}\right] + 0.05 \quad 2.30$$

$$\text{If } 50 \leq (q_{c1N})_{cs} \leq 160 \quad CRR_{7.5} = 93\left[\frac{(q_{c1N})_{cs}}{1{,}000}\right]^3 + 0.08 \quad 2.31$$

Note that these equations are not valid for soils with $(q_{c1N})_{cs} > 160$ because soils in this range are considered too dense to liquefy (Robertson and Wride, 1998), and again, these equations are only applicable for magnitude 7.5 earthquakes. Equations 2.20 and 2.21 must be applied in order to evaluate the liquefaction potential for other earthquake magnitudes.

2.3.4 Advantages and Disadvantages of Field Tests

The DMT and the CPT tests are similar in that they are both highly reproducible, yield an almost continuous soil profile, and are fairly inexpensive to perform (if the capital cost of the equipment is neglected) (Marchetti, 1975 and Robertson and Robertson, 2010). The biggest difference is the amount of soil disturbance observed during testing as illustrated in Figure 2.11 (Baligh and Scott, 1975). The wedge shape of

the DMT allows for much less disturbance than is induced with the conical shape of the CPT; thus the DMT more accurately portrays the in situ soil conditions (Baligh and Scott, 1975). The minimal disturbance of the DMT is the main contributor to its sensitivity to horizontal stresses (Marchetti, 2011). The SPT and CPT cannot detect the effects of stress history (prestraining, aging, cementation, and structure) because the amount of disturbance is so great that it seriously damages or destroys the microstructure effects that result from aging (Monaco and Schmertmann, 2007; Jamiolkowski et al., 1985). As previously mentioned, this ability to detect the effects of stress history is what sets the DMT apart from all other field tests and makes it a superior tool for liquefaction analysis (Monaco et al., 2005).

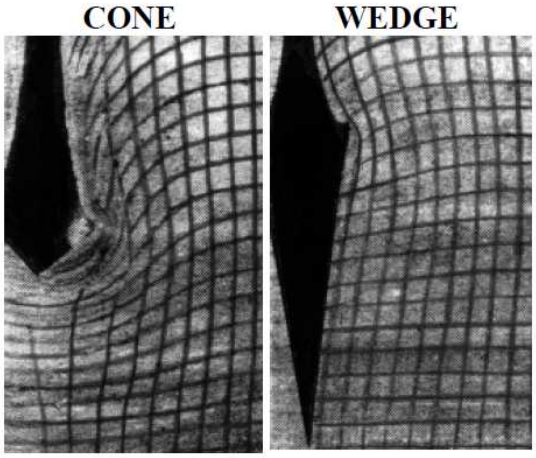

Figure 2.11 Deformed grids by Baligh and Scott (1975)

The main disadvantage of both the CPT and DMT tests is that soil samples are not recovered during testing. The stratigraphy delineated from these test results are based solely on soil behavior. For example, in the CPT test the different soil layers are distinguished from interpreting the tip resistance profile. If the profile is high and wiggly this indicates that the soil at this depth behaves like sand, whereas if the profile is low and

smooth this is indicative of clayey behavior. Therefore, it is important to obtain soil samples from at least one borehole or perform at least one SPT test. Even though the SPT blow counts lack the reproducibility of the CPT and DMT tests, the soil samples retrieved can be used for visual-manual identification as well as index property testing.

2.3.5 Cross Relations with Results from Other In Situ Tests

2.3.5.1 DMT/CPT Relations

The literature presents a number of DMT/CPT relations for certain geologies and soil types. These relationships include those of Mayne and Liao (2004), Robertson (2009), and Tsai et al. (2009).

Mayne and Liao (2004) present a relationship between DMT modulus, E_D, and CPT tip stress, q_t, and between DMT material index, I_D, and CPT friction ratio, FR, that is applicable to piedmont residual soils which are as follows:

$$E_D = 5q_t \tag{2.32}$$

$$I_D = 2.0 - 0.14(FR) \tag{2.33}$$

Robertson (2009) also suggested correlations between DMT and CPT parameters which are presented below.

$$I_D = 10^{(1.67-0.67I_c)} \tag{2.34}$$

$$K_D = 0.3(Q_{t1})^{0.95} + 1.05 \quad \text{when } I_C > 2.60 \tag{2.35}$$

$$\frac{E_D}{\sigma'_{v0}} = 5Q_{t1} \tag{2.36}$$

$$\text{where} \quad Q_{t1} = \frac{(q_t - \sigma'_{v0})}{\sigma'_{v0}} \tag{2.37}$$

Recall from Section 2.3.3.1 that I_C=2.60 is the cut off between sandy and clayey soils where soils with I_C>2.6 are considered too clay-rich to liquefy. Due to this restriction, Robertson's K_D/Q_{t1} relation is not relevant for liquefaction potential analysis.

Marchetti (2011) warns against using any DMT/CPT relations to estimate K_D from q_c. Marchetti argues that because the DMT is sensitive to stress history and the CPT is not then any effects of aging would be lost in translation. To quote Monaco and Schmertmann (2007) "disregarding aging is equivalent to omitting a primary parameter in CRR correlations". When using K_D to evaluate CRR it is critical to use the K_D measured by DMT rather than K_D estimated through correlations with other test data (Marchetti, 2011). Marchetti's (2011) suggested approach to derive CRR-K_D relations is to take the existing large CPT liquefaction database, transform the database into CRR-K_D correlations using translation formulas, use this transformed data as a first approximation, and fine tune the correlation using real life CRR-K_D data.

Tsai et al. (2009) provides some of these "translation formulas". They performed numerous DMT, CPT, and SPT tests side by side so that correlations could be made between the different test parameters. The following translation formulas between DMT and CPT test data in Holocene soils, which were derived using least squares regression to fit a trendline to the data, are as follows:

$$(q_{c1N})_{cs} = 0.4K_D^3 - 7.7K_D^2 + 56K_D - 20: \quad R^2 = 0.39 \qquad 2.38$$

$$(q_{c1N})_{cs} = 0.00078E_D^3 - 0.095E_D^2 + 5E_D + 7; \quad R^2 = 0.54 \qquad 2.39$$

2.3.5.2 DMT/SPT Relations

The DMT/SPT relations found in the literature are those of Tsai et al. (2009) and Tanaka and Tanaka (1998). Tsai et al. (2009) proposed correlations between the normalized, clean-sand- equivalent factor $(N_1)_{60cs}$ and K_D, while Tanaka and Tanaka (1998) present a correlation between the raw, uncorrected factor N and K_D. Tsai et al.'s (2009) correlations are presented in Equations 2.40 and 2.41 and Tanaka and Tanaka's (1998) correlation is shown in Equation 2.42 below.

$$(N_1)_{60cs} = 0.185K_D^3 - 2.75K_D^2 + 17K_D - 15; \quad R^2 = 0.40 \tag{2.40}$$

$$(N_1)_{60cs} = 0.00022E_D^3 - 0.02E_D^2 + 0.9E_D + 3; \quad R^2 = 0.53 \tag{2.41}$$

$$N = \frac{E_D\ (MPa)}{2} \tag{2.42}$$

2.4 Evaluation of Liquefaction Potential using Simplified Procedures

Currently, the SPT and CPT tests are the two most common field tests used for evaluating liquefaction potential. This is because the data bases of results from these two tests far exceed that of the DMT or any other field test (Youd et al. 2001).

2.4.1 Background

The evaluation of liquefaction potential is performed through the estimation of two key variables: cyclic stress ratio (CSR) and cyclic resistance ratio (CRR). CSR is a factor that estimates the seismic loading that is induced on a soil during an earthquake. CRR estimates the strength that a soil has to resist this loading. When CRR is equal to or less than CSR the soil begins to liquefy.

Seed and Idriss (1971) presented the following equation to calculate CSR:

$$\mathrm{CSR} = \left({}^{\tau_{av}}/_{\sigma'_{vo}}\right) = 0.65\left({}^{a_{max}}/_{g}\right)\left({}^{\sigma_{vo}}/_{\sigma'_{vo}}\right) r_d \qquad 2.43$$

where a_{max} = peak horizontal acceleration at the ground surface generated by the earthquake ; g = acceleration of gravity; σ_{vo} and σ'_{vo} are total and effective stresses, respectively; and r_d= stress reduction coefficient. r_d is estimated by Liao and Whitman (1986b) as:

$$r_d = 1.0 - 0.00765z \qquad \text{for } z \leq 9.15\text{m} \qquad 2.44$$

$$r_d = 1.174 - 0.0267z \qquad \text{for } 9.15\text{m} < z \leq 23\text{m} \qquad 2.45$$

Since estimating seismic loading is beyond the scope of this thesis, the presented analysis is based on the assumption that CSR = CRR for all soils within the source sand zones (i.e. all soils within the source sand zones have liquefied).

Estimating CRR is most accurately done through field testing (Youd et al. 2001). Currently, the most widely accepted tests are the SPT, CPT, and shear-wave velocity measurements (V_s). Yet in recent years much interest has been focused on the DMT as it is believed to be a superior tool for evaluating liquefaction (Monaco et al. 2005, Monaco and Marchetti, 2007, Tsai 2009). However, the recent methods that have been proposed to routinely use the DMT for liquefaction analysis are not yet accepted due to the lack of an extensive data base of CRR-DMT data to support these new methods.

2.4.2 Current simplified procedures

Idriss and Boulanger (2006) present the latest SPT-based procedure which builds upon the initial work of Seed et al. (1985) and the revisions made by Youd et al. (2001). The relation between CRR and $(N_1)_{60cs}$ of Holocene soils is expressed through the following equation:

$$\mathrm{CRR}_{7.5} = \exp\left[\frac{(\mathrm{N}_1)_{60\mathrm{cs}}}{14.1} + \left(\frac{(\mathrm{N}_1)_{60\mathrm{cs}}}{126}\right)^2 - \left(\frac{(\mathrm{N}_1)_{60\mathrm{cs}}}{23.6}\right)^3 + \left(\frac{(\mathrm{N}_1)_{60\mathrm{cs}}}{25.4}\right)^4 - 2.8\right] \quad 2.46$$

Robertson and Wride (1988) propose the most recent CPT-based relation between CRR and $(q_{c1N})_{cs}$ of Holocene soils with the following equations:

$$\text{If } (\mathrm{q}_{\mathrm{c1N}})_{\mathrm{cs}} < 50 \quad \mathrm{CRR}_{7.5} = 0.833\left[\frac{(\mathrm{q}_{\mathrm{c1N}})_{\mathrm{cs}}}{1{,}000}\right] + 0.05 \quad 2.47$$

$$\text{If } 50 \le (\mathrm{q}_{\mathrm{c1N}})_{\mathrm{cs}} \le 160 \quad \mathrm{CRR}_{7.5} = 93\left[\frac{(\mathrm{q}_{\mathrm{c1N}})_{\mathrm{cs}}}{1{,}000}\right]^3 + 0.08 \quad 2.48$$

A number of DMT-CRR relations (Monaco et al. (2005), and several by Grasso and Maugeri (2006)) have been formerly recommended but all such relations were derived through indirect means, using relative density (D_r) to draw correlations with SPT and CPT data. Tsai et al. (2009) proposed a DMT-CRR relation that is based on direct relationships between DMT-SPT/CPT data to improve upon the previously proposed indirect DMT-D_r-SPT/CPT relations.

The existing relations include:

Monaco et al. (2005):

$$\mathrm{CRR}_{7.5} = 0.0107\mathrm{K}_\mathrm{D}^3 - 0.0741\mathrm{K}_\mathrm{D}^2 + 0.2169\mathrm{K}_\mathrm{D} - 0.1306 \quad 2.49$$

Grasso and Maugeri (2006)-B:

$$\mathrm{CRR}_{7.5} = 0.0308\mathrm{e}^{0.6054\mathrm{K_D}} \quad 2.50$$

Grasso and Maugeri (2006)-C:

$$\mathrm{CRR}_{7.5} = 0.0111\mathrm{K_D}^{2.5307} \quad 2.51$$

and Tsai et al. (2009):

$$\mathrm{CRR}_{7.5} = \exp\left[\left(\frac{\mathrm{K_D}}{8.8}\right)^3 - \left(\frac{\mathrm{K_D}}{6.5}\right)^2 + \left(\frac{\mathrm{K_D}}{2.5}\right) - 3.1\right] \quad 2.52$$

$$\mathrm{CRR}_{7.5} = \exp\left[\left(\frac{\mathrm{E_D}}{49}\right)^3 - \left(\frac{\mathrm{K_D}}{36.5}\right)^2 + \left(\frac{\mathrm{K_D}}{23}\right) - 2.7\right] \quad 2.53$$

Monaco et al. (2005)'s relation is derived through the study of correlations between q_c-D_r, N-D_r, and K_D-D_r of Holocene soils in Japan and is verified with CSR-K_D data obtained in hydraulic sandfills of southern California after the Loma Prieta 1989 earthquake (M=7.1) reported by Mitchell et al. (1994). The Monaco et al. (2005) CRR-K_D relation suggests that Holocene soils with K_D>5 are too dense to liquefy. Equations 2.50 and 2.51 are two of three CRR-K_D relationships proposed by Grasso and Maugeri (2006) as an update to the Monaco et al. (2005) relationships. Equation 2.50 utilized the D_r-q_c relationship presented in Jamiolkowsi et al. (1985) in its derivation, while Equation 2.51 utilized the D_r-N relationship presented in Gibbs and Holtz (1957). Tsai et al. (2009) formed their direct DMT-SPT/CPT model by deriving correlations between data from DMT, SPT and CPT tests performed side by side (i.e. $(N_1)_{60cs}$ of X is equal to a K_D of Y) in Holocene soils in Taiwan. Tsai et al. (2009) used these correlations (Equation 2.38 and 2.39 for CPT and Equations 2.40 and 2.41 for SPT) to transform the Idriss and Boulanger (2001) CRR-SPT relation and the Robertson and Wride (1998) CRR-CPT

relation into CRR-DMT relations. The correlations between DMT-SPT and DMT-CPT test data derived by Tsai et al. (2009) is presented in Section 2.3.5 (Equations 2.38 through 2.41).

2.4.2.1 The Effects of Aging

Leon et al. (2006) identified the importance of considering the effects of aging when estimating cyclic strength (CRR). It has been reported (Mitchell and Solymar, 1984; Dowding and Hryciw, 1986; Skempton, 1986; Schmertmann, 1987; Mesri et al., 1990) that soil strength and stiffness tend to increase over time through a process called aging. This phenomenon is caused through chemical mechanisms where cementing bonds are formed through the precipitation of silica from solution, taking place with the rise and fall of the ground water table, (Mitchell and Solymar, 1984; Mitchell, 1986; Joshi et al., 1995) and by physical mechanisms where gradual rearrangement of soil particles to a more stable system cause an increased frictional resistance (Schmertmann, 1987; Mesri et al., 1990; Arango and Migues, 1996). As soil strength and stiffness increase due to aging so does the cyclic strength. Prior to Leon et al. (2006) all other methods for estimating CRR were applicable only to relatively young Holocene (<10,000 years) soil deposits. These methods do not consider the increase in CRR over time. Leon et al. (2006) suggest that neglecting the effects of aging result in an underestimation of CRR by as much as 60% and recommend a 4-step procedure shown in Figure 2.12 that corrects field data to account for aging; providing a better estimation of the cyclic strength that accounts for the current aged state of the soil.

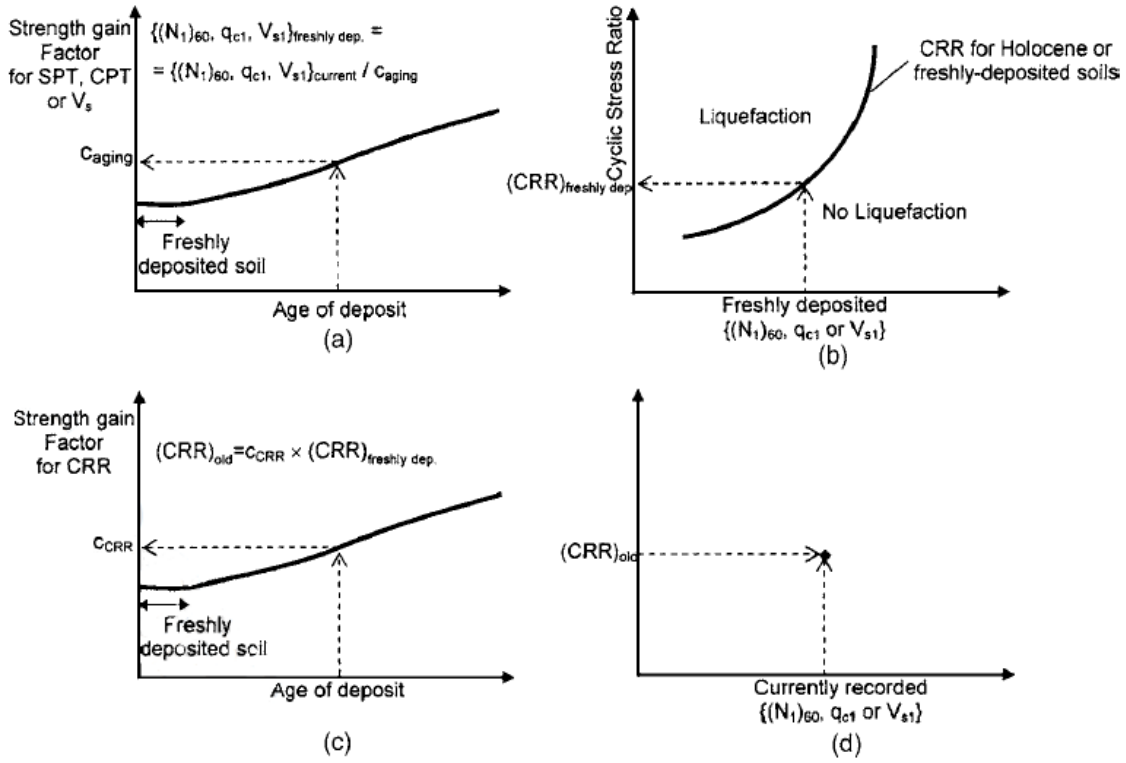

Figure 2.12 Methodology to Account for Aging: (a) Step 1-Correction of in-situ currently recorded data for aging; (b) Step 2-Determination of CRR for freshly deposited soil; (c) Step 3- Determination of CRR for old/aged soil deposit; (d) Step 4-Association of in-situ currently recorded data with CRR for old/aged soil deposit. (After Leon et al., 2006)

The first step of the Leon et al. (2006) methodology is to correct the recorded in situ values of $(N_1)_{60cs}$ and $(q_{c1N})_{cs}$ by reducing the parameters to values indicative of the soil strength at a referenced time before aging occurs and increases the soil strength to its present day strength indicated by the recorded in situ values. The referenced time, *t*, can correspond to two different events. For sites where paleoliquefaction is evident, *t* is taken as the time in years since the liquefaction inducing earthquake. For sites where liquefaction has not previously occurred, *t* is taken as the age of the soil deposit. In this work the "post-earthquake" and "freshly deposited" terms are used interchangeably to describe the soil at time *t*. The correction to account for the strength gain in blow count

and tip resistance is implemented using Kulhawy and Mayne's (1990) correction factor c_A, which is defined as:

$$c_A = 1.2 + 0.05 * \log\left(\frac{t}{100}\right) \quad 2.54$$

The in situ properties at the referenced age are calculated using the following equation (Kulhawy and Mayne, 1990):

$$\frac{(N_1)_{60cs}}{[(N_1)_{60cs}]_R} = \frac{(q_{c1N})_{cs}}{[(q_{c1N})_{cs}]_R} = c_A \quad 2.55$$

where $[(N_1)_{60cs}]_R$ and $[(q_{c1N})_{cs}]_R$ are SPT and CPT values at the referenced time (after liquefaction or deposition).

Step two of Leon et al.'s (2006) approach uses the corrected blow count or tip resistance to estimate the liquefaction resistance of the soil at the referenced time using either the Idriss and Boulanger (2006) SPT-CRR relation or the Robertson and Wride (1998) CPT-CRR relation. The third step is to evaluate the current liquefaction resistance of the soil. In the years that follow liquefaction events, as the effects of aging increase soil strength and stiffness, CRR is also increased. The Arango et al. (2000) strength gain factor, c_{CRR}, is utilized to correct the freshly deposited CRR to the current CRR. Figure 2.13 is used to obtain c_{CRR} while the current CRR is found using Equation 2.56. The fourth and final step of Leon's methodology is to evaluate the liquefaction potential of a soil in its current state by plotting the currently recorded in situ strength parameters with $(CRR)_{aged/current}$.

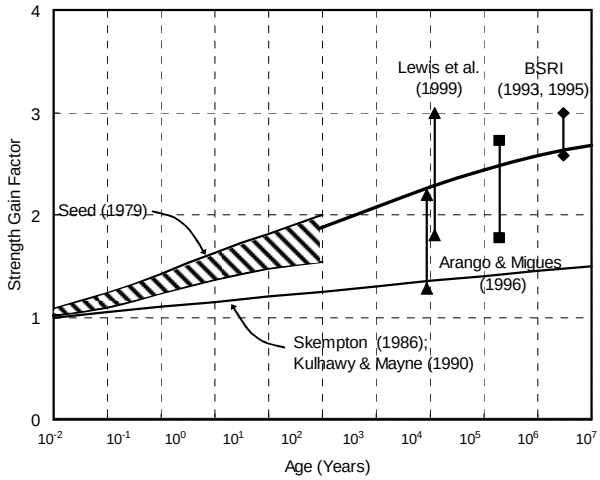

Figure 2.13 Field Cyclic Strength of Aged Sand Deposits: Updated Relationship (after Arango et al., 2000)

$$c_{CRR} = \frac{(CRR)_{aged/current}}{(CRR)_{freshly\ deposited}} \qquad 2.56$$

2.5 Summary

This chapter presents a description of the five geotechnical investigation sites studied in this thesis, test procedures of the DMT, SPT, and CPT tests, cross-relations between DMT and CPT and DMT and SPT found in the literature, and the current simplified methods for estimating liquefaction potential, including the Youd et al. (2001) method of estimating CRR from SPT test data, the Robertson and Wride (1999) method of estimating CRR from CPT test data, and the Leon et al. (2006) method of estimating CRR of aged soils. Marchetti (2011) and Leon et al. (2006) point out differences in the current methods used to estimate the liquefaction potential of soils and recommend procedures that could improve these methods. This thesis follows their recommendations to develop new CRR-DMT relationships that can be used as first approximations for evaluating the liquefaction potential of soils in the South Carolina Coastal Plain.

CHAPTER THREE
METHODOLOGY

3.1 Introduction

This chapter presents the procedures of both field and laboratory testing performed for soils from the five geotechnical investigation sites. The laboratory index tests include visual-manual identification, grain size distribution (with hydrometer and sieve analysis), Atterberg Limits, and specific gravity. The methodologies used in the data analysis and in the identification of the source sand layer at each site are also presented.

3.2 Field Investigation

3.2.1 Dilatometer Test

The flat plate dilatometer test (DMT) was performed using equipment owned and operated by S&ME, Mount Pleasant, SC, in accordance with ASTM D 6635-01 between July 2007 and July 2008. A summary of the DMT tests performed is summarized in Table 3.1. For each test S&ME provided the raw data which consisted of the A, B and C-readings, as well as the DMT derived geotechnical parameters as defined by Marchetti et al. 2001. (See Table 2.1 for a review.) The equations of the main parameters p_o, and p_1, and the intermediate parameters I_D, K_D, and E_D were summarized in Section 2.3.1.2 (see Equations 2.1 to 2.5). It should be noted that in several instances, when DMT testing was attempted in soil that was “too stiff”, the pressure required to inflate the membrane the

full 1.1 mm exceeded the maximum pressure of the equipment and the B-reading was unobtainable. At these points the DMT test was invalid. This condition was encountered with the soils from 3-6 ft (0.9-1.8 m) below the ground surface at HWD and also at 4 and 18-22 ft (1.2 and 5.5-6.7 m) below the ground surface at FHS.

Table 3.1 Summary of DMT tests performed

Test Name	Depth of Test (ft)	Testing Increments (ft)
SAM-DMT	35	2
GAP-DMT	18	1
FD-DMT-NS	12	2
FD-DMT-EW	12	2
HWD-DMT	20	1
FHS-DMT	16	2

3.2.2 Standard Penetration Test

Standard penetration tests were performed with equipment owned and operated by S&ME in accordance with ASTM D 1586. The tests at SAM, HWD, and FHS were performed in April 2010 while the GAP tests were performed in August 1997 as part of a study reported by Hu et al, 2002. The tests at SAM, HWD, and FHS also incorporated hammer energy ratio (ER) measurements. For this research it was elected to sample continuously and drive the 24-in. split spoon samplers through 4 6-in intervals rather than the typical three increments. The blow counts from the upper 6-in. intervals were discarded while the blow counts from the second and third intervals were added together to obtain the N-value. A summary of the SPT tests performed is presented in Table 3.2.

For each test S&ME provided the raw blow counts, the ER measurements for each blow, and placed the split spoon samples in glass jars which were taken to USC's laboratory for index property testing. The raw N-values were transformed into $(N_1)_{60cs}$-values after being corrected for ER measurements, overburden pressures, and fines content per Equations 2.9 through 2.18.

Table 3.2 Summary of SPT data collected

Test Name	Depth of Test (ft)	Number of Samples Obtained
SAM-SPTE-1	36	25
GAP-03	21	17
HWD-SPTE-1	26	14
FHS-SPTE-1	26	21

3.2.3 Cone Penetration Test

Cone penetration tests (CPT) were performed between July and December 2007 at all sites other than Gapway with equipment owned and operated by S&ME. The testing at Gapway was performed by Applied Research Associates, Inc. in 1996. All tests were performed in accordance with ASTM D5778. The testing agencies provided the raw data collected during testing which consisted of q_c, f_s, and u_2 values. This raw data was transformed into $(q_{c1N})_{cs}$-values using Equations 2.22 through 2.29. Table 3.3 shows a summary of the CPT tests performed at each site.

Table 3.3 Summary of CPT tests performed

Test Name	Depth of Test (ft)
SAM-SCPT-1	35
GAP-SCPT-1	24
FD-SCPT-1	14
FD-SCPT-2	35
HWD-SCPT-1	62
FHS-SCPT-1	25

3.2.4 Ground Water Measurements

Piezometers were installed at all sites except GAP. The results of the measured ground water table for each site are shown in Table 3.4.

Table 3.4 Summary of Piezometer Data

Piezometer Site	Date	Ground Water (ft)
SAM	04/29/2010	5.7
FD	01/14/2008	17.5
	03/07/2008	17.0
	07/01/2008	17.4
	08/07/2008	17.8
HWD	04/24/2010	5.5
FHS	01/14/2008	7.3
	04/19/2010	5.2

After reviewing the piezometer data it was noted that the measurements were taken long after the initial geotechnical testing. With the exception of the FHS measurement, which was taken 1 month after the CPT test was performed, the timing of all other piezometer measurements ranged from 6 months to 3 years after the CPT tests. Given the fluctuation of ground water depth with variables such as periods of heavy rain or drought the available piezometer measurements were considered an inaccurate depiction of the depth of the ground water table at the time of the initial geotechnical testing.

Without any valid piezometer data, the CPT pore pressure data was analyzed to determine the depth of the groundwater at the time of testing. The depth of the ground water table was assumed to be at the point where the CPT pore pressures began to build. Table 3.5 shows a summary of the ground water table depths per the CPT data analysis. These depths are used in the calculation of effective stress for all data analysis.

Table 3.5 Summary of Ground Water Table Data from CPT Analysis

CPT Test	Date	Ground Water (ft)
SAM-SCPT-1	07/19/2007	6.5
GAP-SCPT-1	07/19/2007	4.5
FD-SCPT-1	07/26/2007	17
FD-SCPT-2	07/26/2007	17
HWD-CPT-4	07/30/2008	9
FHS-SCPT-1	12/14/2007	9

3.3 Laboratory Investigation

At the Sampit, Gapway, Hollywood, and Four Hole Swamp sites multiple SPT tests were performed and all samples collected from the split spoons were taken back to USC's laboratory for index testing. At the Gapway site the samples from the STP boring GAP-03 were selected for laboratory testing. At the other three sites the samples from the borehole named SPTE-1 were selected to perform visual manual identification, grain size distribution, Atterberg limits, and specific gravity. The samples from SPTE-1 were chosen because, in all cases, this borehole was the closest to the DMT test. In the field the continuous soil samples inside of the split spoons were separated into smaller, more uniform samples based on color, consistency, and texture.

Vibracores were performed in lieu of SPT tests at the Fort Dorchester site by the South Carolina Geological Survey (Doar, 2007). The samples for laboratory testing were obtained from FD-VC-1.

3.3.1 Visual Manual Identification

Visual manual identification (VMID) tests were performed on all samples taken at all sites. VMID tests were performed according to ASTM D 2487-00. In addition to the requirements of the standard, the presence and quantity of shells, fossils, and mica were noted as well as the mineralogy of the soil and its tendency to slake.

3.3.2 Grain Size Distribution

Grain size distribution tests were performed for the samples taken from the SPT split spoon samples at each site in general accordance with ASTM D 422-63

(Reapproved 2007). Testing began by separating the soil sample into two sections: that retained on, and that passing the No. 10 (2.00-mm) sieve. In most cases little to no soil was retained on the No. 10 sieve, but when necessary the ¾-in. (19.0-mm), ⅜-in. (9.5-mm), No. 4 (4.75-mm) and No. 10 sieves were used to determine the size of the larger particles. (This case was mainly reserved for the Hollywood soils which had many large shells mixed in with the soil.) With this portion removed, a representative sample of the soil passing the No. 10 sieve was measured and prepared for hydrometer testing. Due to the small quantity of soil available, the required amount of 115 g was not always obtained; most tests were performed with at least 100 g, but in some cases only 90 g was available. When this soil was weighed a separate small sample of approximately 10 g was collected and used to find the hygroscopic moisture of the sample so that the weight of the dry soil could be determined.

The sample to be used for hydrometer testing was then mixed with 125 mL of a 40 g/L sodium hexametaphosphate solution for at least 16 hours and then further dispersed using a mixing cup and automated stirrer for 1 minute. After stirring, the soil was transferred to the sedimentation cylinder and deionized water was added until a total volume of 1,000 mL was reached. A rubber stopper was used to plug the cylinder and the cylinder was turned upside down and back upright 60 times in one minute to further agitate the soil. Once this action was complete, the cylinder was placed on the lab bench, the stopper was removed, and the stopwatch was started. The soil remaining on the walls of the cylinder was also washed back into the slurry using a squirt bottle. Readings were then taken at 2, 5, 15, 30, 60, 240, and 1440 minutes. All tests were performed in a constant temperature room so the use of a warm bath was not necessary per ASTM

D422-63; instead temperatures were taken after each hydrometer reading to account for slight changes during testing.

The hydrometer used conforms to the requirements for hydrometer 152H in Specification E 100. The hydrometer was calibrated to account for the zero correction, the meniscus correction, and temperature corrections so that accurate readings could be obtained during testing.

After the 24 hour reading was taken the sample was prepared for the mechanical sieve analysis by washing the soil slurry through a No. 200 (75-μm) sieve. Once the No. 200 sieve wash was completed the sieve was placed in a 110°F oven for 24 hours to air dry and then the soil was moved to a metal container and placed in a 230°F oven for another 24 hours to oven dry, at which point it is ready for mechanical sieving.

The stack of sieves used met the requirements of Specification E 11 and included a No. 20 (850-μm), No. 40 (425-μm), No. 60 (250-μm), No. 100 (150-μm), No. 140 (106-μm), and a No. 200 sieve. As testing progressed over the months some of the finer sieves (especially the No. 100 and No. 140 sieves) started to become occluded so the shaking time was increased from 8 minutes to 10 minutes. All tests performed after March 7, 2011 were shaken for 10 minutes.

It should be noted that during the preparation of this test all clumps of soil were broken down into the individual soil particles so that nothing was incorrectly labeled as greater than the No. 10 sieve, except for the case where many clay nodules were found throughout the soil. In these cases the nodules were unaltered so that the natural occurring dimensions of these nodules could be recorded. This was done so that the resulting grain size distribution would better simulate in situ conditions, knowing that the

clay nodules would not break down and mix with the rest of the soil during an earthquake and thus should not be forced to do so when determining the grain size distribution for the purpose of evaluating liquefaction potential. It is also noted that extreme care was taken each time the soil was transferred from one container to another so that nothing was lost in the process.

3.3.3 Atterberg Limits

Atterberg limits were performed in general accordance with ASTM D 4318-00 on soils that had greater than 5% fines. In all cases the wet, multipoint method was used and the soil was allowed to soak in distilled water for at least 16 hours before testing. Before the soil was soaked and prepared for Atterberg limits the portion greater than the No. 40 sieve was removed. (Unless the soil contained less than 1% greater than No. 40, in which case this step was omitted.)

The liquid limit test was performed first. The soil was prepared so that the first test would yield a blow count between 25 and 35. Two more tests were then performed at successively higher water contents aiming for blow counts ranging from 20-30 and 15-25. These three data points were used to determine the liquid limit of the soil. Upon the completion of the liquid limit tests, plastic limit tests were performed using the glass plate method. Three plastic limit tests were run on each soil and the water contents from these tests were averaged together to determine the plastic limit of the soil.

3.3.4 Specific Gravity

Specific gravity tests were also performed on all soil samples collected from the SPT split spoons at each site. The tests were performed by applying a vacuum to soil slurry in calibrated pycnometer flasks which were submerged in a warm water bath in accordance with ASTM D 854-00 Method A. The pycnometers were filled in three stages. In the first stage the pycnometer was filled with the soil slurry to about half the volume of the pycnometer. The pycnometer was then placed in the warm water bath and a vacuum was applied for about one hour. Deaired water was then added to bring the soil slurry just below the neck of the pycnometer and the vacuum was applied for another hour. At the end of the second stage, the pycnometer was removed from the warm water bath and placed in an empty cooler for about 16 hours so that the slurry could reach a constant temperature. When the pycnometer was removed from the cooler it was filled to the calibration line with deaired water using a syringe. The temperature and the mass of the pycnometer and soil slurry were then recorded. Afterwards the soil slurry was then transferred to a 1,000 mL beaker and placed in the 230°F oven overnight to determine the mass of dry soil used in the test.

3.4 Identification of Source Sand Layer

The source sand zone for each site was delineated by analyzing the field and laboratory test data. The boundaries of the source sand layer were determined through "upper bounds" of the DMT, SPT, and CPT tests. The upper bounds of the tests are the limits for which liquefaction can occur. Soils with K_D>5 (Monaco et al., 2005), $(N_1)_{60,cs}$>30 (Seed et al., 1985) or $(q_{c1N})_{cs}$>160 (Robertson and Wride, 1998) are

considered too dense to liquefy. The CPT soil behavior type index, I_c, was also used to determine the range of the source sand as soils with I_c>2.6 are considered too clay-rich to liquefy (Robertson and Wride (1998)). The DMT, SPT, and CPT data profiles were analyzed together and soil that exceeded any of the thresholds was excluded from the source sand zone. Analyzing the test data in this way suggests that Monaco et al.'s (2005) upper limit of K_D>5 may not be applicable to SCCCP soils. While each site encountered distinct layers that meet the SPT and CPT liquefaction criteria, only a very few data points meet the $K_D \leq 5$ criteria. Monaco's method was ultimately not used to define the source sand layer because it would predict that nearly all of the source sand would not be considered liquefiable based on the $K_D \leq 5$ limit. The theory that Monaco's method is not applicable to SCCP soils is further verified in chapter four.

The visual-manual ID results and the laboratory fines content data were used to confirm the range of the source sand zone by identifying distinct changes in material type. Finally, the ground water table was reviewed to ensure that the depicted source sand zone is saturated. Note that restricting the classification of a source sand layer to the depth of the water table to ensure saturation is not practical in routine engineering practice. Given the nature of seasonal variability in the ground water depth, it would be incorrect to say that loose clean sand immediately above the water table is unliquefiable based solely on its unsaturated state. However, this was a necessary assumption given the definition of liquefaction used for the simplified procedure.

3.5 Summary

This chapter presents the field and laboratory tests performed at five sites within the SCCP and addresses the methodologies used to analyze the test data and identify the source sand layer. Geotechnical field exploration tests consisted of DMT, SPT, CPT, and vibracore tests. Laboratory tests including visual-manual identification, grain size distribution, Atterberg Limits, and specific gravity were performed on samples taken from SPT and vibracore samples. Piezometers that were installed at the sites were used to find the depth of the groundwater.

CHAPTER FOUR
RESULTS

4.1 Introduction

This chapter presents the results of the field exploration testing along with the associated data reduction and laboratory testing data analysis. The data from the various tests was used to create a soil stratigraphy for each site. The most critical stratus that was delineated for each site was the source sand. This was done by identifying layers that met all of the conditions necessary for liquefaction: saturated soils, loose consistency, and low fines content, as presented in Section 3.4. Once the source sand layers were identified at each site, the data from within these zones was evaluated and the DMT results were paired with the corresponding SPT and CPT results to develop direct relationships between DMT and SPT data and DMT and CPT data for soils in the South Carolina Coastal Plain. These relationships were then used to transform the existing CRR-SPT curves and CRR-CPT curves (developed by Idriss and Boulanger (2006) and Robertson and Wride (1998), respectively, for Holocene soils, and by Leon et al. (2006) for aged soils) into new CRR-DMT curves using the simplified procedure. The results of the simplified procedure and the proposed CRR-DMT curves are presented and serve as new tools, which can be used as first approximations, for evaluating the liquefaction potential of soils in the South Carolina Coastal Plain.

4.2 Field and Laboratory Testing Results

For all sites, both the raw and the normalized, corrected data from the DMT, SPT, and CPT tests performed are presented along with a description of the major steps in the data reduction. The laboratory index testing data, which consists of fines content, C_u, C_c, Atterberg limits, specific gravity, USCS classification, and grain size distribution curves, from each site is also presented. The source sand zone for each site was delineated by analyzing the field and laboratory test data as presented in Section 3.4.

4.2.1 Sampit Results

Figure 4.1 shows the results of SAM-DMT presented by S&ME. The raw parameters p_0 and p_1 were used to calculate I_D and E_D using Equations 2.3 and 2.5, respectively. The parameters M, s_u, ϕ', and OCR were calculated using the equations from Table 2.1 and Equations 2.6 through 2.8. Note that Figure 4.1 uses the variable s_u in place of the previously used variable c_u to represent undrained shear strength. Also note that s_u and OCR are only applicable when $I_D<1.2$ (clayey soils), while ϕ' is only applicable when $I_D \geq 1.2$ (sandy soils).

Figure 4.2 presents the results and data reduction of SAM-SPTE-1. N_{60}, $(N_1)_{60}$, and $(N_1)_{60,cs}$ were calculated using the methods described in Section 2.3.2.1. Note that $(N_1)_{60,cs}$ is not plotted from 23-27 ft (7.0-8.2 m) because $(N_1)_{60cs}$ is not valid for either fine-grained soils or soils with N=0. The fines content shown in the last plot of the figure comes from the laboratory test data (as described in Section 3.3.2) and is used to calculate $(N_1)_{60,cs.}$

Figure 4.3 shows the results and data reduction of SAM-SCPT-1. q_{c1N}, and $(q_{c1N})_{cs}$ were calculated using the methods discussed in Section 2.3.3.1. The fines content presented comes from the laboratory test data (as described in Section 3.3.2) and is used to calculate $(q_{c1N})_{cs}$.

The field data is summarized in Figure 4.4, showing the I_D, K_D, E_D, fines content, N, $(N_1)_{60,cs}$, I_c, q_c, and $q_{c1N,cs}$ profiles. This figure was used to delineate the source sand layer by evaluating the data with regards to the upper limits of liquefaction for each test. Using the upper bounds of the field tests, the locations of the water table, visual manual ID, and index tests the source sand layer was identified to range from 9-22 ft (2.7-6.7 m). The upper boundary is refined by first noticing that the CPT data at 7 ft (2.1 m) exceeds the liquefaction limit and secondly by noting the significant decrease in K_D and E_D from 8-9 ft (2.4-2.7 m). While the Monaco et al. (2005) upper limit of K_D>5 was deemed inapplicable to SCCP soils (see Section 3.4) and was not used to define the source sand, further analysis of K_D through the DMT-SPT/CPT correlation derivation shows that the points above 9 ft (2.7 m) are outliers when compared to the other data points from the source sand. (See Figure 4.28 for an illustration). The lower boundary of the source sand was identified by the change in soil strata. At 22 ft (6.7 m) the soil changes from poorly graded sand with clay (SP-SC) to sandy clay (CL). This change in strata is also clearly shown in the fines content and I_c data profiles.

Table 4.1 shows a summary of the laboratory index testing results for the source sand layer. For each sample within the source sand percent fines, C_u, C_c, LL, PL, PI, G_s, and the USCS classification are presented. Note that Atterberg limit tests were not performed on many of the samples due to insufficient sample sizes remaining after the

grain size distribution tests. The percent silt, clay and colloid from the grain size distribution tests shown in Figures 4.5 and 4.6 were analyzed in lieu of Atterberg limit test data for classification purposes.

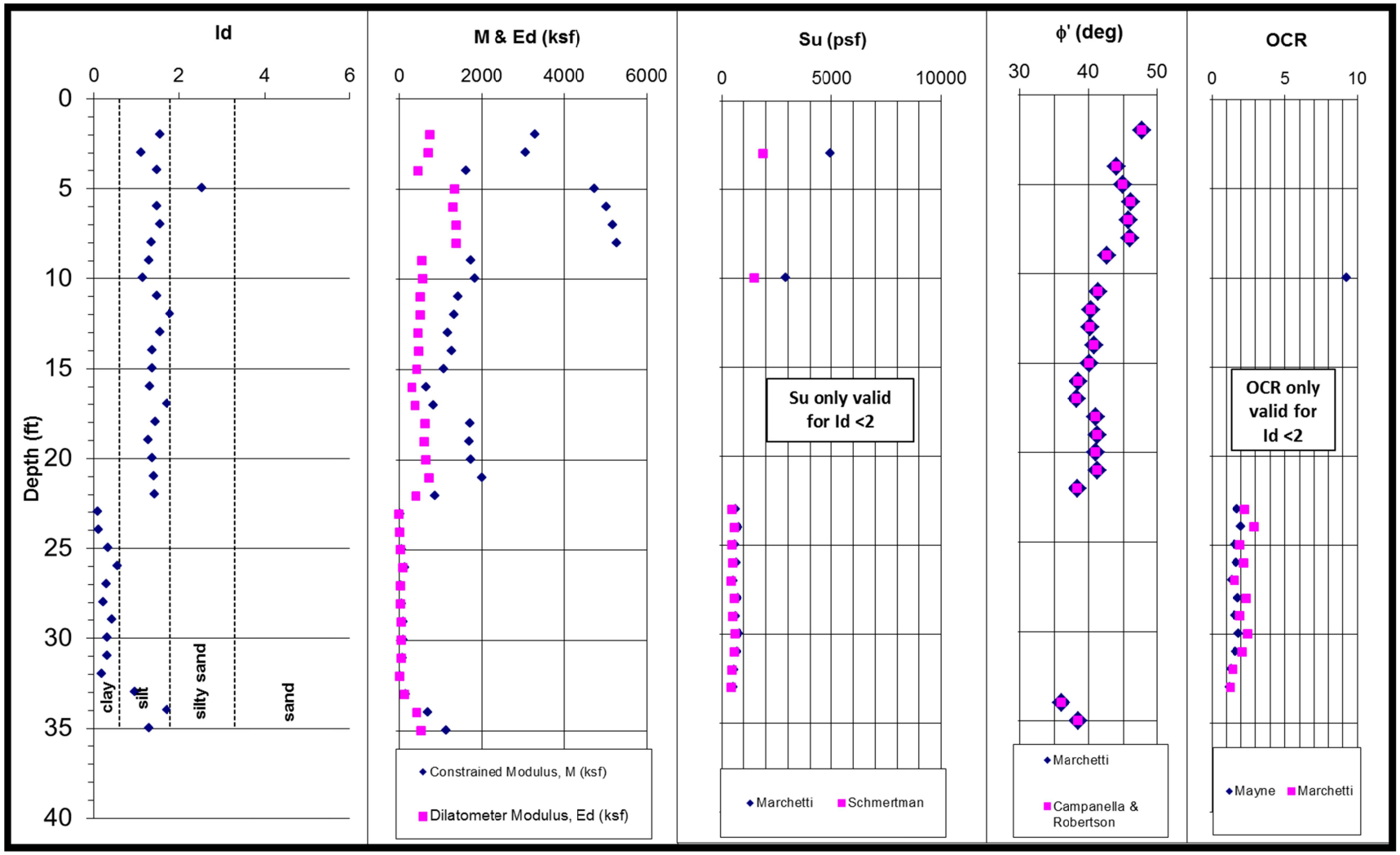

Figure 4.1 SAM-DMT Results (Provided by S&ME,Inc,)

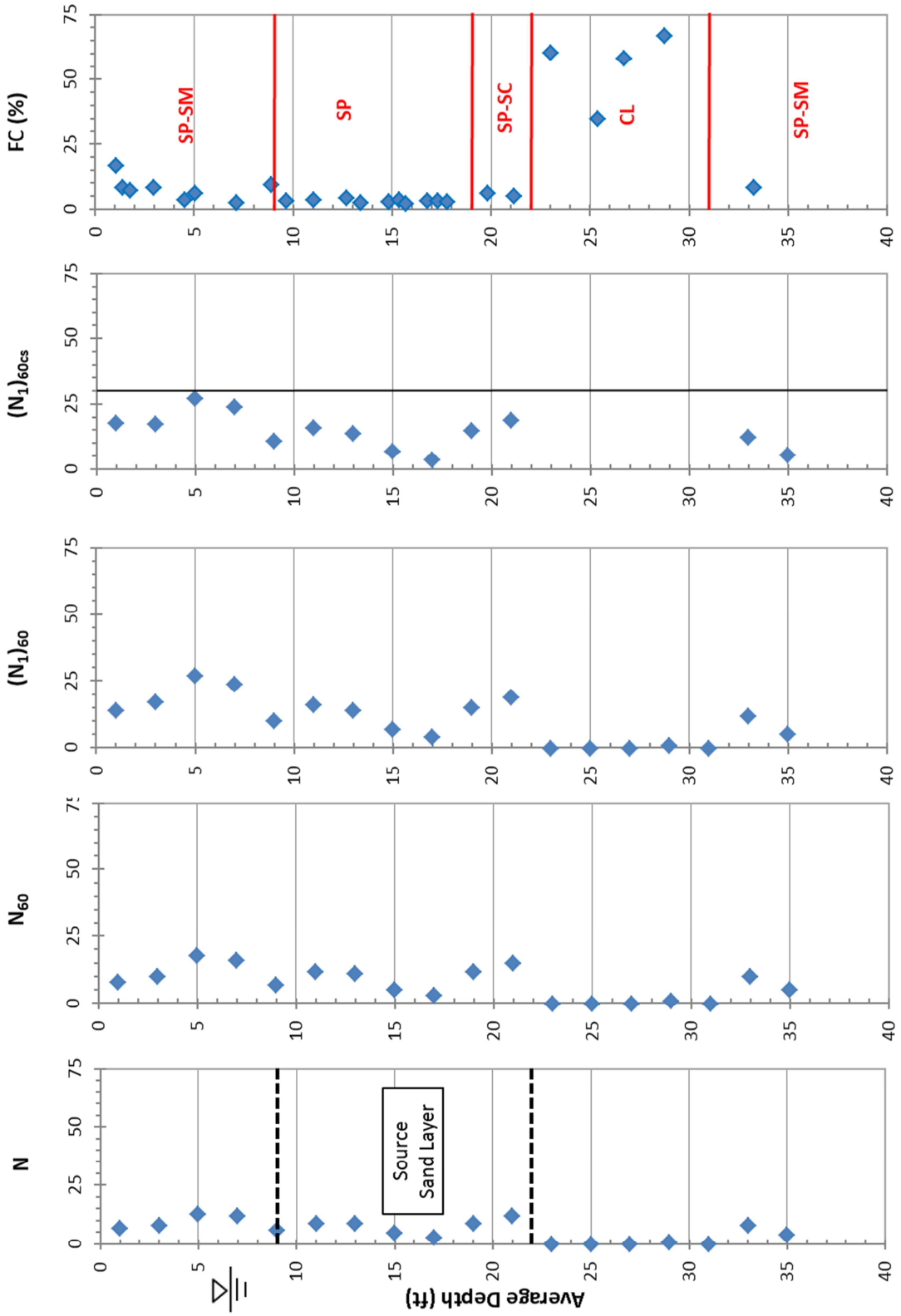

Figure 4.2 SAM-SPTE-1 Results

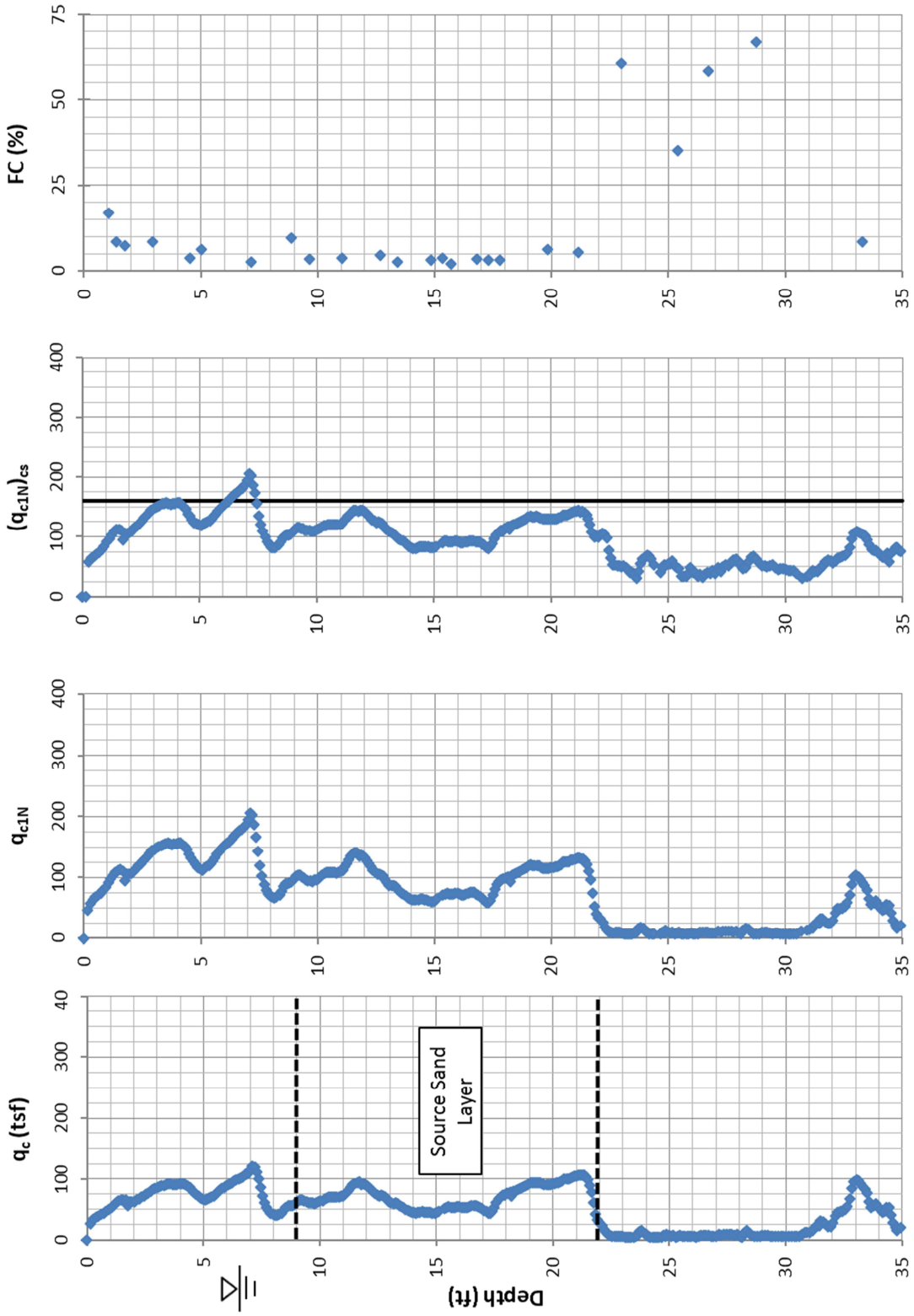

Figure 4.3 SAM-SCPT-1 Results

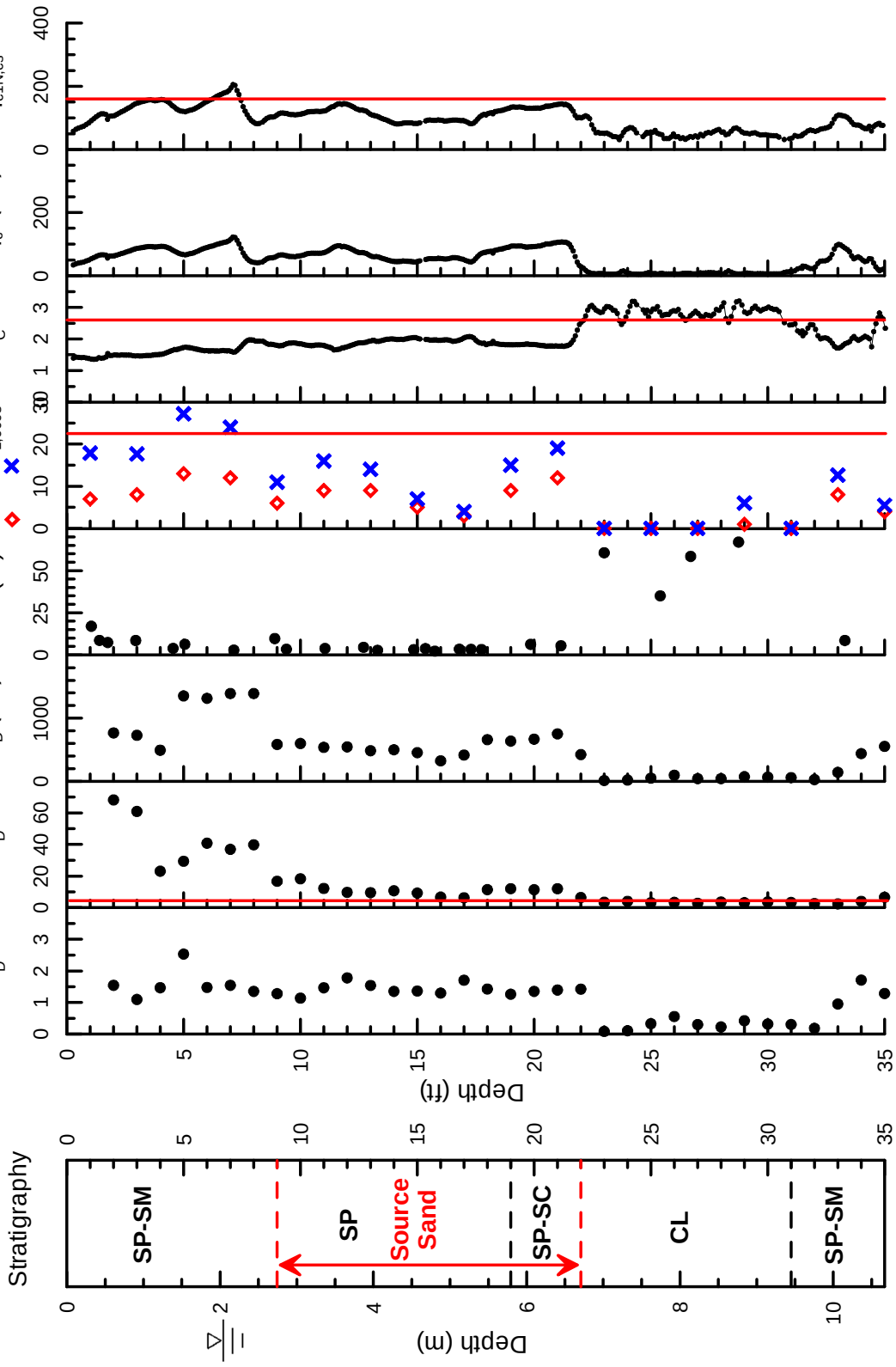

Figure 4.4 Summary of Sampit Field Testing Results

Table 4.1 Summary of the Sampit Index Testing Results for the Source Sand Layer

Sample Name	Sample Depth (ft)	Sample Depth (m)	% Fines	C_u	C_c	LL	PL	PI	G_s	USCS
F66	9.3 – 9.5	2.8 – 2.9	3.4	1.4	1.0	-	-	-	2.650	SP
F46	10.6 – 11.5	3.2 – 3.5	3.8	1.2	1.0	NP	22	NP	2.640	SP
F64	12.6 – 12.8	3.8 – 3.9	4.5	1.4	1.0	-	-	-	-	SP
F47	13.1 – 13.5	4.0 – 4.1	2.7	1.3	1.0	NP	22	NP	2.640	SP
F48	14.4 – 15.3	4.4 – 4.7	3.1	1.2	1.1	24	25	0	2.649	SP
F67	15.3 – 15.4	4.7	3.8	4.2	0.3	-	-	-	-	SP
F20	15.5 – 16.0	4,7 – 4.9	2.2	1.4	1.0	-	-	-	2.651	SP
F49	16.6 – 17.0	5.1 – 5.2	3.4	1.3	1.0	-	-	-	2.652	SP
F50	17.0 – 17.5	5.2 – 5.3	3.3	3.0	0.4	16	16	0	2.642	SP
F18	17.5 – 18.0	5.3 – 5.5	3.2	1.4	1.0	-	-	-	2.645	SP
F51	18.7 – 19.7	5.7 – 6.0	-	-	-	22	21	1	2.652	SP
F69	19.7 – 20.0	6.0 – 6.1	6.25	1.4	1.2	-	-	-	2.653	SP-SC
F52	20.8 – 21.5	6.3 – 6.6	5.42	1.6	1.0	-	-	-	2.662	SP-SC

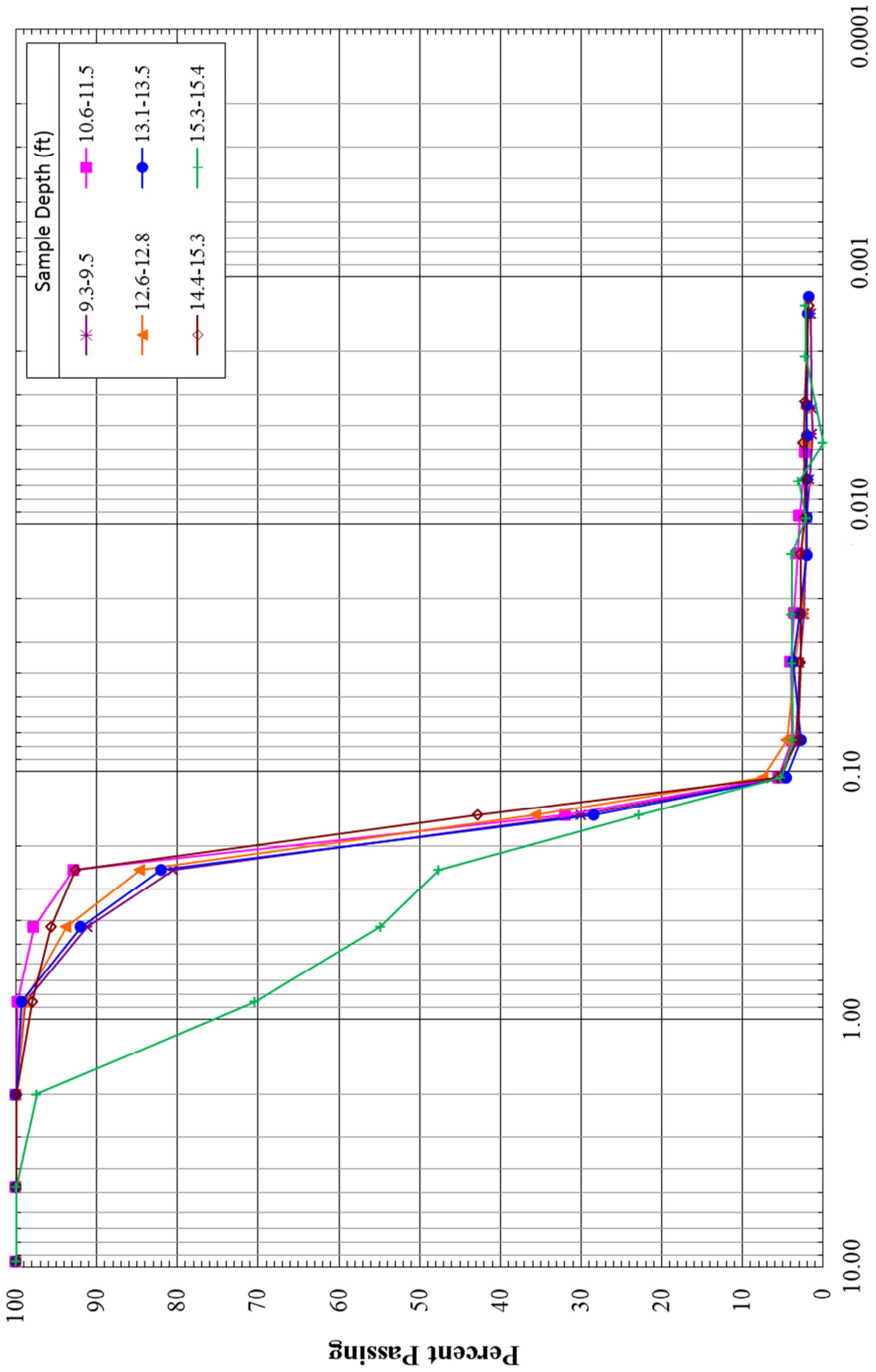

Figure 4.5 Grain Size Distribution Curves for Sampit Source Sand (1 of 2) (Modified from Hasek, 2013)

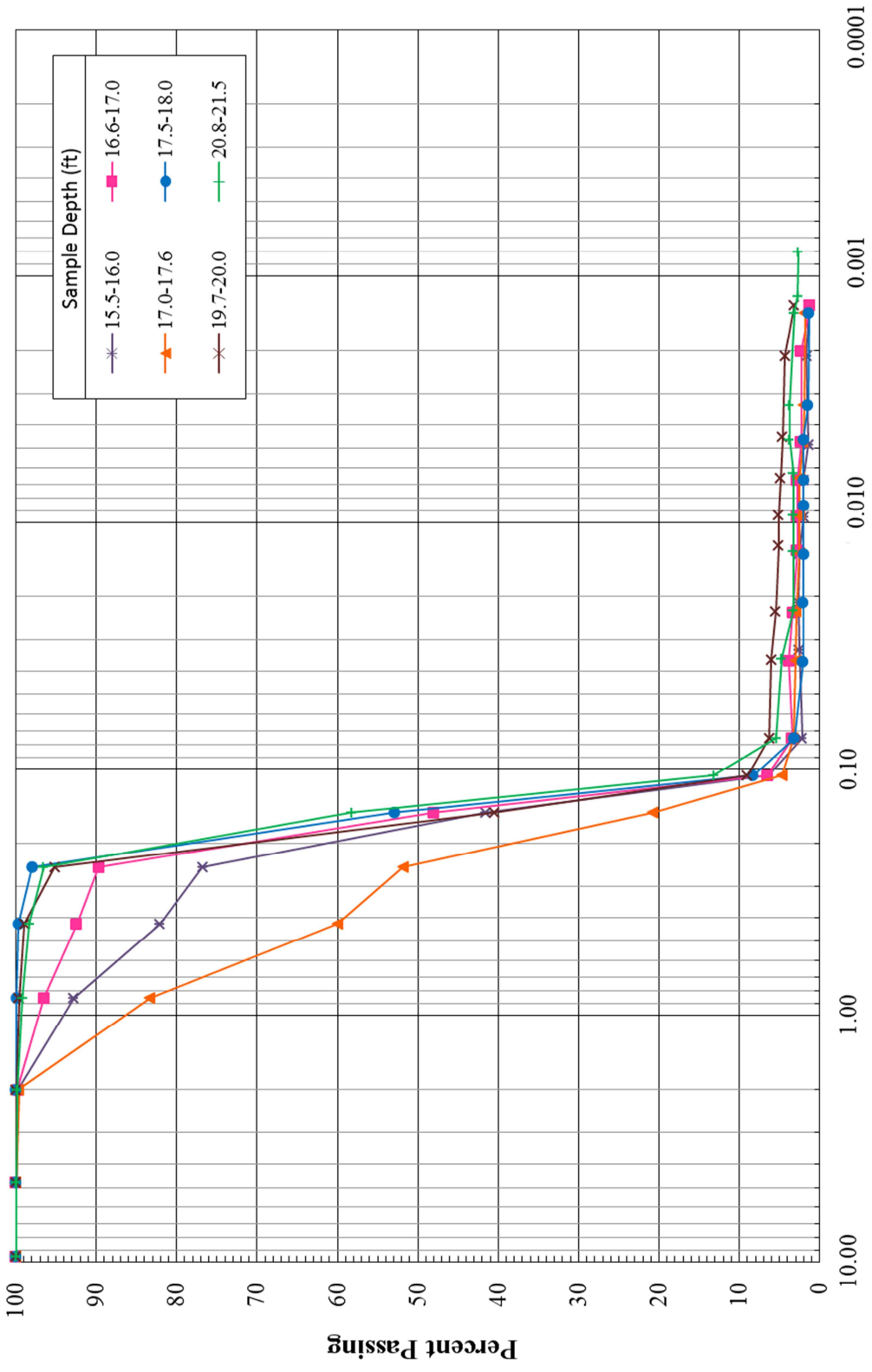

Figure 4.6 Grain Size Distribution Curves for Sampit Source Sand (2 of 2) (Modified from Hasek, 2013)

4.2.2 Gapway Results

The results of the DMT, SPT, and CPT tests performed at Gapway are shown in Figures 4.7, 4.8 and 4.9, respectively. A summary of these results is shown in Figure 4.10.

Figure 4.8 presents $(N_1)_{60}$, $(N_1)_{60,cs}$, and the fines content data from GAP-03 per Hu et al. (2002). The raw N-values are not presented as Hu et al. (2002) only provided $(N_1)_{60}$ data. The $(N_1)_{60}$ values were reduced to clean sand equivalent values using the methods outlined in Section 2.3.2.1 so that the SPT data could be used for the liquefaction analysis. Note that $(N_1)_{60cs}$ is not available from 10-15 ft (3-4.6 m) due to the lack of fines content data in this range.

As shown in Figure 4.9, the source sand ranges from 4-7 ft (1.2-2.1 m). This comes from the interpretation of the CPT and DMT data. Both of these tests clearly show the clay cap layer from 3-4 ft (0.9-1.2 m), whereas the clay cap layer was not identified in the SPT data. The lower bound of 7 ft (2.1 m) for the source sand was also depicted from the CPT data where I_C exceeds the liquefaction maximum of 2.6 per Robertson and Wride (1998).

Table 4.2 presents a summary of Hu's (2002) laboratory data for the source sand layer, which includes percent fines, C_u, C_c, and USCS classifications. C_u and C_c were found using the gran size distribution curves in Figure 4.11. The grain size distribution curve for the 5.3-6.0 ft (1.6-1.8 m) sample is not plotted in Figure 4.11 because the sieve data was not available. The USCS classifications shown in Table 4.2 are incomplete due to a lack of Atterberg limit data (tests not performed by Hu et al. (2002)). The source

sand layer is classified SP-SM/SC, although it is noted that SP-SC is deemed more probable than SP-SM because of the clay layers above and below the source sand.

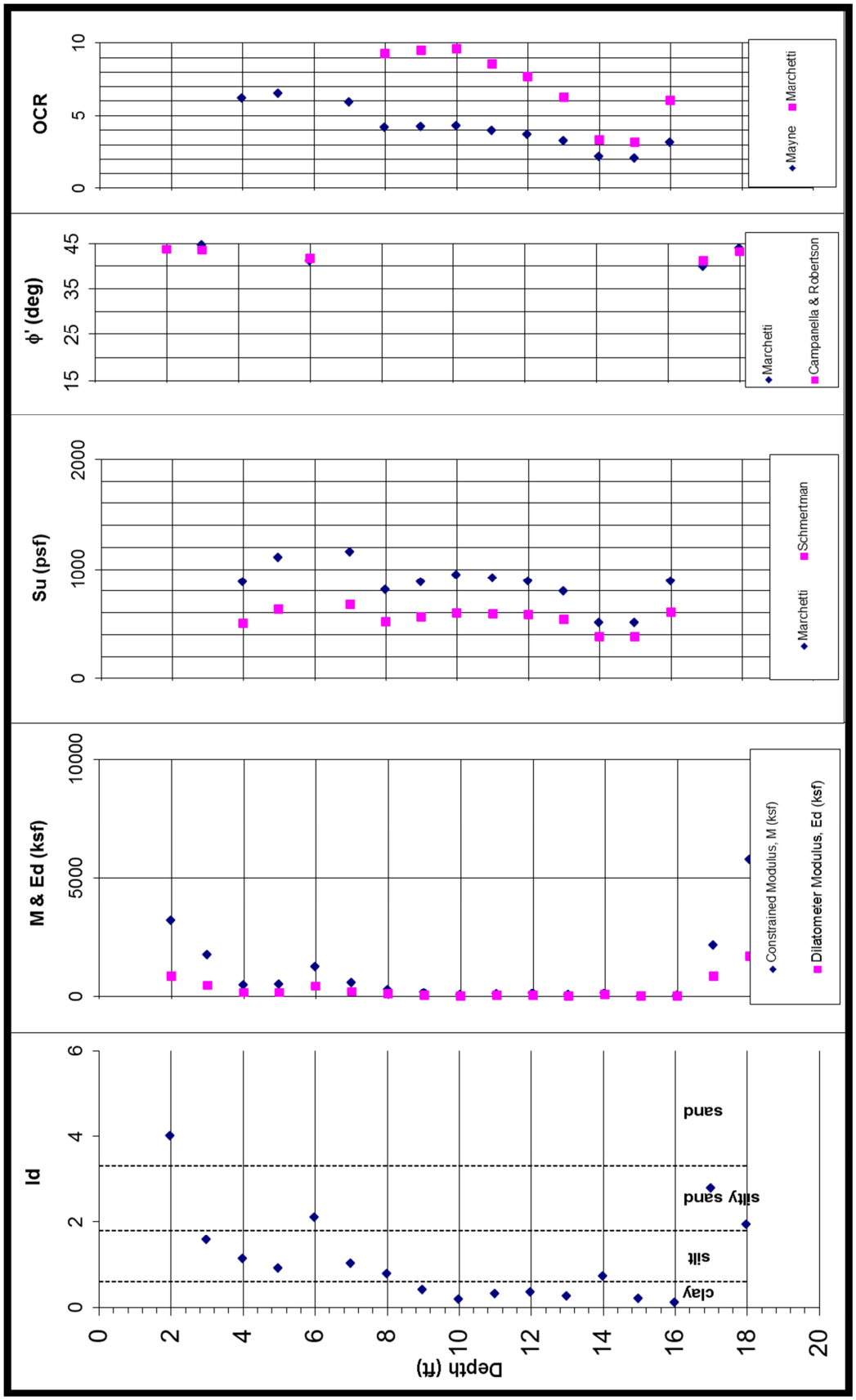

Figure 4.7 GAP-DMT Results (Provided by S&ME,Inc,)

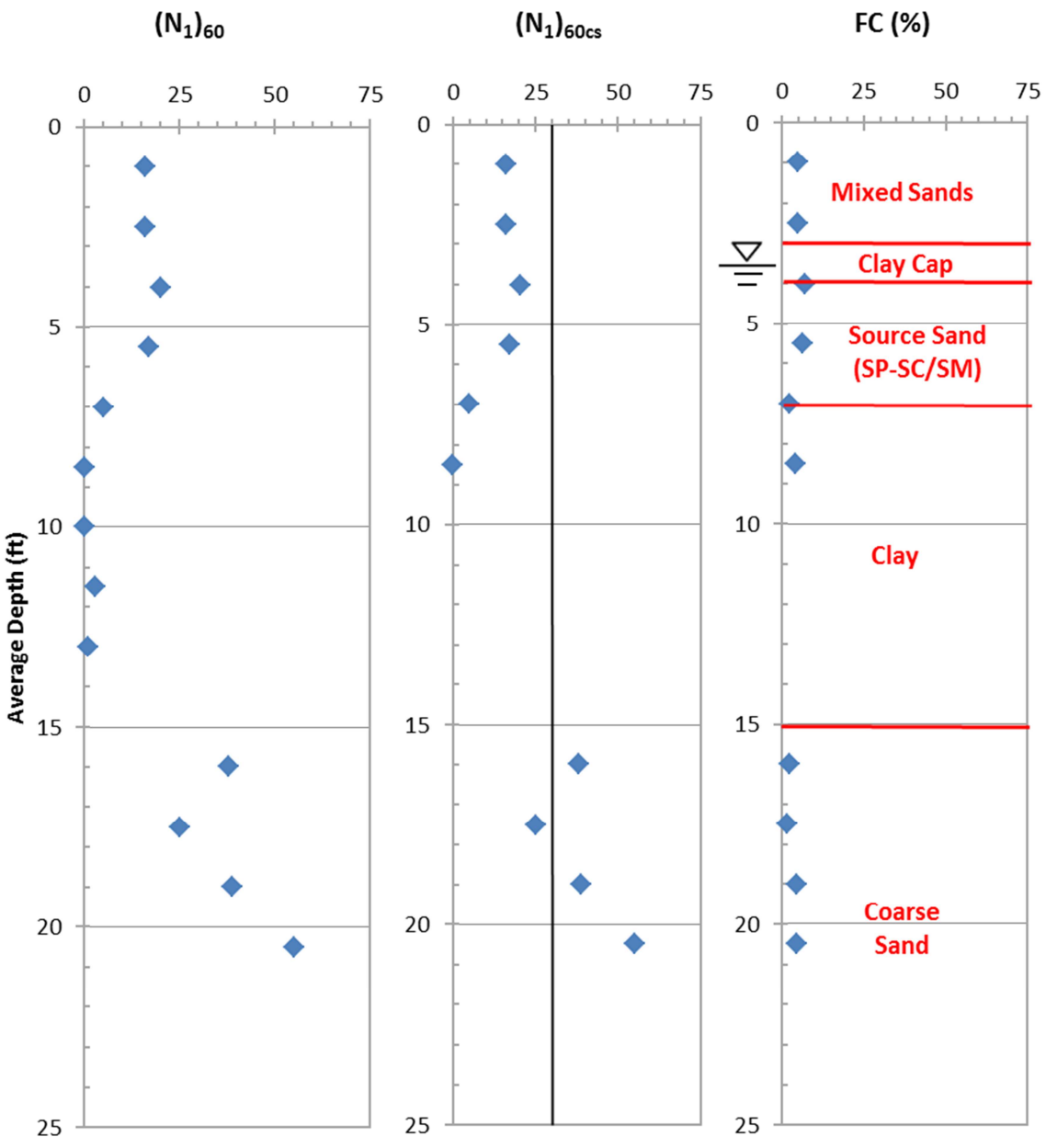

Figure 4.8 SPT GAP-03 Results (modified after Hu et al. (2002))

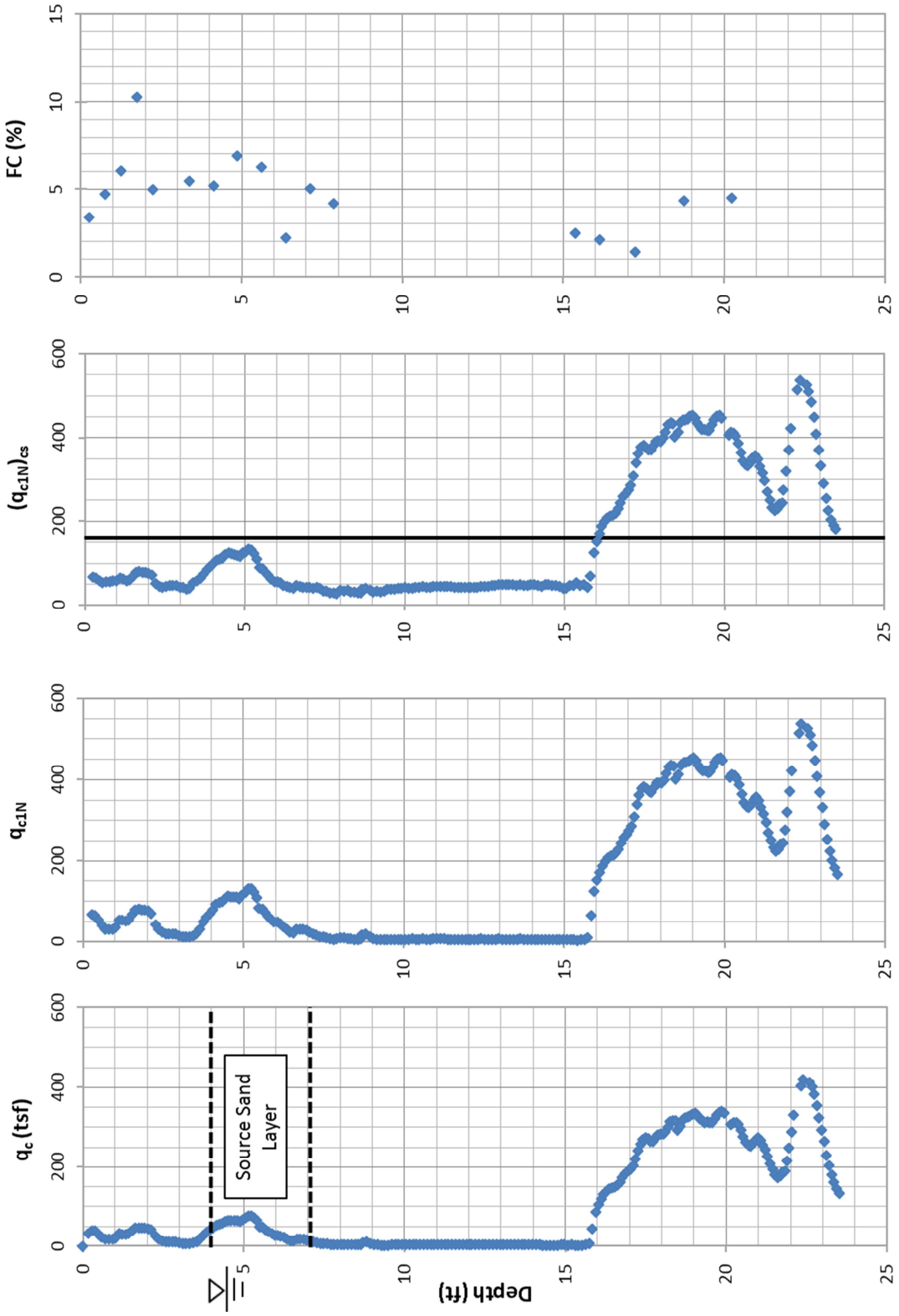

Figure 4.9 GAP-SCPT-1 Results

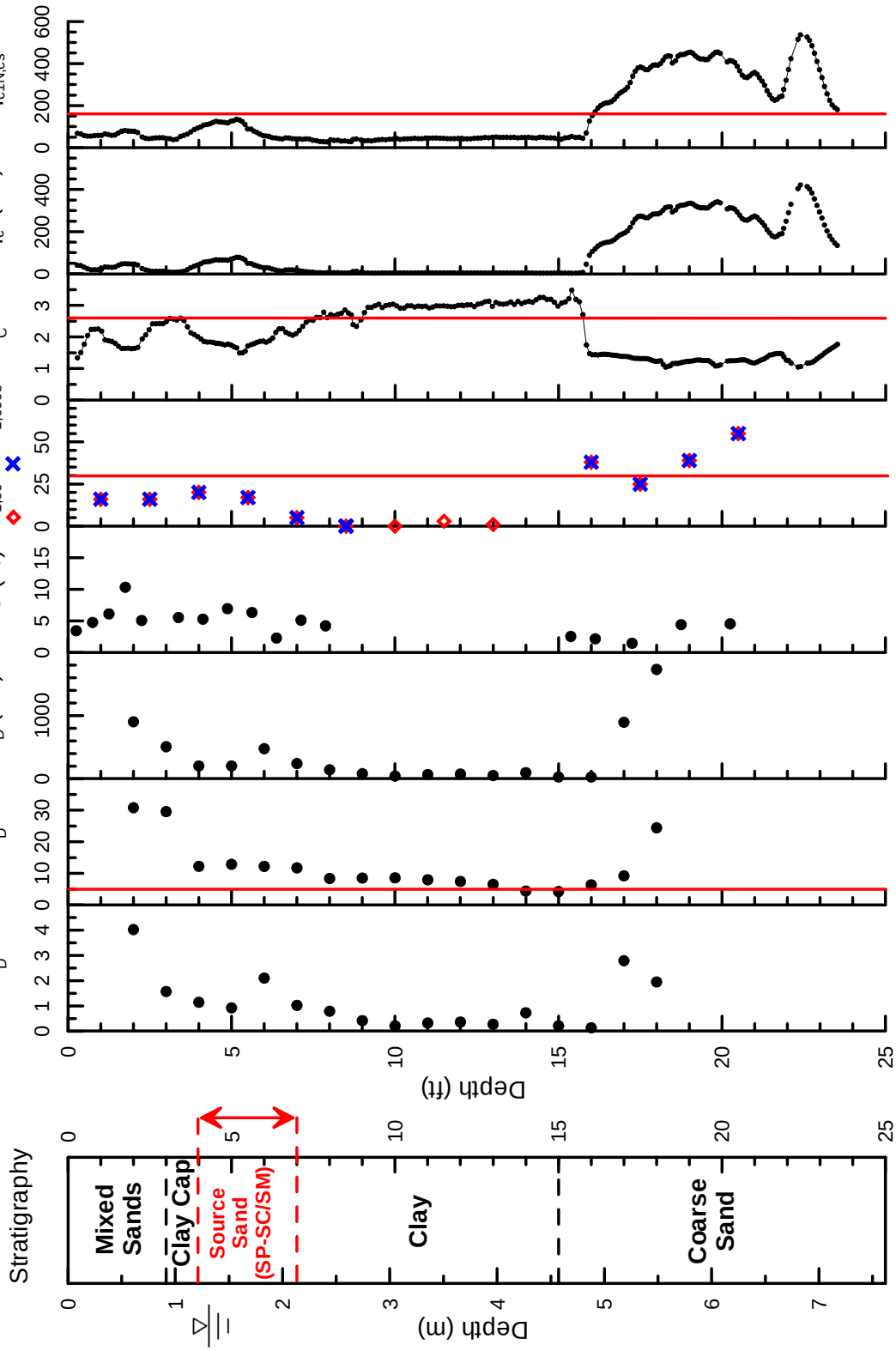

Figure 4.10 Summary of Gapway Field Testing Results

Table 4.2 Summary of Gapway Index Testing Results for the Source Sand Layer (after Hu et al., 2002 and Hasek, 2013)

Sample Depth (ft)	Sample Depth (m)	% Fines	C_u	C_c	USCS
3.8 - 4.5	1.2 – 1.4	5.3	0.5	1.7	SP-[a]
4.5 – 5.3	1.4 – 1.6	6.9	0.4	1.7	SP-[a]
5.3 – 6.0	1.6 – 1.8	6.3	0.5	1.7	SP-[a]
6.0 – 6.8	1.8 – 2.1	2.3	0.6	1.5	SP

[a] Note: Fines 5-12%, thus soil might be SP-SM or SP-SC (Atterberg limits not available)

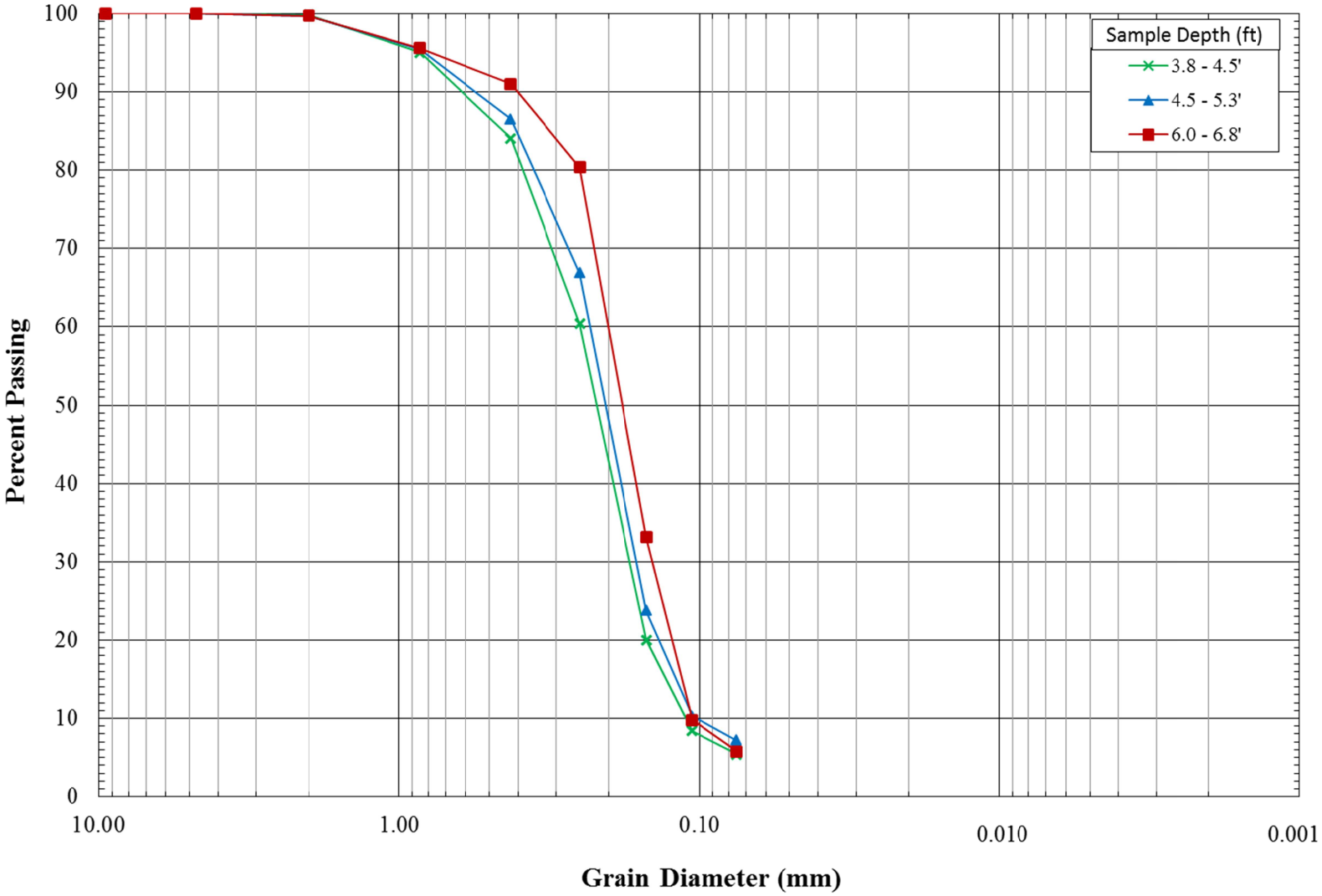

Figure 4.11 Grain Size Distribution Curves for Gapway Source Sand (Modified from Hu et al., 2002 and Hasek, 2013)

4.2.3 Fort Dorchester Results

The results of the DMT and CPT tests performed at Fort Dorchester are shown in Figures 4.12 through 4.14. A summary of these results is shown in Figure 4.15. Note that S_u and OCR are not plotted in Figures 4.12 and 4.13 because $I_D \geq 1.2$ for the entire profile. For Figures 4.14 and 4.15, recall from Section 2.2.4 and Figure 2.5 that FD-SCPT-1 corresponds to FD-DMT-EW and FD-SCPT-2 corresponds to FD-DMT-NS.

As shown in Figure 4.15, the source sand layer ranges from 8-16 ft (2.4-4.9 m). The CH/SC-SM interface that caps the source sand at 8 ft (2.4 m) is clearly distinguished in the DMT and CPT data. The lower boundary of 16 ft (4.9 m) was designated through the evaluation of the fines content data which jumps from 12.9 to 37.3% in samples from depths of 15.2 and 17.0 ft (4.6 and 5.2 m), respectively.

Note that FD-SCPT-2 exceeds the upper limit for liquefaction throughout much of the soil profile, indicating that the soil in this vicinity is too dense to liquefy. This indicates that the source sand range of 8-16 ft (2.4-4.9 m) is only valid in the vicinity of FD-SCPT-1 and the two DMT tests and it does not extend laterally to FD-SCPT-2. (Refer to Figure 2.5 for illustration.) As such, the FD-SCPT-2 data was not included in the simplified procedure.

Also, recall that even though the ground water table was consistently measured to be around 17 ft (5.2 m), it was assumed that the ground water was high enough to saturate the source sand layer at the time of the paleoliquefaction event.

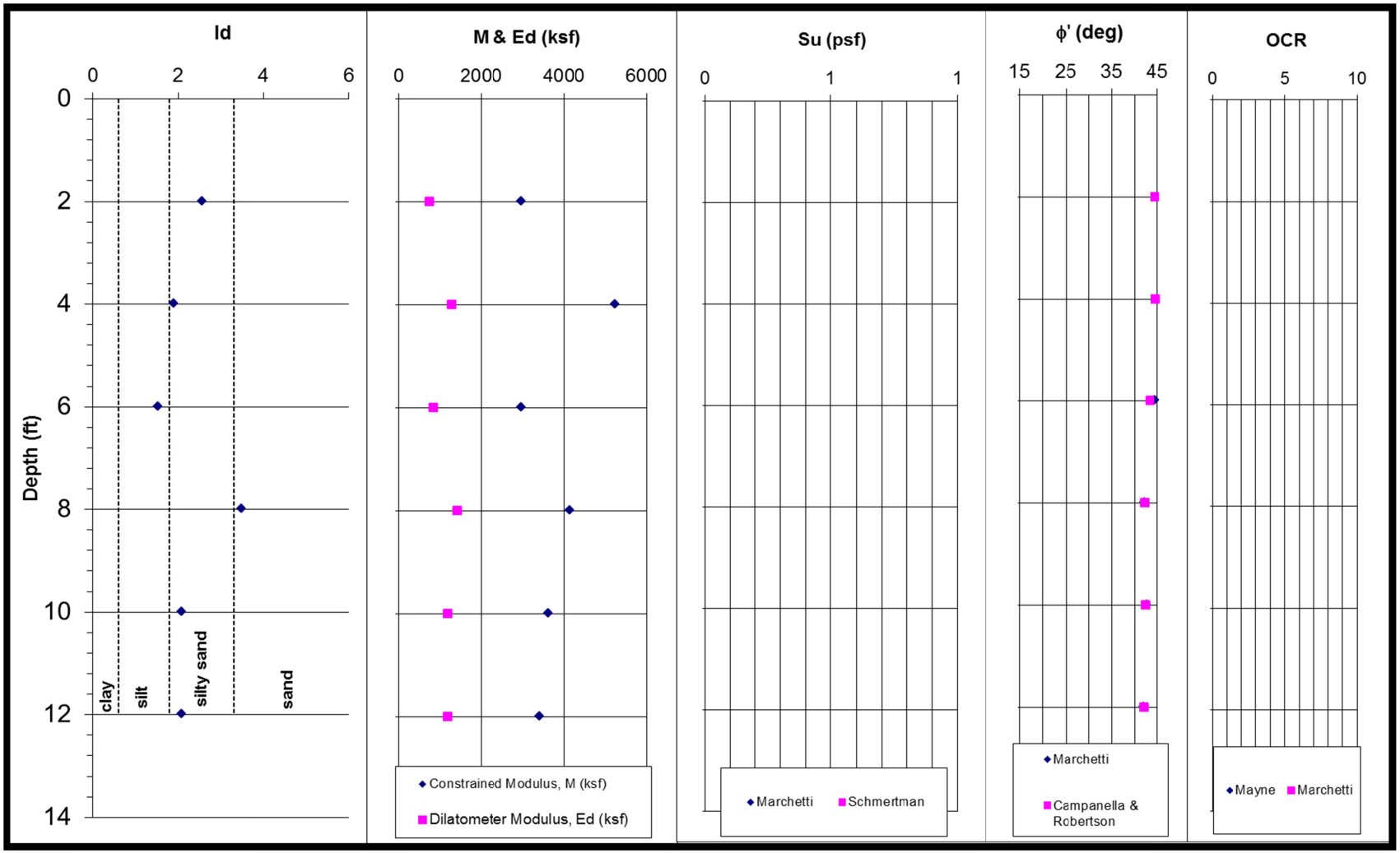

Figure 4.12 FD-DMT-NS Results (Provided by S&ME,Inc,)

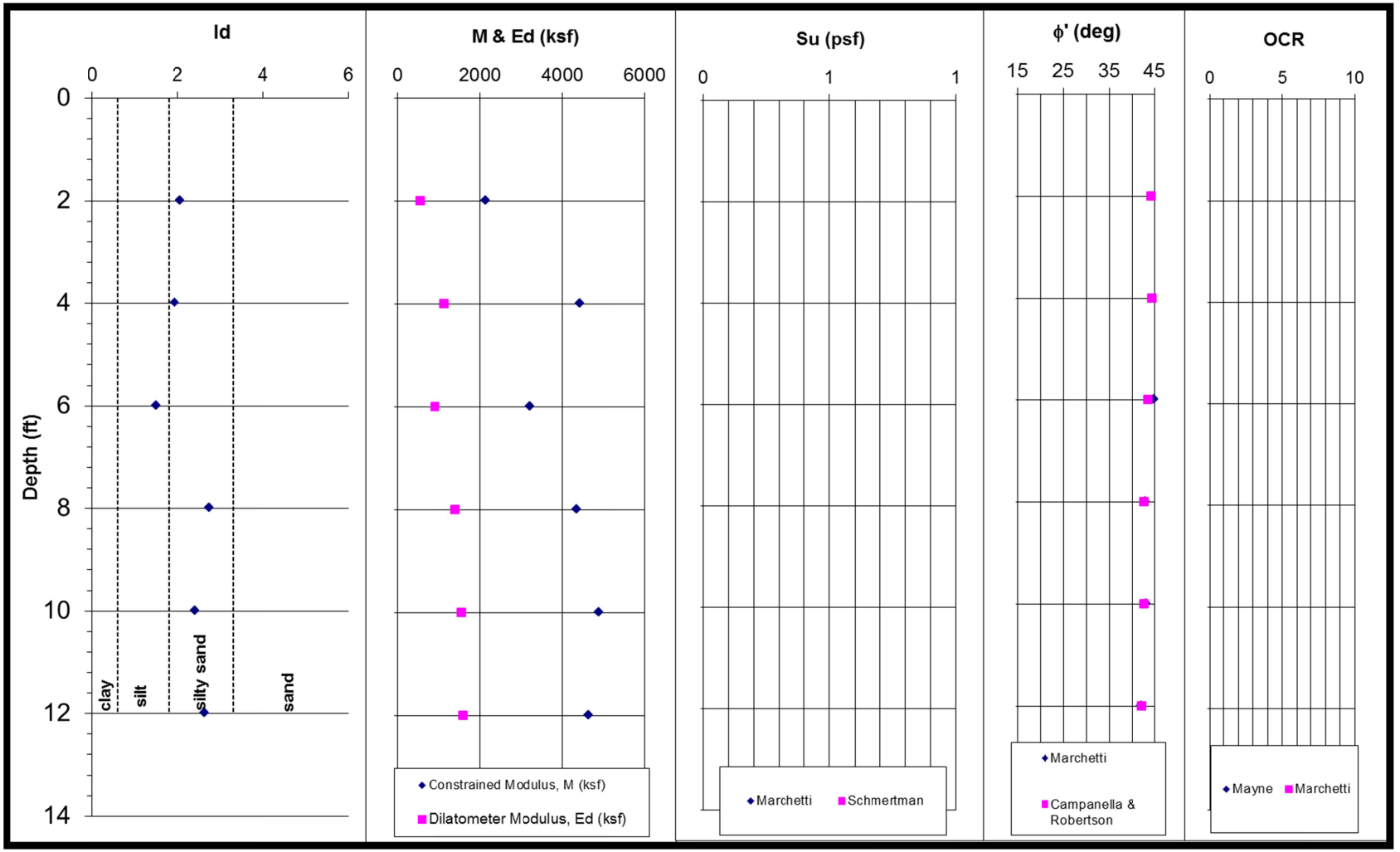

Figure 4.13 FD-DMT-EW Results (Provided by S&ME,Inc,)

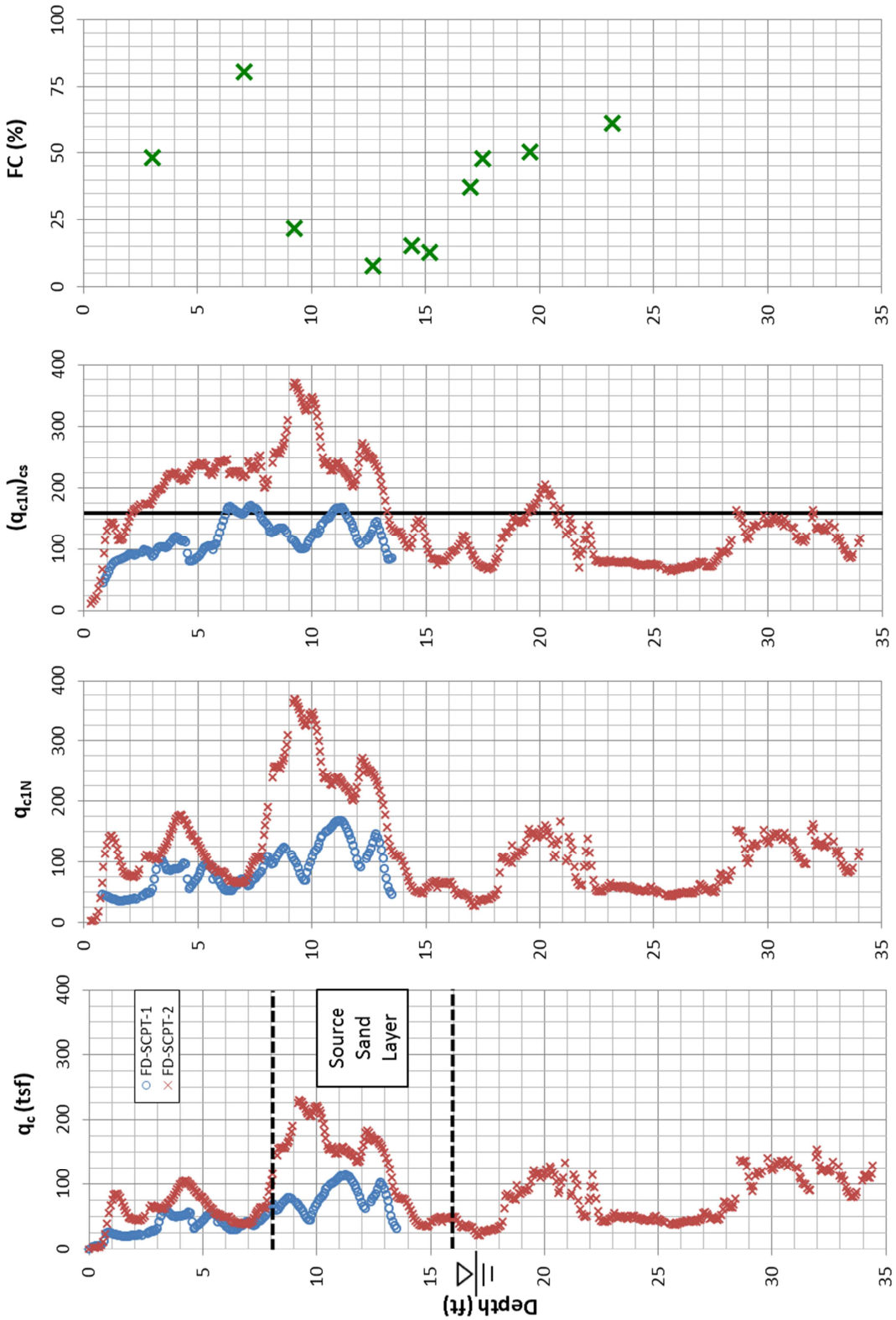

Figure 4.14 FD-SCPT-1 and 2 Results

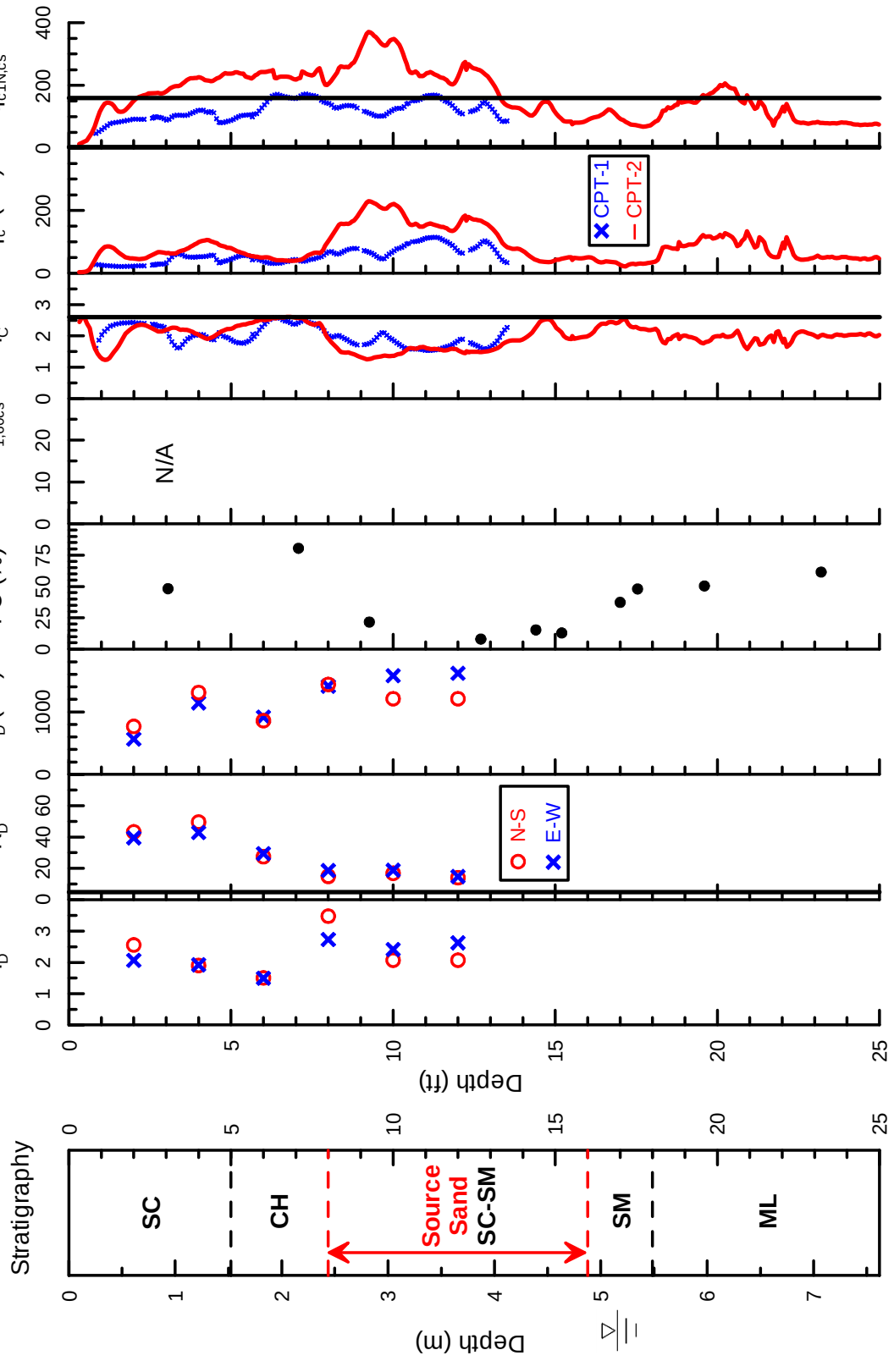

Figure 4.15 Summary of Fort Dorchester Field Testing Results

Table 4.3 presents a summary of the laboratory index testing results from the source sand layer. Note that Atterberg limit tests were unable to be performed for samples FDVC1D, FDVC1E, and FDVC1F due to insufficient sample sizes remaining after the grain size distribution tests. The percent silt, clay and colloid from the grain size distribution tests were analyzed in lieu of Atterberg limit test data for the classification of these samples. Figure 4.16 presents the grain size distribution curves for the samples in the source sand layer.

Table 4.3 Summary of the Fort Dorchester Index Testing Results for the Source Sand Layer

Sample Name	Sample Depth (ft)	Sample Depth (m)	% Fines	C_u	C_c	LL	PL	PI	G_s	USCS
VC1C	8.9 – 9.7	2.7 – 3.0	21.6	N/A[a]	N/A[a]	26	21	5	2.700	SC-SM
VC1D	12.3 – 13.1	3.7 – 4.0	8.0	1.8	1.2	-	-	-	2.700	SP-SM [c]
VC1E	14.1 – 14.7	4.3 – 4.5	15.3	722[b]	90[b]	-	-	-	2.690	SC-SM [c]
VC1F	15.0 – 15.4	4.6 – 4.7	12.9	5.1	4.2	-	-	-	2.680	

[a]Cu and Cc unobtainable- 24-hour hydrometer reading was insufficient to extend grain size distribution curve to 10% finer
[b] - 24-hour hydrometer reading was insufficient to extend grain size distribution curve to 10% finer (Cu and Cc calculated by assuming $D_{11} \approx D_{10}$)
[c] USCS classification obtained through grain size distribution curve analysis

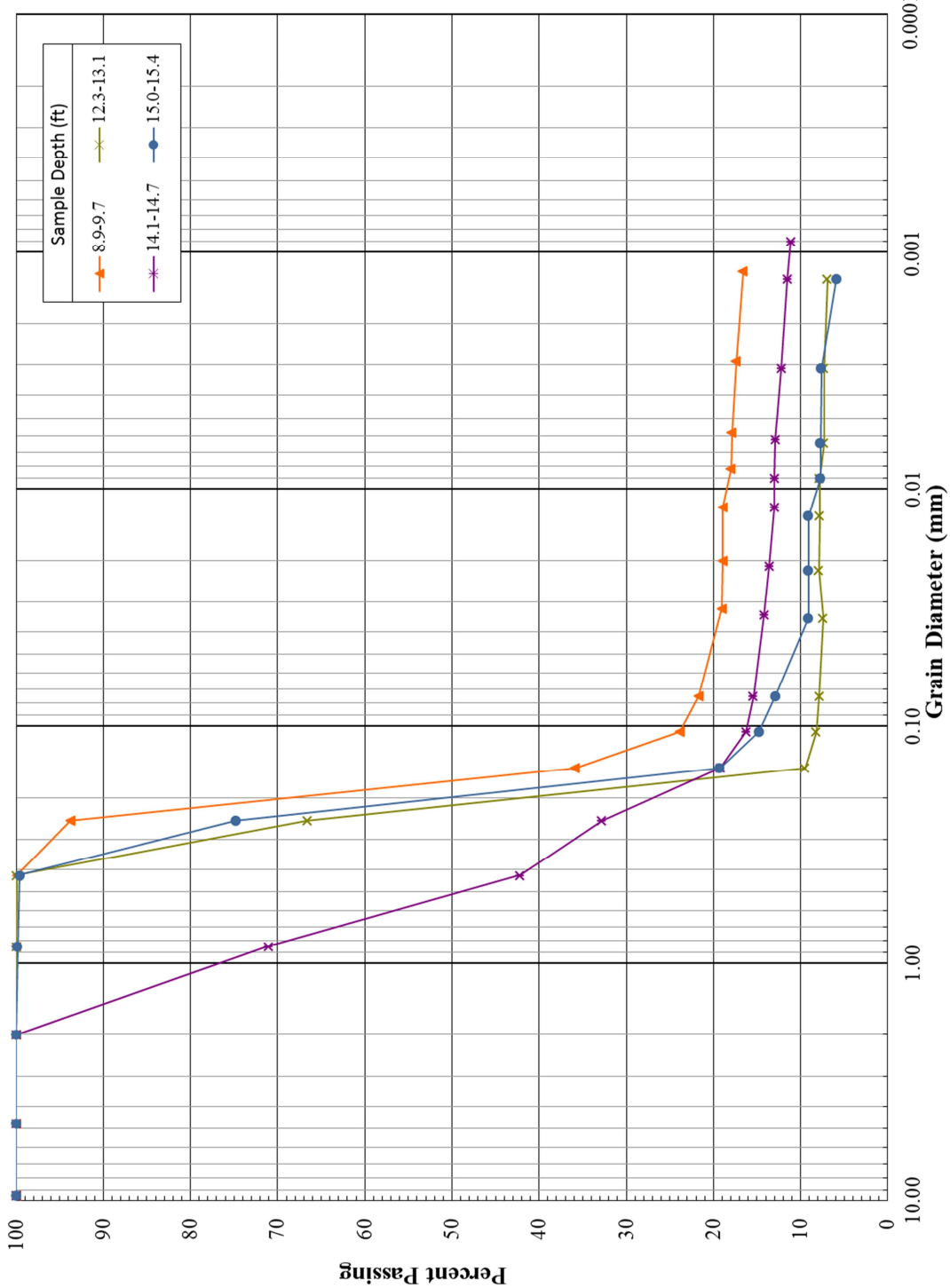

Figure 4.16 Grain Size Distribution Curves for Fort Dorchester Source Sand (Modified from Hasek, 2013)

4.2.4 Hollywood Results

The results of the DMT, SPT, and CPT tests performed at Hollywood are shown in Figures 4.17, 4.18 and 4.19, respectively. A summary of these results is shown in Figure 4.20.

In Figure 4.17, I_D, M, and E_D are unknown from 3-6 ft (0.9-1.8 m) because the B-values were unobtainable at these depths. This often occurs in dense soils where the pressure required to fully inflate the membrane exceeds the maximum pressure of the equipment. In Figure 4.18, ER measurements were not collected from 4-6 ft (1.2-1.8 m) in HWD-SPTE-1, thus N_{60} is not available in this range.

As shown in Figure 4.20, the source sand ranges from 9-14 ft (2.7-4.3m), per the interpretation of the CPT data which indicates that the soils just above and below the referenced depths are unliquefiable.

Table 4.4 presents a summary of the laboratory index testing results for the source sand layer. Note that Atterberg limit tests were unable to be performed for samples F78 and F79 due to insufficient sample sizes remaining after the grain size distribution tests. The percent silt, clay and colloid from the grain size distribution test were analyzed in lieu of Atterberg limit test data for the classification of these samples. Figure 4.21 presents the grain size distribution curves for the samples in the source sand layer.

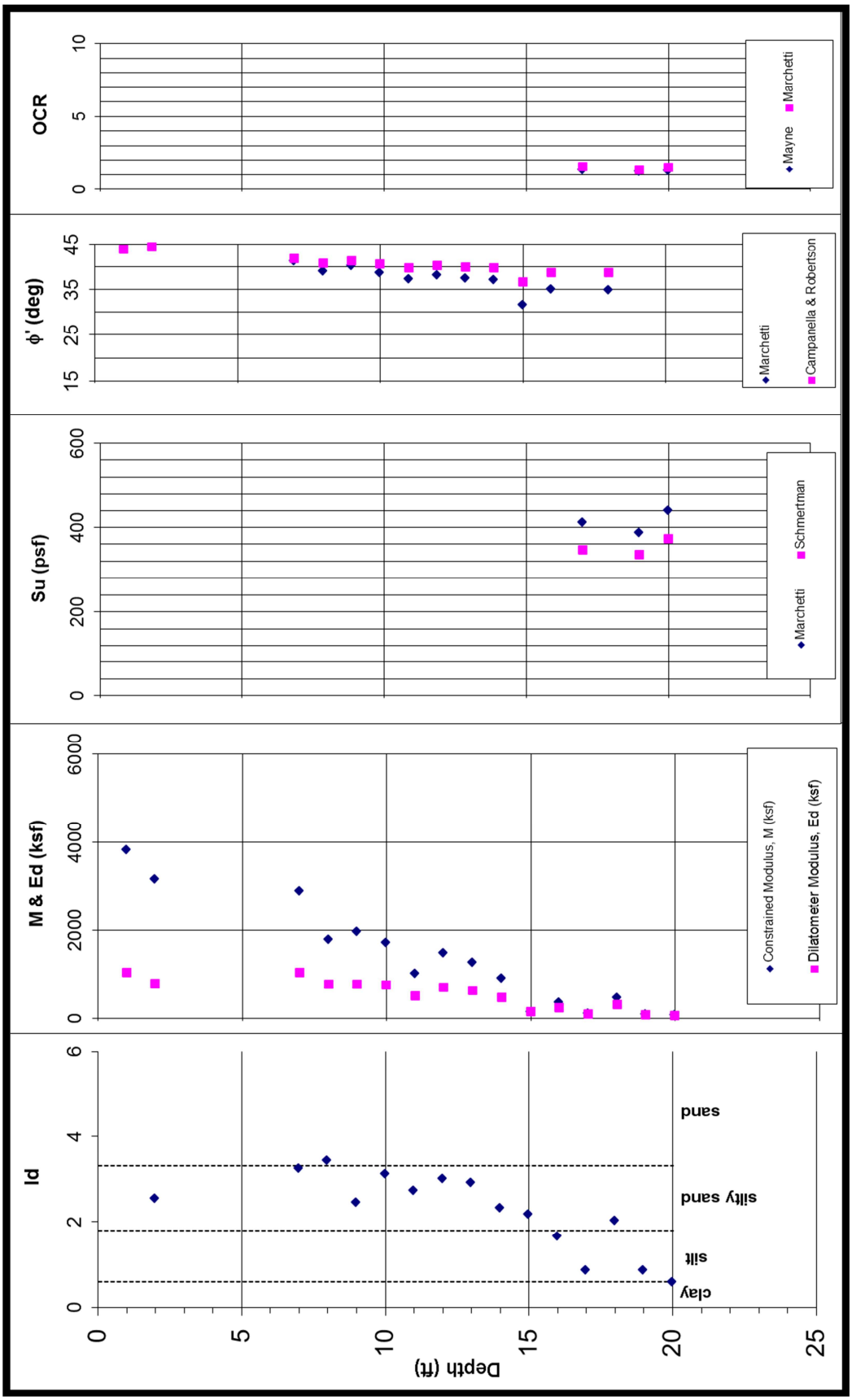

Figure 4.17 HWD-DMT Results (Provided by S&ME,Inc,)

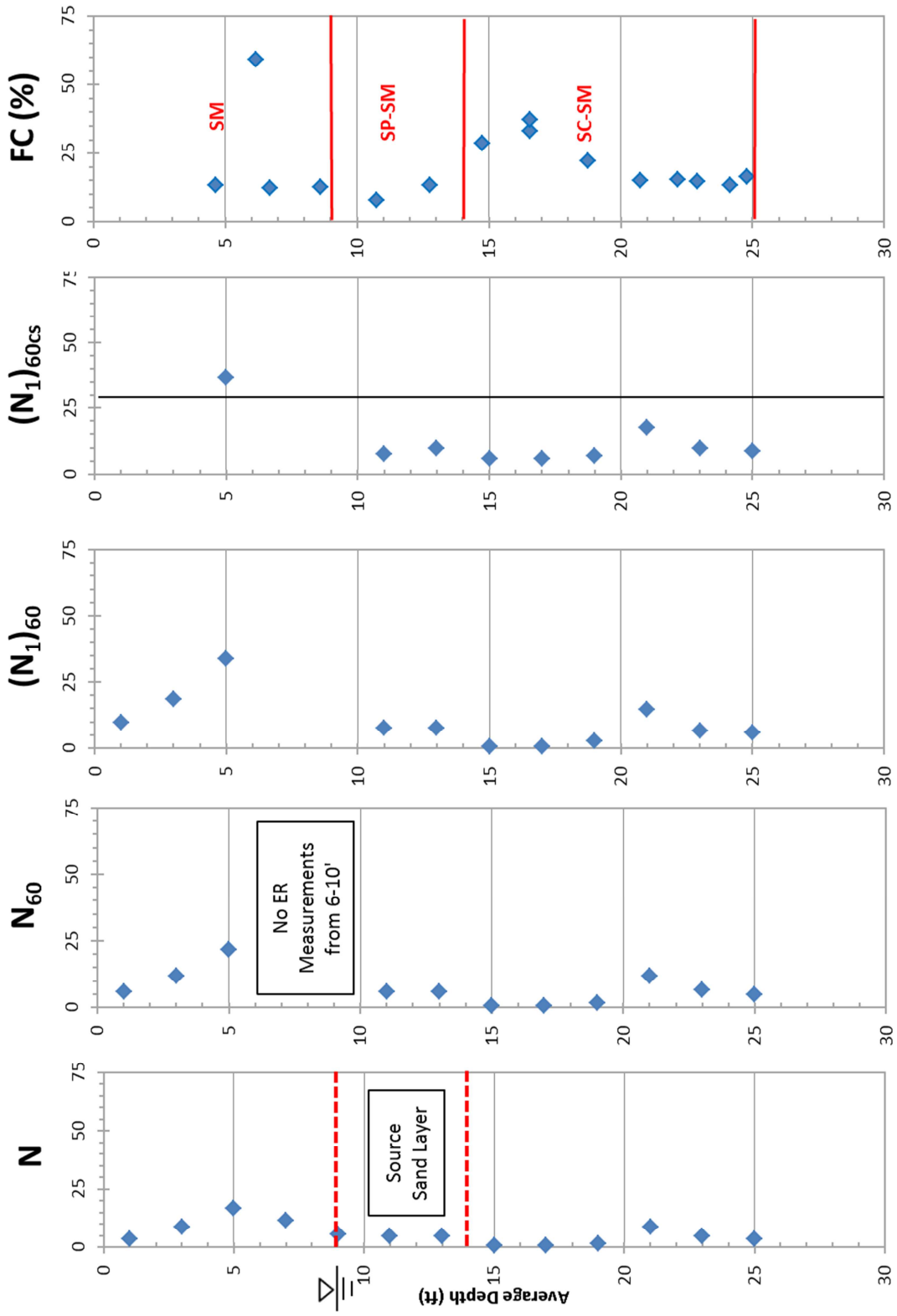

Figure 4.18 HWD-SPTE-1 Results

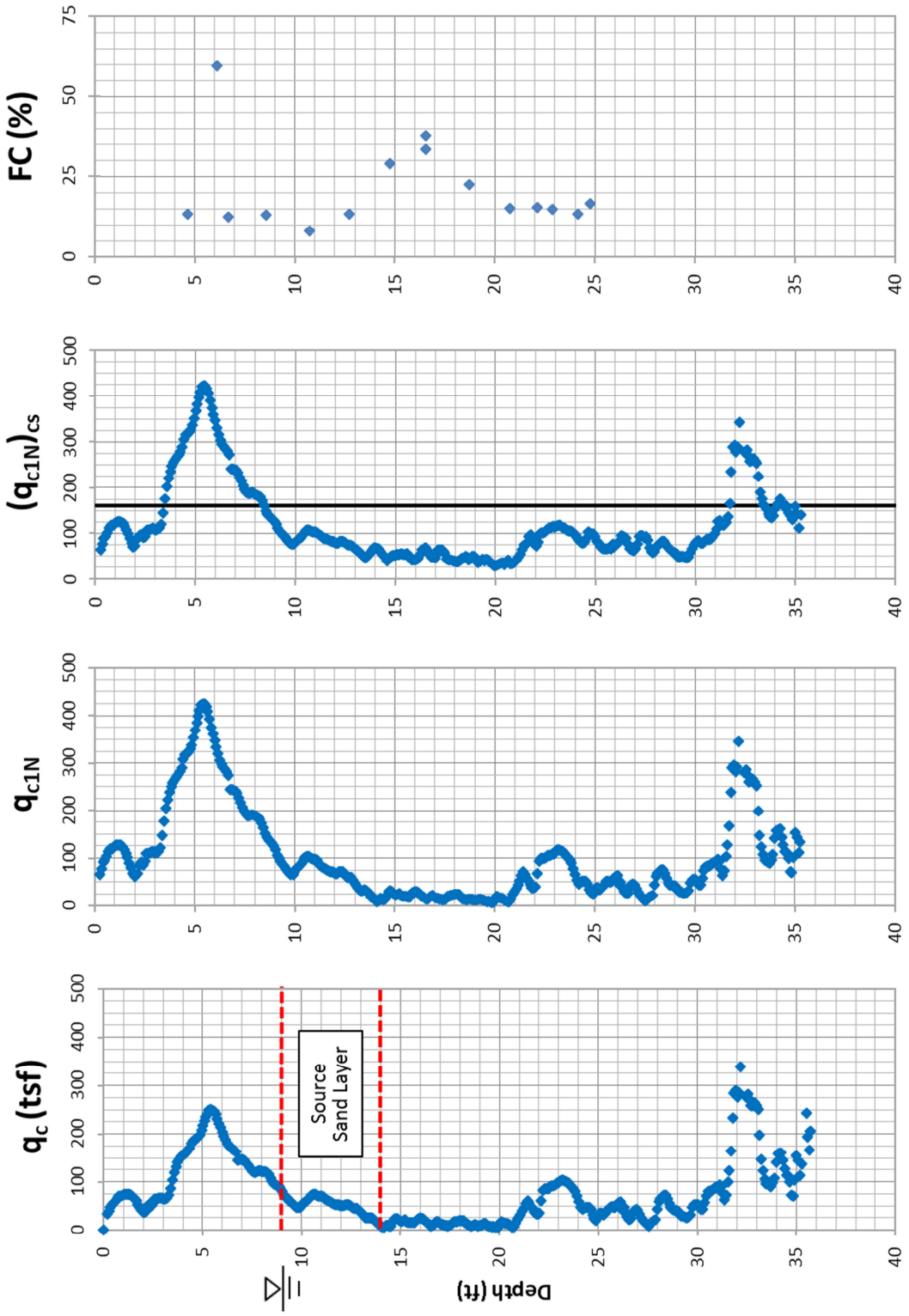

Figure 4.19 HWD-CPT-4 Results

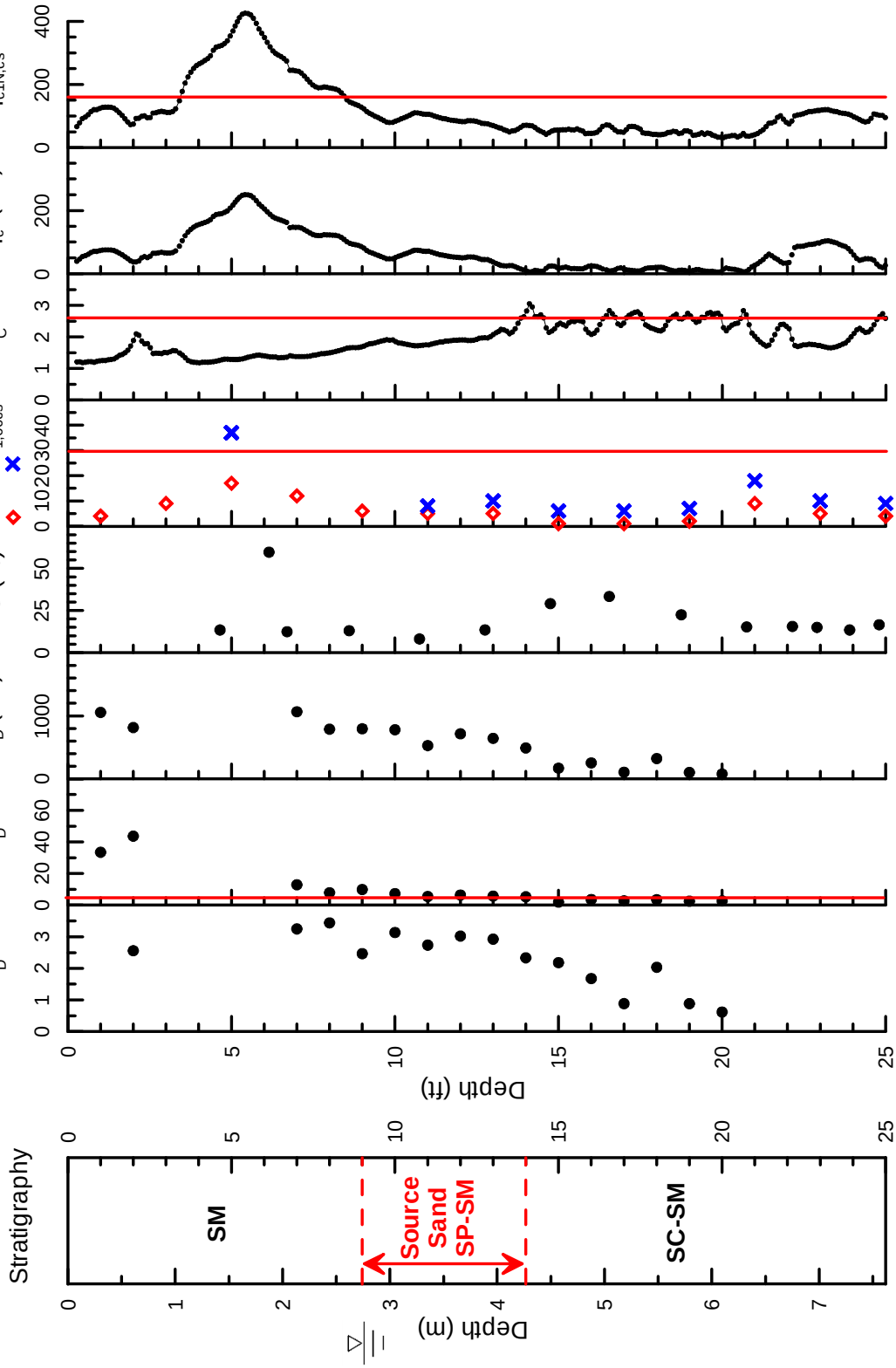

Figure 4.20 Summary of Hollywood Field Testing Results

Table 4.4 Summary of the Hollywood Index Testing Results for the Source Sand Layer

Sample Name	Sample Depth (ft)	Sample Depth (m)	% Fines	C_u	C_c	LL	PL	PI	G_s	USCS
F78	10.0 – 11.5	3.0 – 3.5	8.11	1.62	0.98	-	-	-	2.665	SP-SM[a]
F79	12.0 – 13.5	3.7 – 4.1	13.43	1.83	1.23	-	-	-	2.675	SM[a]

[a] USCS classification obtained through grain size distribution curve analysis

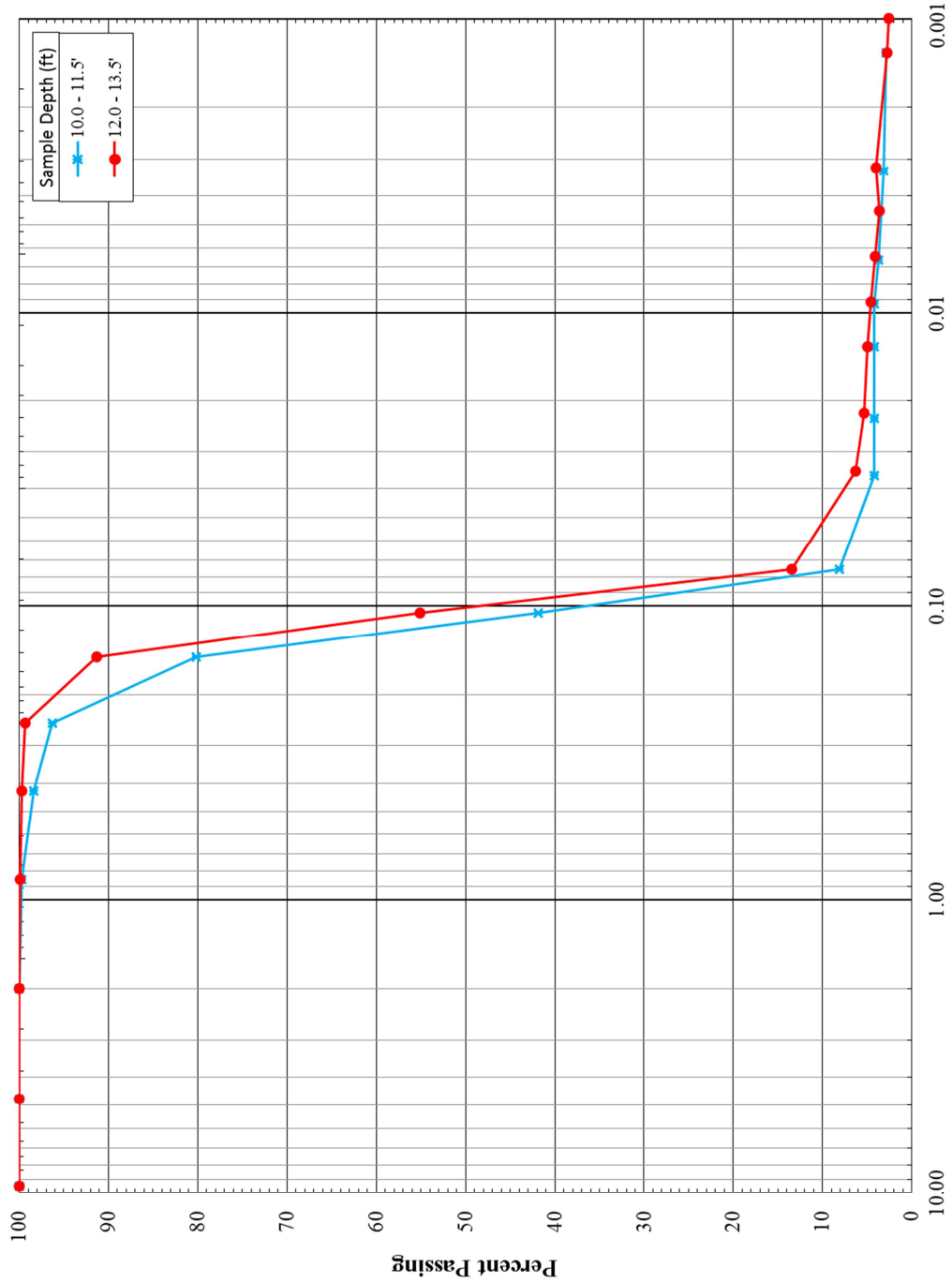

Figure 4.21 Grain Size Distribution Curves for Hollywood Source Sand (Modified from Hasek, 2013)

4.2.5 Four Hole Swamp Results

The results of the DMT, SPT, and CPT tests performed at Four Hole Swamp are shown in Figures 4.22, 4.23, and 4.24, respectively. A summary of these results is shown in Figure 4.25.

In Figure 4.22, I_D, M, and E_D are unknown at 4, 18, 20 and 22 ft (1.2, 5.5, and 6.1 m) due to unobtainable B-values at these depths. In Figure 4.23, FHS-SPTE-1 N_{60} is unavailable above 6 ft (1.8 m), as no ER measurements were available in the first two drives. Also, $(N_1)_{60cs}$ is unknown below 20 ft (6.1 m) due to the lack of fines content data.

As shown in Figure 4.25, the source sand ranges from 9 -15 ft (2.7-4.6 m). The CPT results indicate that the soil in this range would be considered unliquefiable; however, the laboratory index results show that the soils in this range are granular with little fines and potentially liquefiable. This case is a prime example of how the CPT test (as well as the DMT) only measures soil *behavior* types and stresses the need to supplement CPT and DMT test with testing of soil samples (e.g. SPT split spoon samples) to ensure soil types.

The lower boundary of the source sand was determined by a clear jump in fines content at 15 ft (4.6 m). The upper boundary of 9 ft (2.7 m) was selected because of the location of the ground water table at the time of testing. While the soil directly above 9 ft (2.7 m) would be considered liquefiable if it were saturated, this was not the case at the time of testing; as such, the data points from these soils were not included in the simplified procedure analysis.

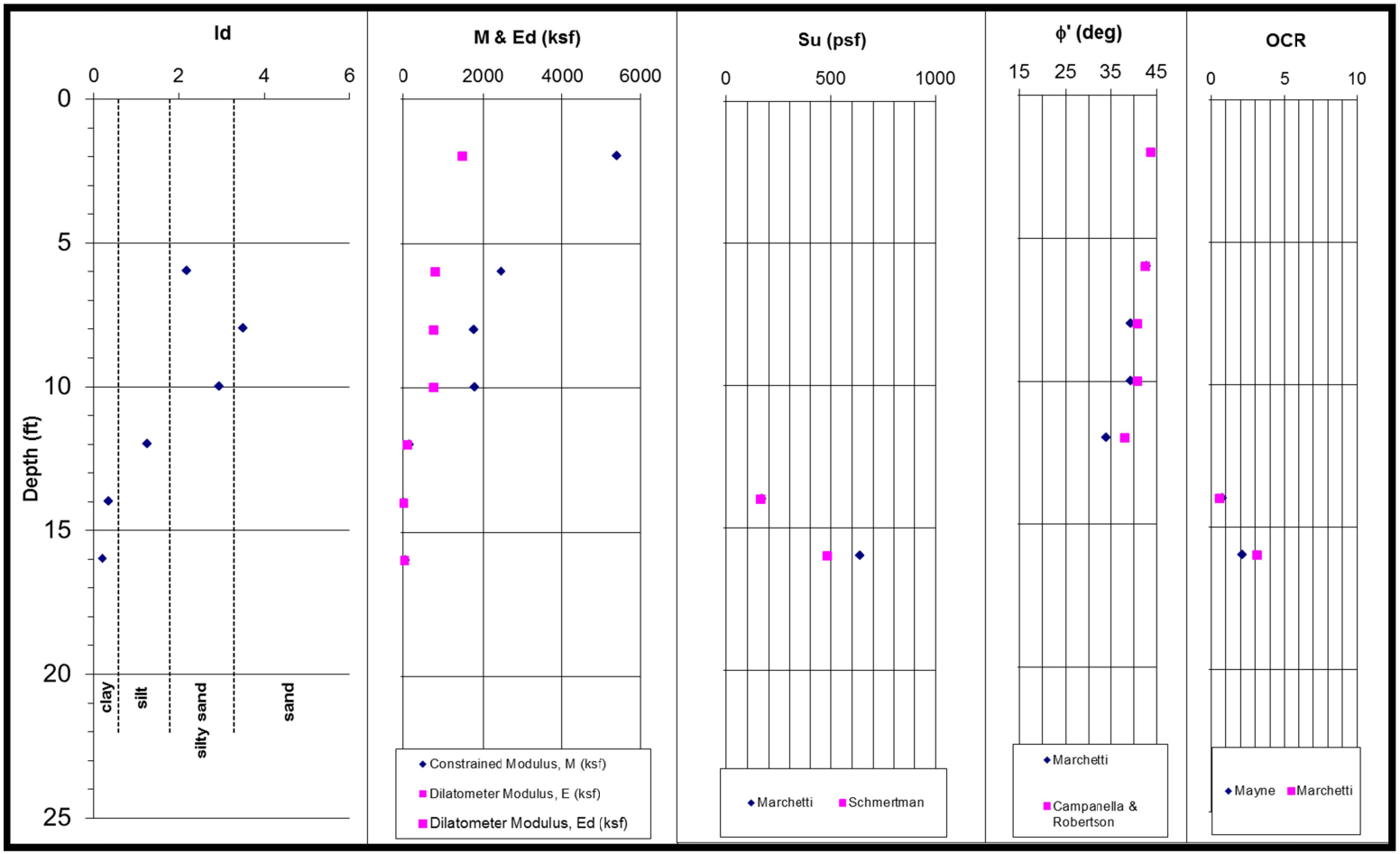

Figure 4.22 FHS-DMT Results (Provided by S&ME,Inc,)

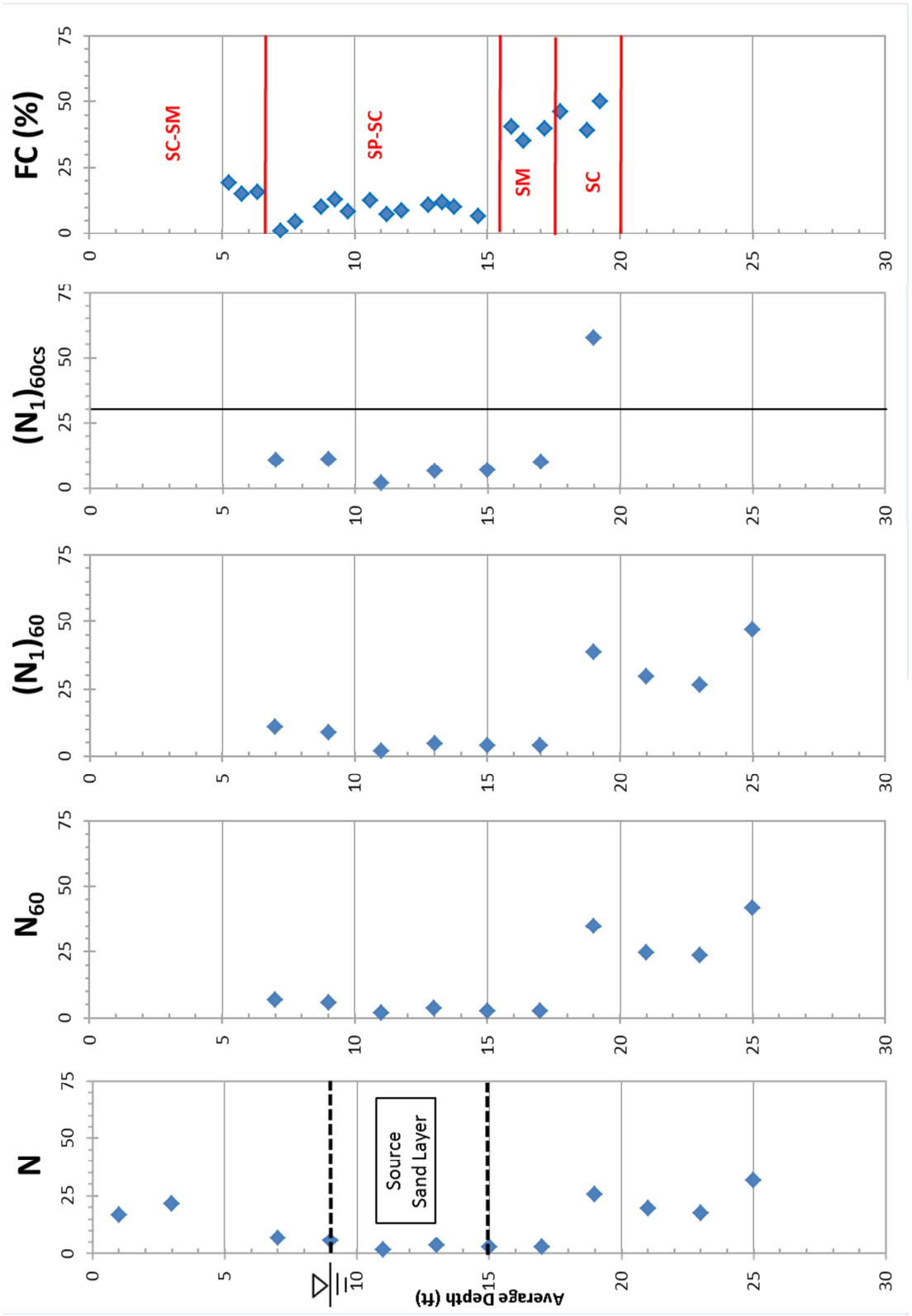

Figure 4.23 FHS-SPTE-1 Results

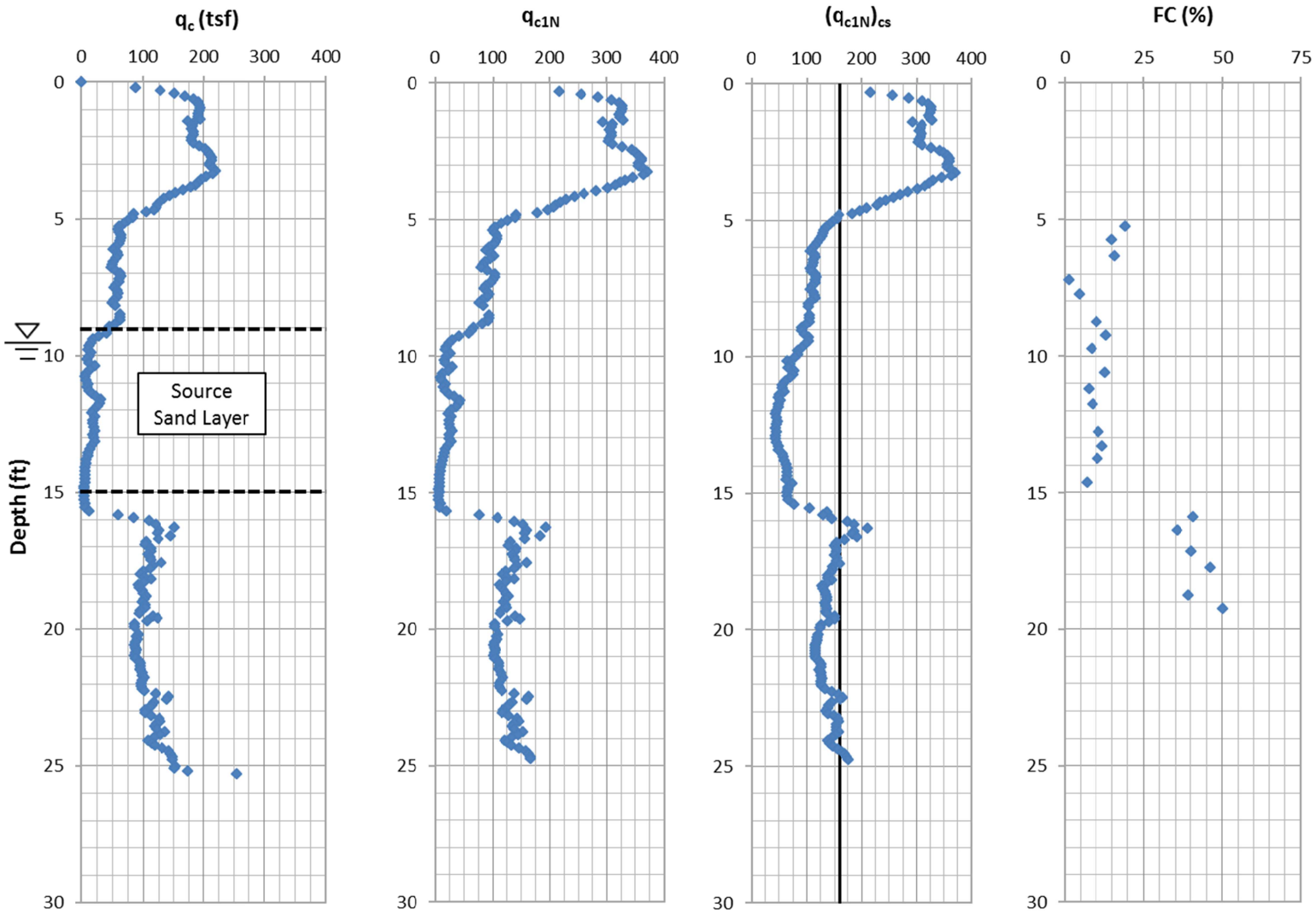

Figure 4.24 FHS-SCPT-1 Results

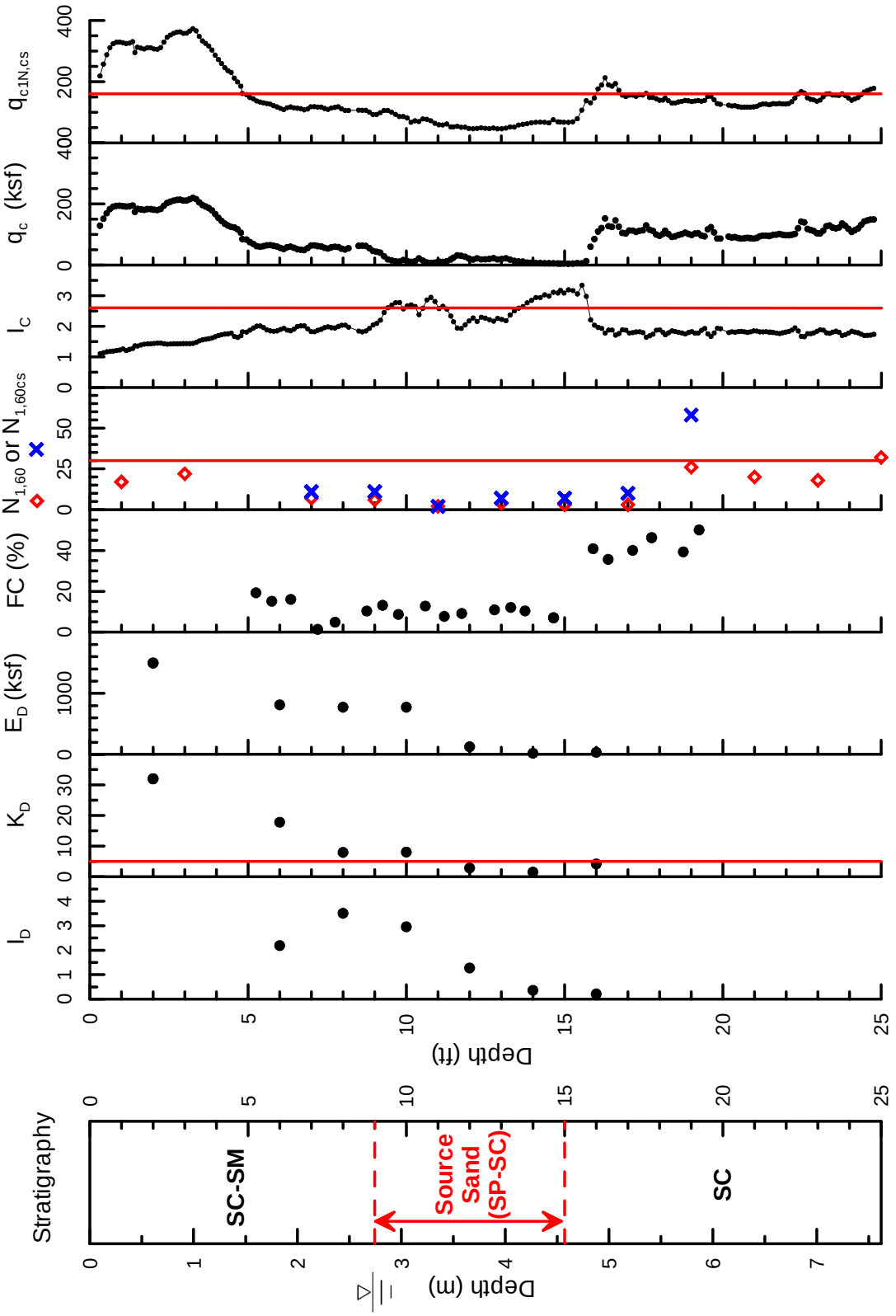

Figure 4.25 Summary of Four Hole Swamp Field Testing Results

Table 4.5 presents a summary of the laboratory index testing results. Note that Atterberg limit tests were unable to be performed for many of the samples due to insufficient sample sizes remaining after the grain size distribution tests. Once again, the percent silt, clay and colloid from the grain size distribution test were analyzed in lieu of Atterberg limit test data for the classification of these samples. Figures 4.26 and 4.27 present the grain size distribution curves for the samples in the source sand layer.

Table 4.5 Summary of the Four Hole Swamp Index Testing Results for the Source Sand Layer

Sample Name	Sample Depth (ft)	Sample Depth (m)	% Fines	C_u	C_c	LL	PL	PI	G_s	USCS
F35	9.0 – 9.5	2.7 – 2.9	13.1	54.5	33.3	-	-	-	2.651	SC-SM[a]
F44	9.5 – 10.0	2.9 – 3.0	8.6	2.3	1.2	-	21	-	2.659	SP-SC[a]
F82	10.3 – 10.9	3.1 – 3.3	12.8	48.5	36.1	-	-	-	2.650	SP-SC[a]
F36	10.9 – 11.5	3.3 – 3.5	7.7	1.7	1.2	-	-	-	2.660	SP-SC[a]
F45	11.5 – 12.0	3.5 – 3.7	9.1	3.2	1.7	-	-	-	2.658	SP-SM[a]
F37	12.7 – 12.9	3.9	10.9	7.4	4.3	25	17	8	2.648	SP-SC
F39	13.1 – 13.5	4.0 – 4.1	12.1	28.0	11.2	20	13	7	2.650	SP-SC
F46	13.5 – 14.0	4.1 – 4.3	10.4	3.1	1.9	-	-	-	2.668	SP-SC[a]
F38	14.2 – 15.1	4.3- 4.6	7.0	2.3	1.0		-	-	2.663	SP-SM[a]

[a] USCS classification obtained through grain size distribution curve analysis

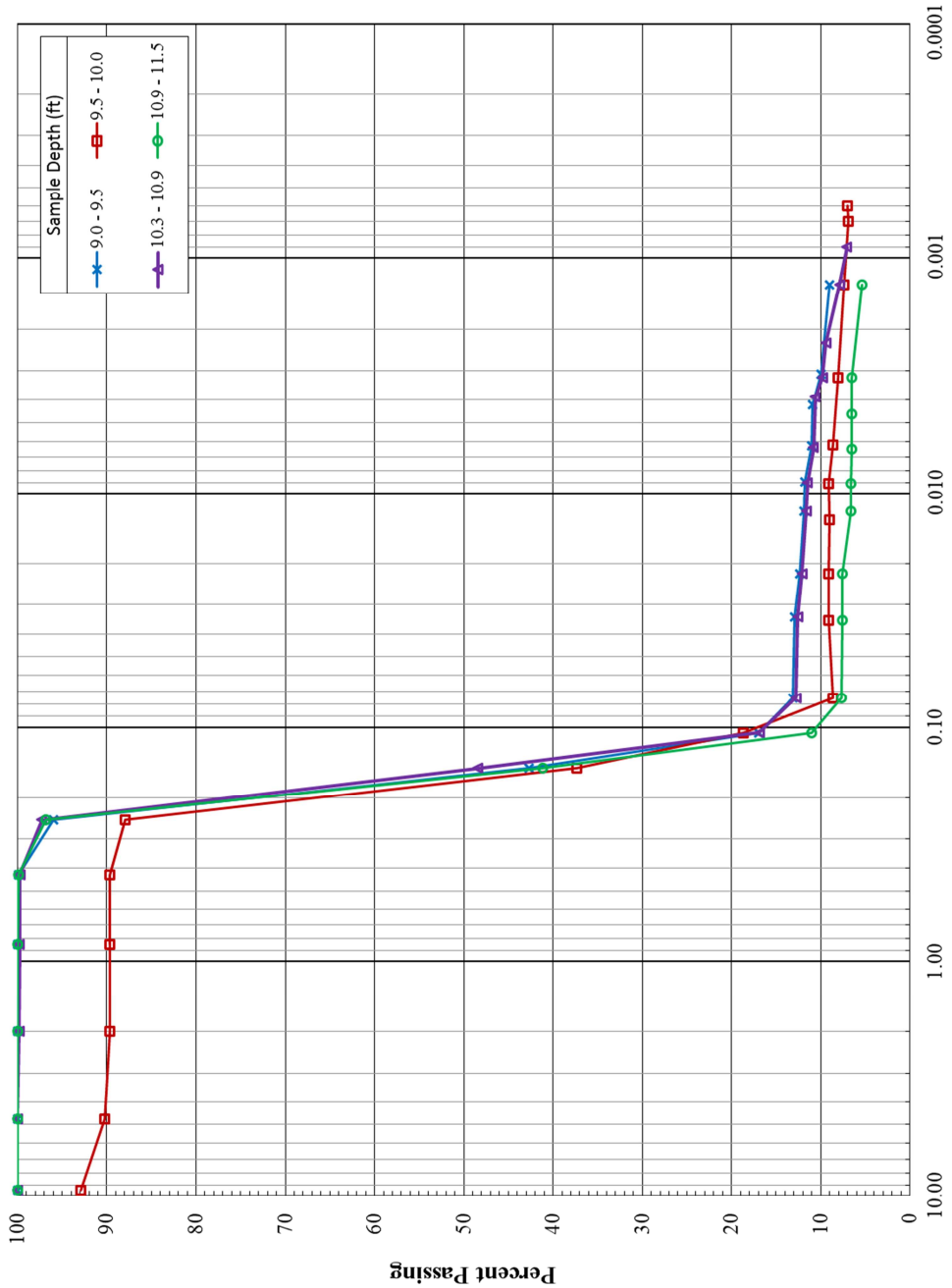

Figure 4.26 Grain Size Distribution Curves for Four Hole Swamp Source Sand (1 of 2)
(Modified from Hasek, 2013)

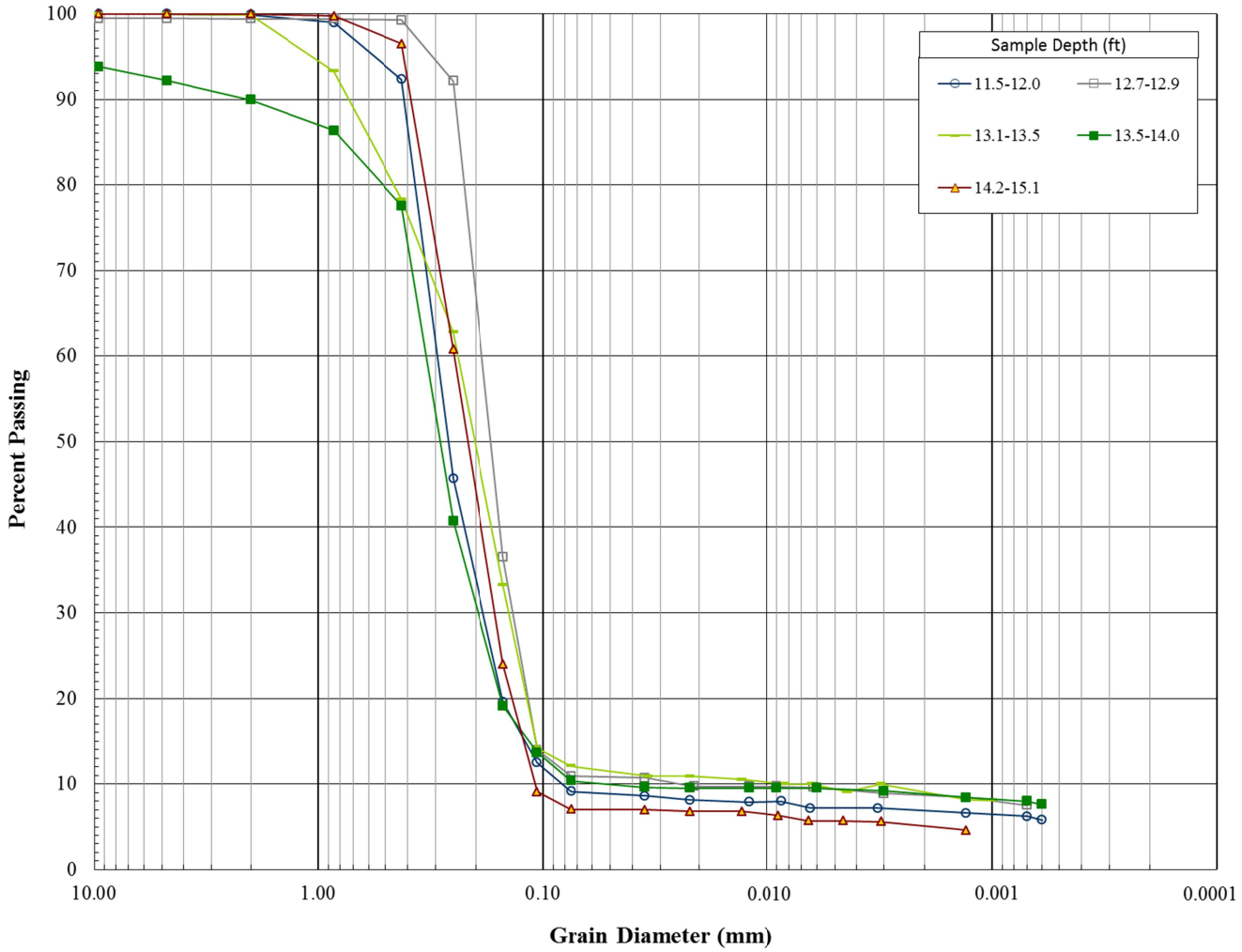

Figure 4.27 Grain Size Distribution Curves for Four Hole Swamp Source Sand (2 of 2)
(Modified from Hasek, 2013)

4.3 Simplified Procedure Results

The goal of the simplified procedure analysis is to develop a DMT-CRR relation that is based on a direct relationship between DMT-SPT/CPT data and can be used as a first approximation of liquefaction analysis for SCCP soils. Recall from Section 2.4.2 that the current DMT-CRR relations of Monaco et al. (2005) and Grasso and Maugeri (2006) were derived through indirect means using relative density (D_r) as a mediator between DMT and SPT/CPT data. Tsai et al. (2009) developed a DMT-CRR relation that was based on direct relations between DMT-SPT/CPT data. The procedure outlined in Tsai et al. (2009) was followed for the five SCCP sites to develop relationships between DMT, SPT, and CPT test data that is specific to SCCP soils. These relations were used to transform the existing CRR-SPT and CRR-CPT relations into CRR-DMT relations. The first analysis does not consider the effects of aging while the second analysis does. A third analysis considers CRR relations with data where CRR was obtained from stress-controlled cyclic triaxial tests performed by Hasek (2013) on high-quality fixed-piston tube samples.

4.3.1 Development of correlations between DMT and CPT and SPT

SPT, CPT, and DMT test results performed in close proximity with one another were used to establish correlations between the results of the different tests. These correlations were used to establish a new CRR-DMT relation for the South Carolina Coastal Plain soils by transforming the CRR-SPT and CRR-CPT relations from the well-established simplified procedure (see Section 2.4.2). As shown in the test data profiles for each site (Figures 4.4, 4.10, 4.15, 4.20, and 4.25) the pattern of the variation of N-

values, q_c, K_D, and E_D have similar trends with depth suggesting that there is a relationship between each of the parameters. Section 2.3.5 discusses existing relationships between DMT/CPT and DMT/SPT presented by Mayne and Liao (2004), Robertson (2009), and Tsai et al. (2009). The existing relationships apply to soil types that are different from what is encountered in the SCCP while the correlations derived in this thesis are specific to SCCP soils.

4.3.1.1 Direct Correlations

Correlations between the different tests were obtained following a two-step procedure similar to the Tsai et al. (2009). The first step uses the field test data to derive direct correlations that are specific to both the site and the depth from which the data originates. This is done by taking the results from the three tests and setting the different parameters equal to each other. For example, consider the data from 11 and 21 ft (3.4 and 6.4 m) below the ground surface at SAM. At 11 ft (3.4 m) K_D = 12, q_{c1Ncs}= 122, and $N_{1,60cs}$ = 16. At 21 ft (6.4 m) K_D is again equal to 12 but q_{c1Ncs} is equal to 143 and $N_{1,60cs}$ is equal to 19. The first step in obtaining the correlation is to say that for the point 11 ft (3.4 m) deep at SAM, a K_D of 12 is equal to a q_{c1Ncs} of 122 and an $N_{1,60cs}$ of 16 but at 21 ft (6.4 m) deep a K_D of 12 is equal to a q_{c1Ncs} of 143 and an $N_{1,60cs}$ of 19 . In this way the direct correlations are both site and depth specific. Table 4.6 presents a summary of the direct correlations developed for the source sand layers at each site.

Table 4.6 SCCP Direct Correlations for Collected Field Data in Source Sand Layers

	Depth (ft)	Depth (m)	Field Data			
			$(N_1)_{60cs}$	(qc1N)cs	KD	ED (MPa)
Sampit	9	2.7	11	108.7	16.7	28.0
	10	3.0	-	112.4	18.2	28.7
	11	3.4	16	121.5	12.1	25.8
	12	3.7	-	142.4	9.7	26.2
	13	4.0	14	112.1	9.5	23.2
	14	4.3	-	81.8	10.6	24.0
	15	4.6	7	82.8	9.2	21.8
	16	4.9	-	92.7	6.7	15.6
	17	5.2	4	91.7	6.2	20.0
	18	5.5	-	113.7	11.4	31.6
	19	5.8	15	134.2	12.0	30.5
	20	6.1	-	130.7	11.3	32.0
	21	6.4	19	142.9	11.9	36.0
	22	6.7	-	99.9	6.4	20.3
Gapway	4	1.2	20	93.0	12.2	9.8
	5	1.5	17	124.9	12.9	9.8
	6	1.8	-	57.2	12.2	22.9
	7	2.1	5	41.9	11.7	11.6
Fort Dorchester	8	2.4	-	141.9	18.6	67.6
	10	3	-	123.5	18.8	75.6
	12	3.7	-	118.6	14.8	77.4
Hollywood	9	2.7	-	122.8	9.8	38.1
	10	3.0	-	83.8	7.3	37.3
	11	3.4	8	105.6	5.4	25.3
	12	3.7	-	83.3	6.4	34.2
	13	4.0	10	69.7	5.7	30.8
	14	4.3	-	71.1	5.2	23.5
Four Hole Swamp	10	3	11	81.4	8.0	37.1
	12	3.7	4	47.0	2.8	6.1
	14	4.3	6	67.3	1.5	1.0

4.3.1.2 Regression Correlations

The second step of the procedure plots the results of the direct correlations from all sites and uses least squares regression to fit a trendline to the data and establish general correlations between $N_{1,60cs}$–K_D, $q_{c1N,cs}$-K_D, $N_{1,60cs}$ –E_D, and $q_{c1N,cs}$-E_D.

In making these correlations two assumptions were made. The first was to assume that the effects of any soil variability between the test locations are minimal; as such the effects of such variability are neglected in this study. Table 4.7 summarizes the range of distances between test locations at each site. Among SAM, FD, HWD, and FHS the approximate distance between any of the three DMT, SPT or CPT test locations ranges from 3-70 ft (1-21 m). At GAP, for purposes outside the scope of this thesis, the DMT was performed further away from the SPT and CPT tests. The maximum distance between test locations at GAP is approximately 335 ft (102 m). The vast spatial distance at GAP was considered during the simplified procedure analysis and reserved as a reason to exclude any potential "outlying" data points. Secondly, it was assumed that the minimal changes in elevation (< 2 ft (0.6 m)) between DMT, SPT and CPT test locations does not alter the stratification laterally between test locations (i.e. the source sand at SAM ranges from 9-22 ft (2.7-6.7 m) at all three test locations).

Table 4.7 Summary of Distances between Test Locations at Each Site

Site	Distances between Test Locations	
	(ft)	(m)
SAM	3 – 18	1 – 5.5
GAP	270 – 335	82 - 102
FD	18 – 70	5.5 – 21
HWD	26 – 43	8 – 13
FHS	10 – 18	3 - 5.5

Two different regression correlations were made for each relationship. The first regression correlation followed Tsai et al (2009)'s procedure and used data points from the entire soil profiles of each site and thus included multiple soil types (clays and sands). The second correlation only used the data from the source sand zones of each site, limiting the analysis to the sandy soils that were prone to liquefaction.

4.3.1.2.1 Entire Soil Profile

The results of the first regression correlation, which includes data from the entire soil profile, are shown in Figures 4.28 through 4.31. As shown by the R^2 values of each relation, this method produced rather large scatter and yielded relatively weak relationships compared to the results of Tsai et al. (2009), shown in Figure 4.32. Both the $N_{1,60cs}$–K_D and the $q_{c1N,cs}$–K_D correlations presented in Tsai et al. (2009) (Figure 4.32 (a) and (b), respectively) exhibit an R^2 value of approximately 0.40 while the correlations of this thesis have R^2 values of 0.22 and 0.33 for the $N_{1,60cs}$–K_D and the $q_{c1N,cs}$–K_D relations, respectively. Tsai et al.'s (2009) $N_{1,60cs}$–E_D, and $q_{c1N,cs}$–E_D correlations (Figures 4.32 (c) and (d), respectively) have R^2 values of 0.53 and 0.54, respectively while the $N_{1,60cs}$–E_D, and $q_{c1N,cs}$–E_D correlations of this thesis exhibit R^2 values of 0.56 and 0.50, respectively. Even though the R^2 value of this thesis' $N_{1,60cs}$–E_D correlation is greater than that of Tsai et al. (2009), the relation is still considered relatively weak and is improved by the procedure described in Section 4.3.1.2.2.

The amount of scatter in Figures 4.28 through 4.31 is not unexpected considering that the analysis includes data from a variety of soil types that each behaves differently during SPT, CPT, and DMT testing and in liquefaction inducing events. These poor results

prompted the second regression correlation, where the analysis was restricted to the source sand layers (i.e. one soil type that behaves similarly during liquefaction inducing events).

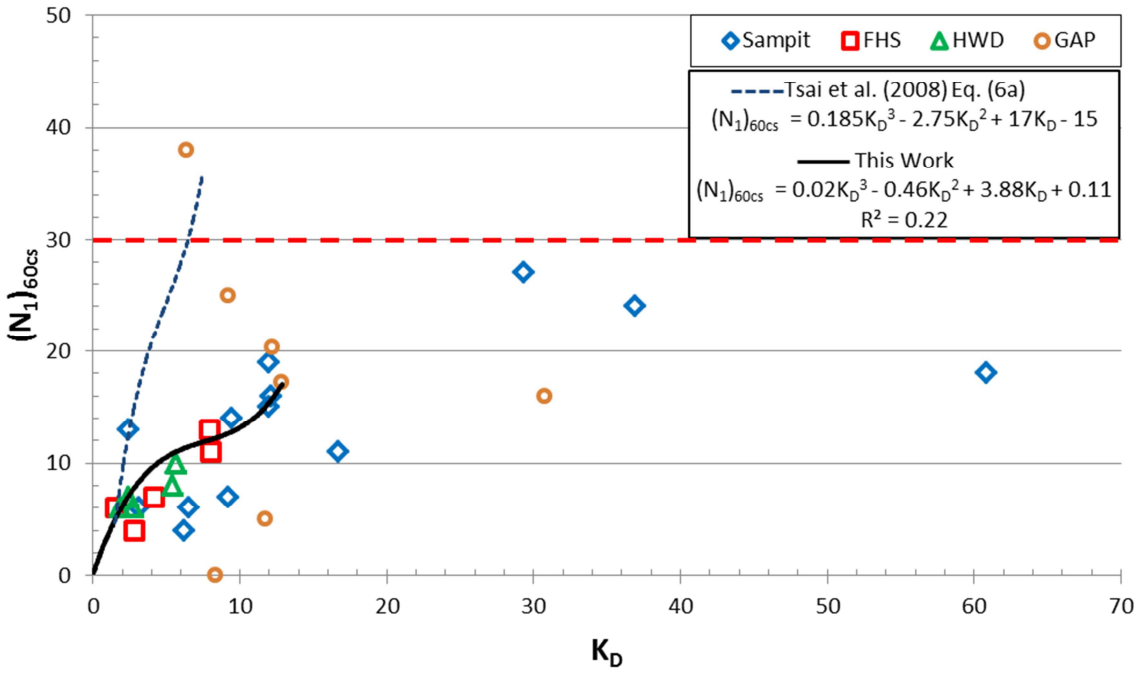

Figure 4.28 Correlations between $(N_1)_{60cs}$ and K_D using the entire soil profile

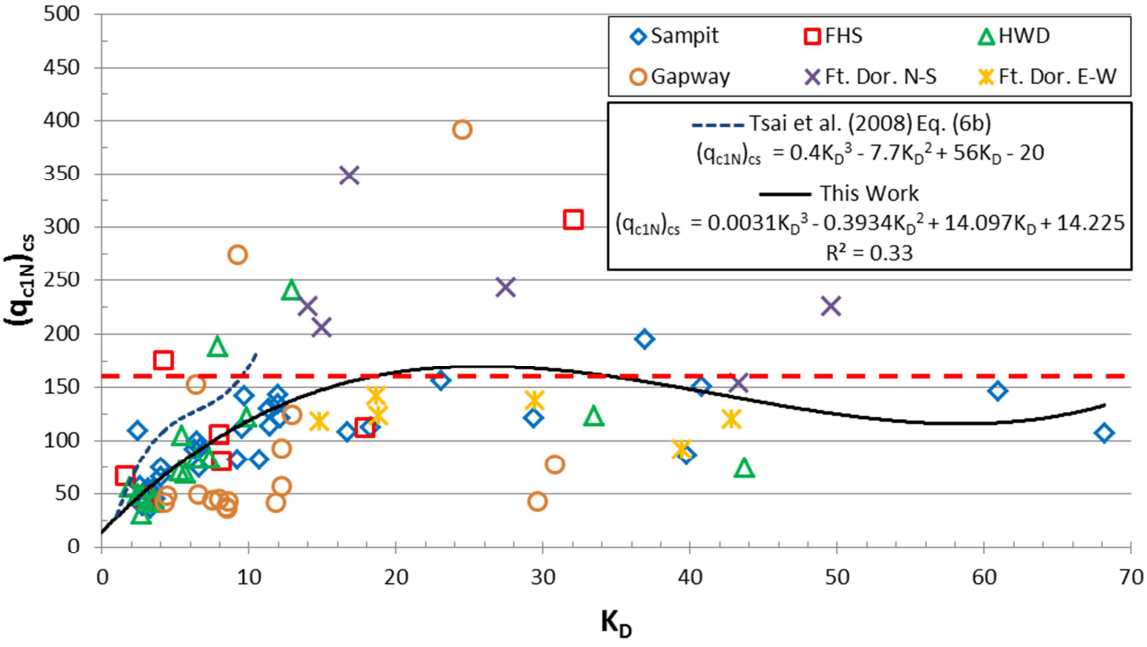

Figure 4.29 Correlations between $(q_{c1N})_{cs}$ and K_D using the entire soil profile

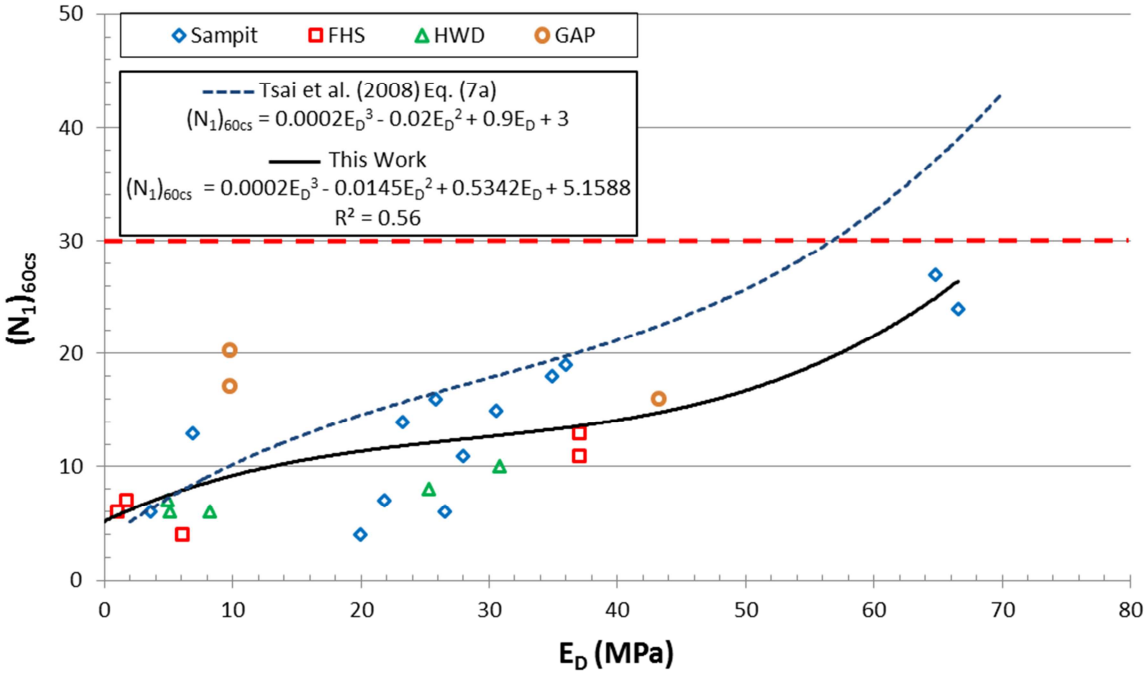

Figure 4.30 Correlations between $(N_1)_{60cs}$ and E_D using the entire soil profile

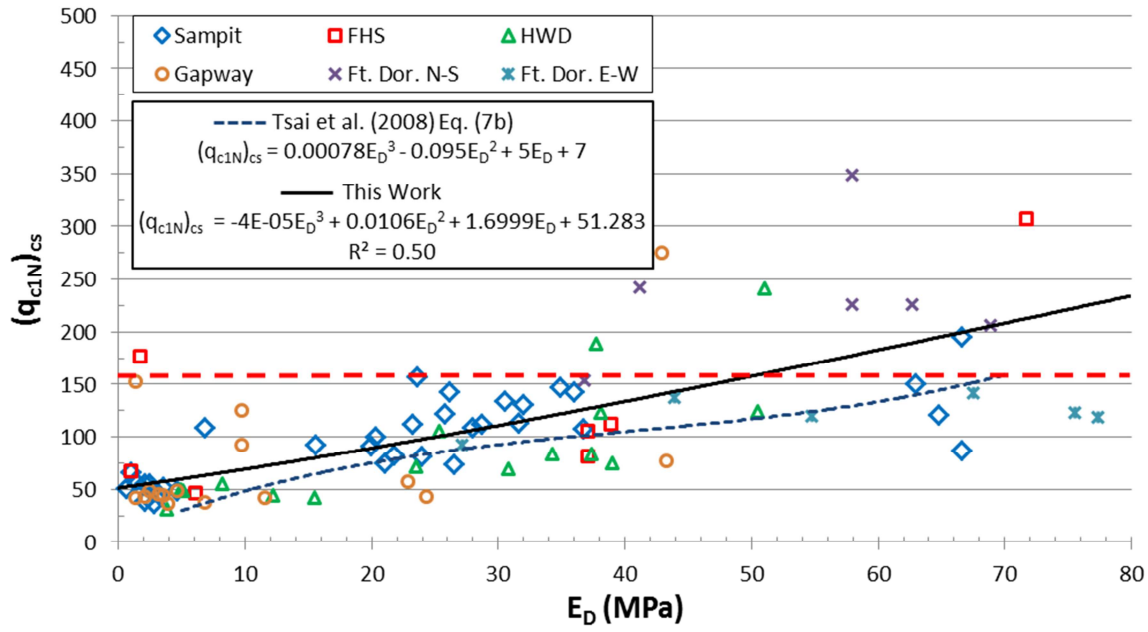

Figure 4.31 Correlations between $(q_{c1N})_{cs}$ and E_D using the entire soil profile

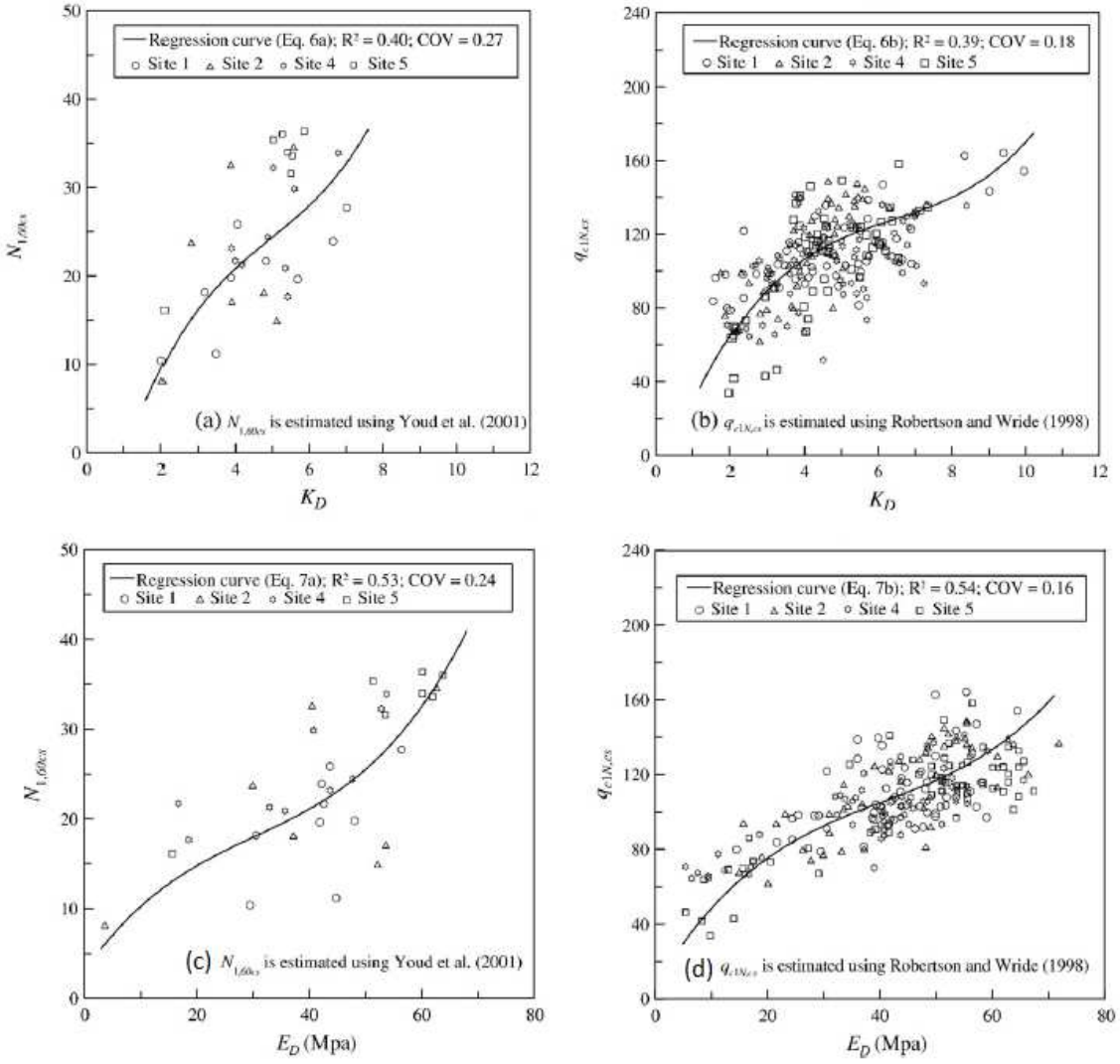

Figure 4.32 Correlations presented by Tsai et al. (2009) for: (a) $(N_1)_{60,cs}$-K_D; (b) $(q_{c1N})_{cs}$-K_D; (c) $(N_1)_{60,cs}$-E_D; (d) $(q_{c1N})_{cs}$-E_D

It should be noted that several points were considered outliers and were excluded from the $N_{1,60cs}$–K_D analysis shown in Figure 4.28. Doing so provided a curve with a similar shape to that presented in Tsai et al. 2009 (Figure 4.32(a); Equation 2.39). Four of the five excluded points had K_D>29 which is relatively high compared to the rest of the data which has a max K_D=17. The fifth excluded point (K_D = 16.7, $N_{1,60cs}$ =11) is from 9 ft (2.7 m) below the ground surface at SAM on the boundary of the source sand layer (9-

22 ft (2.7-6.7 m)). Including this point in the regression analysis not only reduced the R^2 value of the trendline but also changed the concavity of the curve and produced a shape much different than the shape presented by Tsai et al. (2009). Excluding this point is justified by considering that it lies on the boundary of the source sand zone and as such, its inclusion in the analysis is uncertain in the first place.

4.3.1.2.2 Source Sand Only

The results of the second regression correlation, where the analysis was restricted to only include data from the source sand layer, are shown in Figures 4.33 through 36. This analysis provided slightly stronger relationships, with R^2 values ranging from 0.31-0.66. The relation with the lowest R^2 value is the $N_{1,60cs}$–E_D relation. Upon further review of Figure 4.35 it is noted that the low R^2 is caused by the outlying points from Gapway. It is assumed that the irregularity of the GAP data points (with respect to the rest of the data) is due to the vast spatial difference between the DMT and the SPT at GAP (approximately 335 ft (102 m)). If the Gapway data were excluded from Figure 4.35 the resulting R^2 value would be greater.

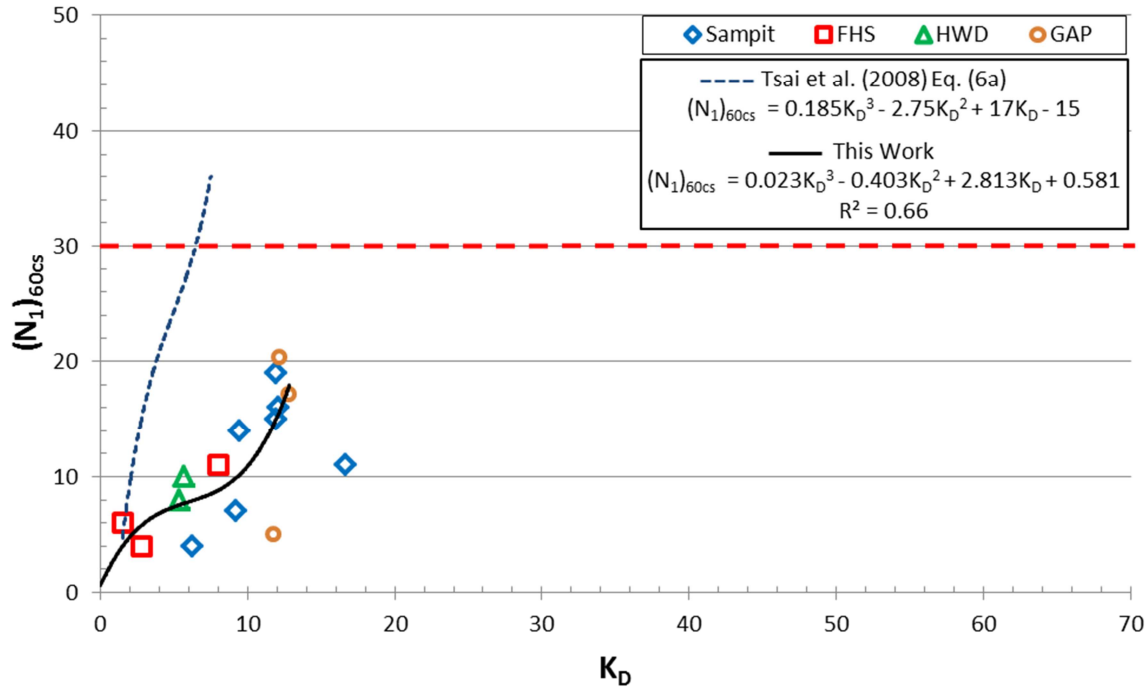

Figure 4.33 Correlations between $(N_1)_{60cs}$ and K_D for the source sand layer

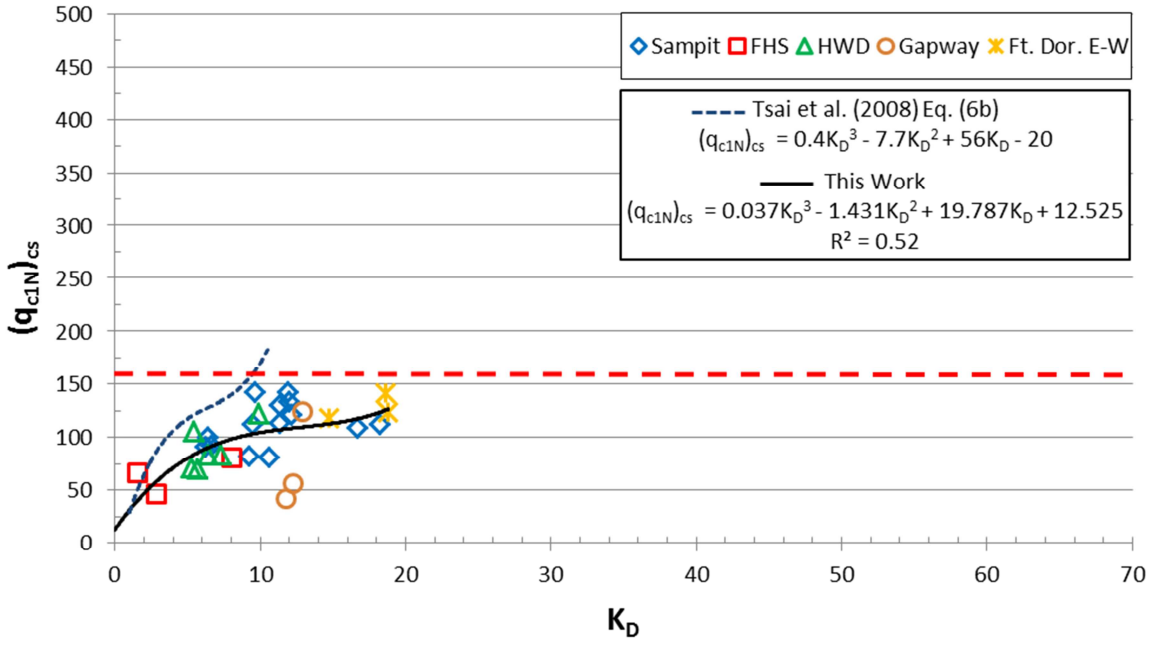

Figure 4.34 Correlations between $(q_{c1N})_{cs}$ and K_D for the source sand layer

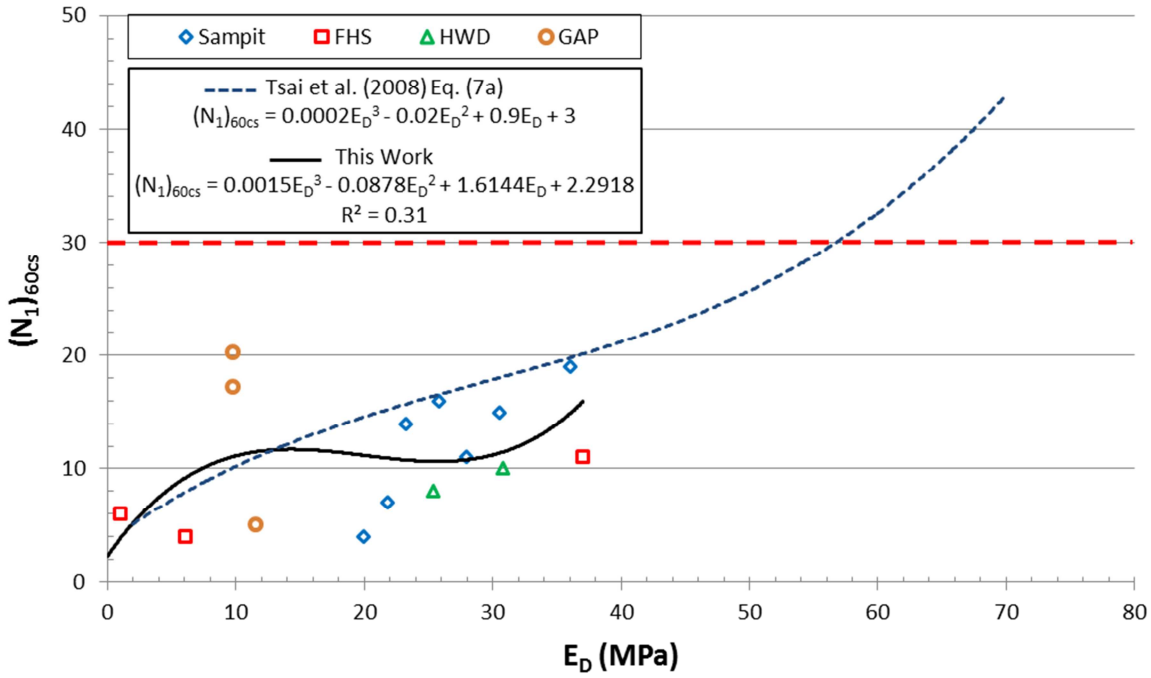

Figure 4.35 Correlations between $(N_1)_{60cs}$ and E_D for the source sand layer

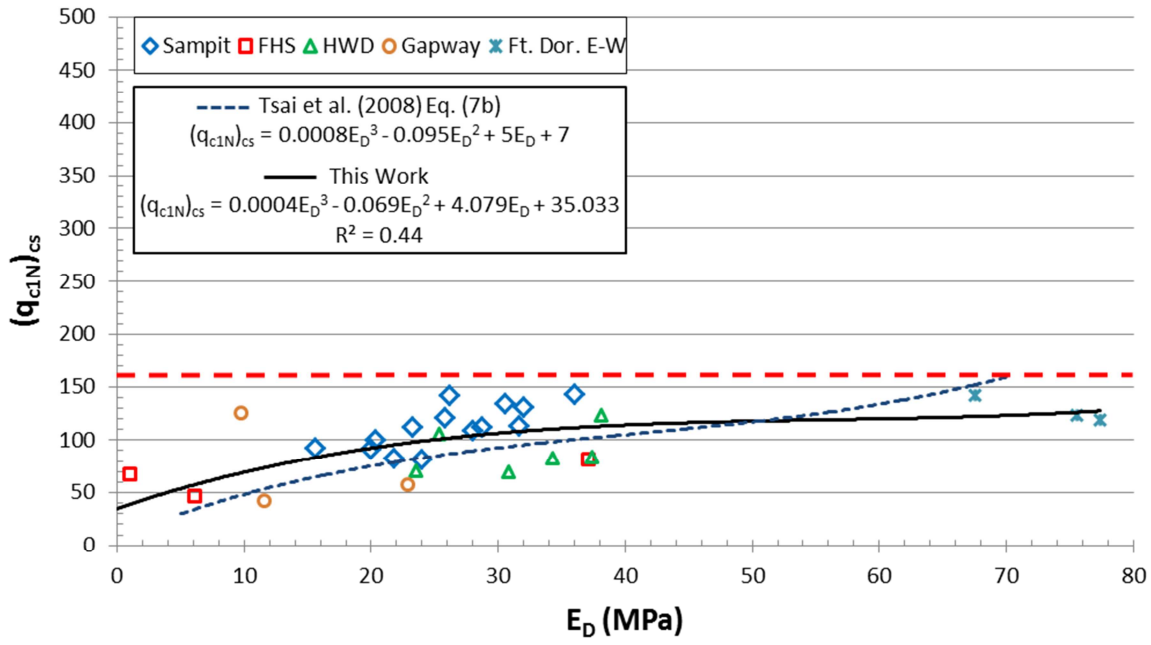

Figure 4.36 Correlations between $(q_{c1N})_{cs}$ and E_D for the source sand layer

The best fit relations of the data from the source sand zones only are as follows:

For the correlations related to K_D (Figure 4.33 and 4.34):

$$N_{1,60cs} = 0.023K_D^3 - 0.403K_D^2 + 2.813K_D + 0.581; \quad R^2 = 0.66 \tag{4.1}$$

$$q_{c1N_{cs}} = 0.037K_D^3 - 1.431K_D^2 + 19.787K_D + 12.525; \quad R^2 = 0.52 \tag{4.2}$$

For the correlations related to E_D (Figure 4.35 and 4.36):

$$N_{1,60cs} = 0.0015E_D^3 - 0.0878E_D^2 + 1.6144E_D + 2.2918; \quad R^2 = 031 \tag{4.3}$$

$$q_{c1N_{cs}} = 0.0004E_D^3 - 0.069E_D^2 + 4.079E_D + 35.033; \quad R^2 = 0.44 \tag{4.4}$$

It should be noted that the R^2 values of the K_D relations of this thesis (Equations 4.1 and 4.2) are greater than that presented by Tsai et al. (2009) (Equations 2.40 and 2.38) while the R^2 values of the E_D relations of this thesis (Equations 4.3 and 4.4) are less than that presented by Tsai et al. (2009) (Equations 2.41 and 2.39). The degree of scatter in Figures 4.33 through 4.36 should not be unexpected due to the different means and methods associated with the three tests and because of the actual soil variability between test locations at each site. However, it is noted that all source sand zone only curves (Figures 4.33 through 4.36) have a similar shape to that which is presented in Tsai et al. (2009) (Figure 4.32), yet Tsai's curves overestimate much of the SCCP data. Nearly all of the data points fall below Tsai's $(N_1)_{60cs}$-K_D, $(q_{c1N})_{cs}$-K_D, and $(N_1)_{60cs}$-E_D curves, while Tsai's $(q_{c1N})_{cs}$-E_D curve has numerous data points both above and below the curve. The incompatibility between the two relationships is to be expected considering that Tsai's relations are derived from test data of Holocene soils in Taiwan. Still, the fact that the relations have similar graphical shapes suggests that the same general relationships exist between both cases' data, but that Tsai's curves must be shifted in order to be applicable to SCCP soils.

Figures 4.37 through 4.40 compare the measured SPT/CPT values to those calculated from Equations 4.1 through 4.4 to illustrate the accuracy of the proposed correlations. Figure 4.37 compares the accuracy of the $N_{1,60cs}$–K_D correlations presented in this thesis (Equation 4.1) with that presented in Tsai et al.(2009) (Equation 2.40). This figure shows that for a given K_D, Tsai's correlation overestimates $N_{1,60cs}$ in SCCP soils by as much as 350%. Figures 4.38 and 4.39 compare the correlations for $q_{c1N,cs}$-K_D and $N_{1,60cs}$ –E_D, respectively, and show that Tsai's correlations overestimate $q_{c1N,cs}$ and $N_{1,60cs}$ by up to 180 and 55 %, respectively. Figure 4.40 shows a similar degree of scatter for the $q_{c1N,cs}$-E_D correlations from both this thesis (Equations 4.4) and Tsai et al. (2009) (Equation 2.39). In summary, Tsai et al. (2009)'s $N_{1,60cs}$–K_D, $q_{c1N,cs}$–K_D, and $N_{1,60cs}$–E_D correlations consistently over predict the $N_{1,60cs}$ and $q_{c1N,cs}$ values for SCCP soils, whereas their $q_{c1N,cs}$–E_D correlation provides reasonable estimates for SCCP soils.

It seems unique that the SCCP data agrees with Tsai's correlation for $q_{c1N,cs}$-E_D but not with his $q_{c1N,cs}$-K_D correlations. The reason for this may lie in the differences in the soil parameters themselves and what each one actually measures. Considering that E_D measures stiffness, K_D measures earth pressure, and q_c measures bearing capacity, it may be that there is more scatter in the K_D data because this is the only parameter that can measure stress history (aging and cementation) (Marchetti, 2011; Tsai et al., 2009; and Monaco et al., 2005). Because E_D, and q_c cannot detect the increased liquefaction resistance that results from aging and cementation the data from these two parameters would be different from the K_D data which is sensitive to stress history. Marchetti et al. (2001) states that because E_D lacks information on stress history it should only be used in combination with I_D and K_D.

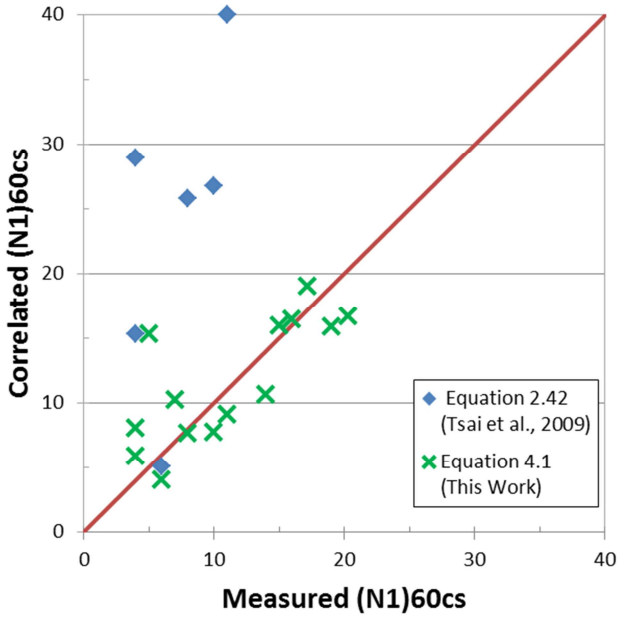

Figure 4.37 Correlation between measured $N_{1,60cs}$ and $N_{1,60cs}$ calculated from Equation 4.1 (This Work) and Equation 2.42 (Tsai et al., 2009) using K_D from DMT tests

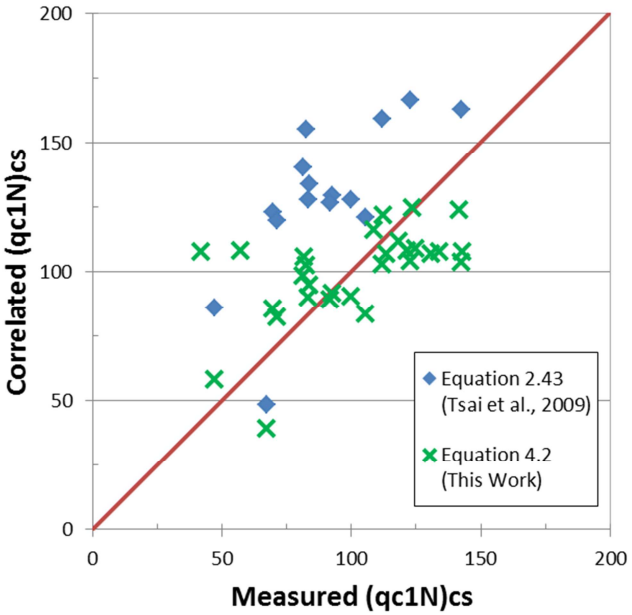

Figure 4.38 Correlation between measured $q_{c1N,cs}$ and $q_{c1N,cs}$ calculated from Equation 4.2 (This Work) and Equation 2.43 (Tsai et al., 2009) using K_D from DMT tests

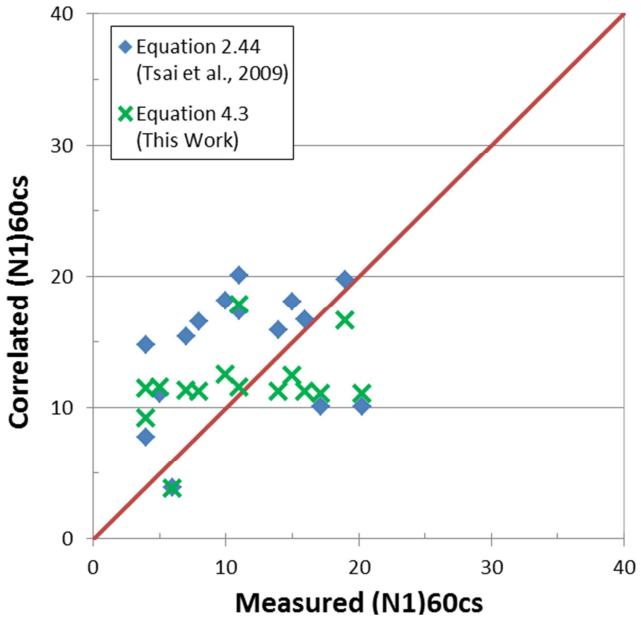

Figure 4.39 Correlation between measured $N_{1,60cs}$ and $N_{1,60cs}$ calculated from Equation 4.3 (This Work) and Equation 2.44 (Tsai et al., 2009) using E_D from DMT tests

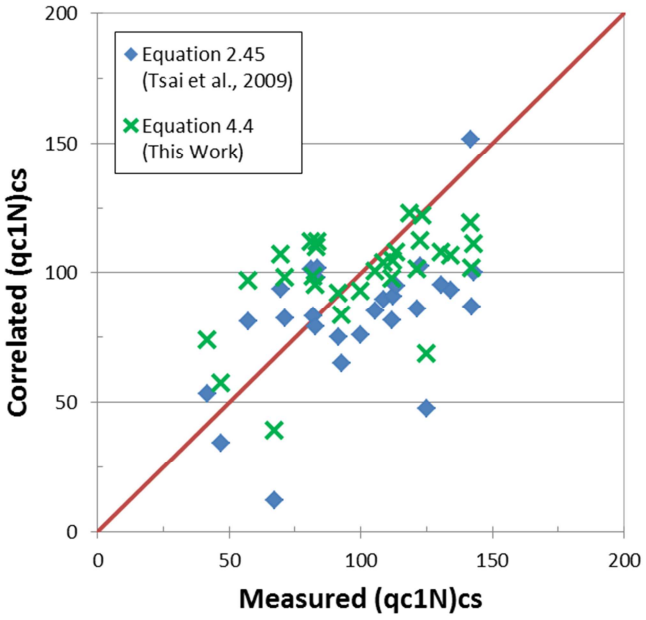

Figure 4.40 Correlation between measured $q_{c1N,cs}$ and $q_{c1N,cs}$ calculated from Equation 4.4 (This Work) and Equation 2.45 (Tsai et al., 2009) using E_D from DMT tests

4.3.2 Liquefaction Analysis of SCCP Soils Using the Existing Relations

Figure 4.41 presents the existing CRR-K_D relations presented by Grasso & Maugeri (2006), Monaco et al. (2005), and Tsai et al. (2009) plotted with the SCCP data. The CRR of the SCCP data was calculated using the Idriss and Boulanger (2006) CRR-$N_{1,60cs}$ relation (Eq 2.46) and the Robertson and Wride (1998) CRR- $q_{c1N,cs}$ relation (Eq 2.47 and 2.48) using the measured $N_{1,60cs}$ and $q_{c1N,cs}$ at the same depth as the measured K_D. In this way each K_D value has two CRR values: one calculated from $N_{1,60cs}$ and one calculated from $q_{c1N,cs}$. The open symbols in Figure 4.41 denote the points where CRR was calculated using $N_{1,60cs}$ data while the closed symbols represent points from which CRR was calculated using $q_{c1N,cs}$ data. Table 4.8 presents the CRR values calculated by both methods and the difference between the two values. Although there is a significant difference (35% on average) in the CRR obtained from the two methods, with the exception of a couple points, the SCCP data plots below and to the right of the existing CRR-K_D relations.

The CRR-K_D relations represent lines that distinguish potentially liquefiable soils from unliquefiable soils. The data points shown in Figure 4.41 all come from the source sand zones of the different sites, where sandblows have been found as evidence of prehistoric liquefaction. Figure 4.41 indicates that all of the SCCP source sands would be considered currently not prone to liquefaction. Recall from Chapter 2 that the equations used to calculate CRR in Figure 4.41 and Table 4.8 (the Idriss and Boulanger (2007) CRR-SPT relation (Equation 2.46) and the Robertson and Wride (1998) CRR-CPT relation (Equations 2.47 and 2.48)) were derived from data from Holocene soils. Figure 4.41 supports Leon et al.'s (2006) work that shows the Idriss and Boulanger (2007) CRR-

SPT relation and the Robertson and Wride (1998) CRR-CPT relation for Holocene soils are not applicable to SCCP soils; therefore, soil aging must be taken into effect.

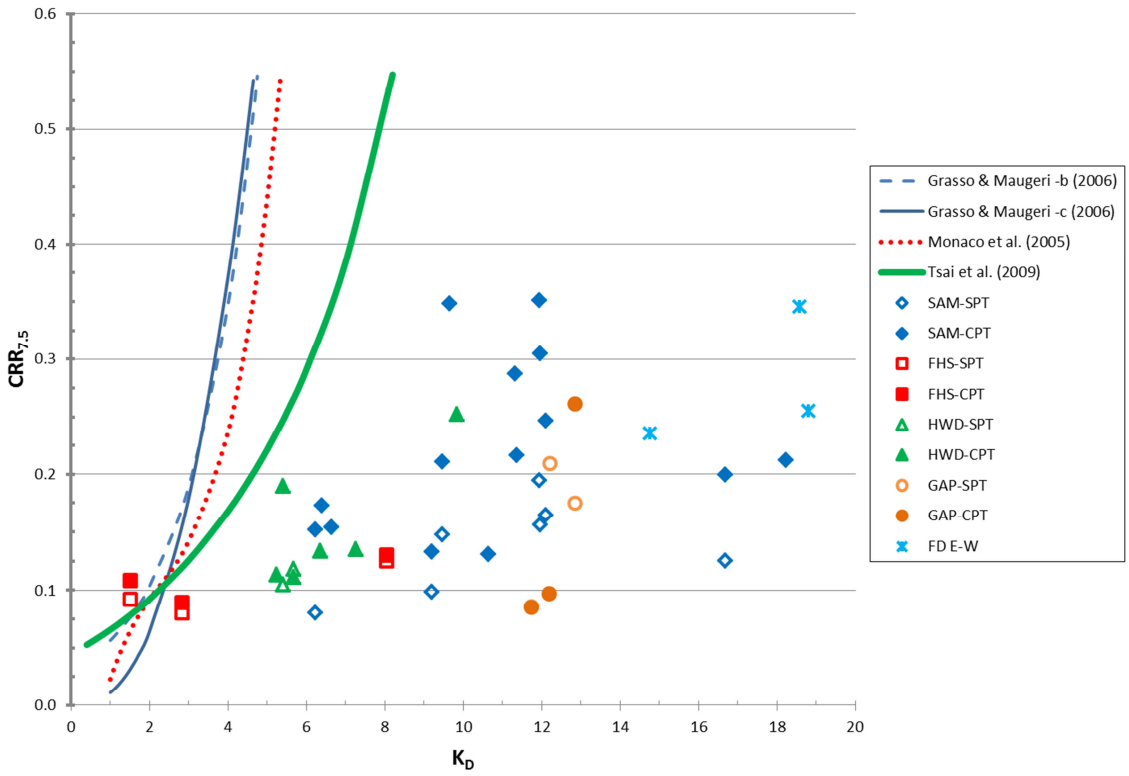

Figure 4.41 Comparison of SCCP Data with Existing CRR-K_D Relations
Note: Open symbols denote CRR calculated through $N_{1,60cs}$,
Closed symbols denote CRR calculated through $q_{c1N,cs}$

Table 4.8 Summary of CRR Calculations

	Depth (ft)	Depth (m)	K_D	E_D (MPa)	$(N_1)_{60cs}$	$(q_{c1N})_{cs}$	SPT derived $CRR_{7.5}$ [1]	CPT derived $CRR_{7.5}$ [2]	Δ
SAM	9	2.7	16.7	28.0	11	108.7	0.13	0.20	0.07
	10	3.0	18.2	28.7	-	112.4	-	0.21	-
	11	3.4	12.1	25.8	16	121.5	0.16	0.25	0.08
	12	3.7	9.7	26.2	-	142.4	-	0.35	-
	13	4.0	9.5	23.2	14	112.1	0.15	0.21	0.06
	14	4.3	10.6	24.0	-	81.8	-	0.13	-
	15	4.6	9.2	21.8	7	82.8	0.10	0.13	0.03
	16	4.9	6.7	15.6	-	92.7	-	0.15	-
	17	5.2	6.2	20.0	4	91.7	0.08	0.15	0.07
	18	5.5	11.4	31.6	-	113.7	-	0.22	-
	19	5.8	12.0	30.5	15	134.2	0.16	0.30	0.15
	20	6.1	11.3	32.0	-	130.7	-	0.29	-
	21	6.4	11.9	36.0	19	142.9	0.19	0.35	0.16
	22	6.7	6.4	20.3	-	99.9	-	0.17	-
FHS	10	3.0	8.0	37.1	11	81.4	0.13	0.13	0.01
	12	3.7	2.8	6.1	4	47.0	0.08	0.09	0.01
	14	4.3	1.5	1.0	6	67.3	0.09	0.11	0.02
HWD	9	2.7	9.8	38.1	-	122.8	-	0.25	-
	10	3.0	7.3	37.3	-	83.8	-	0.13	-
	11	3.4	5.4	25.3	8	105.6	0.10	0.19	0.09
	12	3.7	6.4	34.2	-	83.3	-	0.13	-
	13	4.0	5.7	30.8	10	69.7	0.12	0.11	0.01
	14	4.3	5.2	23.5	-	71.1	-	0.11	-
GAP	5	1.5	12.9	9.8	17	124.9	0.18	0.26	0.08
	6	1.8	12.2	22.9	-	57.2	-	0.10	-
	7	2.1	11.7	11.6	5	41.9	0.09	0.08	0.01
FD-EW	8	2.4	18.6	67.6	-	141.9	-	0.35	-
	10	3.0	18.8	75.6	-	123.6	-	0.25	-
	12	3.7	14.8	77.4	-	118.8	-	0.24	-
						average	0.17		0.06
							average difference		35%

[1] CRR calculated using Equation 2.44
[2] CRR calculated using Equations 2.45 and 2.46

4.3.3 Liquefaction Analysis of SCCP Soils Considering the Effects of Aging

The effects of aging on SCCP soils were accounted for by implementing the Leon et al. (2006) methodology presented in Section 2.4.2.1. The $(N_1)_{60cs}$ and $(q_{c1N})_{cs}$ values from the source sand zones at each site were used in conjunction with Equations 2.54 through 2.56 to evaluate the liquefaction resistance of the soils in their aged/current state. Through utilization of this thesis' direct correlations (presented in Section 4.3.1.1 and summarized in Table 4.6) the $(CRR)_{aged/current}$ values obtained from Leon's methodology were then plotted with the measured K_D and E_D values associated with the depth that $(N_1)_{60cs}$ and $(q_{c1N})_{cs}$ originated. The data was then compared to the CRR-K_D and CRR-E_D relations presented in the literature to reevaluate the liquefaction potential of the source sand layers; this time accounting for aging.

The CRR-SPT and CRR-CPT boundary curves for SCCP aged soils developed by Leon et al. (2006) for 546-5,038 years, 200,000 years, and 450,000 years were transformed into CRR-K_D and CRR-E_D curves by reproducing Leon's CRR-SPT and CRR-CPT curves by picking points off of the curves so that equations for each of the curves could be derived. The equations of Leon's curves were then used in conjunction with this thesis' SPT-DMT and CPT-DMT regression correlations (Equations 4.1 through 4.4) to derive CRR-DMT curves. The equations of Leon's curves used in this analysis are as follows:

CRR-SPT curves:

For $546 - 5{,}038$ years:

$$\mathrm{CRR} = 0.0911 * e^{0.067*(N_1)_{60cs}} \qquad 4.5$$

For 200,000 years:

$$\mathrm{CRR} = 0.0028 * [(\mathrm{N_1})_{60cs}]^2 - 0.0268 * (\mathrm{N_1})_{60cs} + 0.1984 \quad (4.6)$$

For 450,000 years:

$$\mathrm{CRR} = 0.0955 * \mathrm{e}^{0.0739*(\mathrm{N_1})_{60cs}} \quad (4.7)$$

CRR-CPT curves:

For $546 - 5038$ years:

$$\mathrm{CRR} = 0.0036 * [(\mathrm{q_{c1N}})_{cs}]^2 - 0.0473 * (\mathrm{q_{c1N}})_{cs} + 0.3616 \quad (4.8)$$

For 200,000 years:

$$\mathrm{CRR} = 0.0033 * [(\mathrm{q_{c1N}})_{cs}]^2 - 0.025 * (\mathrm{q_{c1N}})_{cs} + 0.2267 \quad (4.9)$$

For 450,000 years:

$$\mathrm{CRR} = 0.0014 * [(\mathrm{q_{c1N}})_{cs}]^2 - 0.0035 * (\mathrm{q_{c1N}})_{cs} + 0.1676 \quad (4.10)$$

Note that the equations above are only valid over the range for which Leon et al. (2006) presented the curves. This range was preserved in the transformation into CRR-DMT curves. Table 4.9 below presents the range of validity of all parameters.

Table 4.9 Range of Validity for Leon et al.'s (2006) CRR-SPT and CRR-CPT Curves

Equation	Range of $(N_1)_{60cs}$	Range of $(q_{c1N})_{cs}$	Range of K_D	Range of E_D (Mpa)
4.5	8 - 18	-	6.2 - 12.6	4.6 - 37.2
4.6	5 - 9	-	2.2 - 7.9	1.9 - 5.8
4.7	9 - 16	-	7.9 - 12.0	5.8 - 35.4
4.8	-	5.5 - 15.5	2.8 - 23.1	6.1 - 78.0
4.9	-	4.0 - 6.5	1.7 - 3.7	1.7 - 9.5
4.10	-	3.0 – 11.0	1.0 - 16.1	0 - 42.8

Note: Range of K_D and E_D derived through this thesis' SPT-DMT and CPT-DMT regression correlations (Equations 4.1 through 4.4)

For each point in the soil profile CRR was calculated multiple ways. Leon's methodology was implemented using both the SPT and CPT data. (This yields two different CRR values for the same point in the soil profile.) CRR was also calculated using two different values of *t*, where *t* is equal to the age of the liquefaction inducing earthquake and where *t* is equal to the age of the soil deposit (this assumes the soil has never liquefied and yields a greater CRR value for comparison). In short, there are as many as four different values of CRR for each point in the soil profile. Table 4.10 presents a summary of CRR values obtained through the different methods, along with the different field test parameters used in the calculation of CRR. Table 4.11 presents a summary of the different ages used in the analysis.

Table 4.10 Summary of CRR values obtained through the different methods

			Field Data				Holocene CRR Values		Aged CRR Values			
	Depth (ft)	Depth (m)	$(N_1)_{60cs}$	(qc1N)cs	K_D	E_D (MPa)	SPT-derived CRR [1]	CPT-derived CRR [2]	SPT-derived CRR [3] (t=1,021 years)	SPT-derived CRR [3] (t=450,000 years)	CPT-derived CRR [4] (t=1,021 years)	CPT-derived CRR [4] (t=450,000 years)
Sampit	9	2.7	11	108.7	16.7	28.0	0.13	0.20	0.21	0.25	0.27	0.30
	10	3.0	-	112.4	18.2	28.7	-	0.21	-	-	0.28	0.31
	11	3.4	16	121.5	12.1	25.8	0.16	0.25	0.26	0.31	0.31	0.34
	12	3.7	-	142.4	9.7	26.2	-	0.35	-	-	0.41	0.43
	13	4.0	14	112.1	9.5	23.2	0.15	0.21	0.24	0.28	0.28	0.31
	14	4.3	-	81.8	10.6	24.0	-	0.13	-	-	0.20	0.24
	15	4.6	7	82.8	9.2	21.8	0.10	0.13	0.17	0.21	0.20	0.24
	16	4.9	-	92.7	6.7	15.6	-	0.15	-	-	0.22	0.26
	17	5.2	4	91.7	6.2	20.0	0.08	0.15	0.14	0.18	0.22	0.25
	18	5.5	-	113.7	11.4	31.6	-	0.22	-	-	0.28	0.31
	19	5.8	15	134.2	12.0	30.5	0.16	0.30	0.25	0.30	0.37	0.39
	20	6.1	-	130.7	11.3	32.0	-	0.29	-	-	0.35	0.38
	21	6.4	19	142.9	11.9	36.0	0.19	0.35	0.30	0.35	0.41	0.43
	22	6.7	-	99.9	6.4	20.3	-	0.17	-	-	0.24	0.27
	Average		12	112.0	11.0	16.5	0.13	0.21	0.22	0.26	0.28	0.31

			Field Data				Holocene CRR Values		Aged CRR Values			
	Depth (ft)	Depth (m)	$(N_1)_{60cs}$	(qc1N)cs	K_D	E_D (MPa)	SPT-derived CRR [1]	CPT-derived CRR [2]	SPT-derived CRR [3] (t=5,038 years)	SPT-derived CRR [3] (t=450,000 years)	CPT-derived CRR [4] (t=5,038 years)	CPT-derived CRR [4] (t=450,000 years)
Gapway	4	1.2	20	93.0	12.2	9.8	0.21	0.15	0.33	0.36	0.23	0.26
	5	1.5	17	124.9	12.9	9.8	0.18	0.26	0.29	0.32	0.33	0.35
	6	1.8	-	57.2	12.2	22.9	-	0.10	-	-	0.18	0.20
	7	2.1	5	41.9	11.7	11.6	0.09	0.08	0.16	0.19	0.16	0.18
	Average		14	109.0	12.5	9.8	0.15	0.20	0.25	0.28	0.27	0.30

Note: Average CRR values calculated Using Average Field Data Values

[1] Equation 2.35

[2] Equation s 2.36-2.37

[3] CRR calculated using $(N_1)_{60,cs}$ and the Leon et al. (2006) methodology for SPT data

[4] CRR calculated using $(q_{c1N})_{cs}$ and the Leon et al. (2006) methodology for CPT data

Table 4.10 Summary of CRR values obtained through the different methods (continued)

			Field Data				Holocene CRR Values		Aged CRR Values			
	Depth (ft)	Depth (m)	$(N_1)_{60cs}$	(qc1N)cs	K_D	E_D (MPa)	SPT-derived CRR [1]	CPT-derived CRR [2]	SPT-derived CRR [3] (t=5,000 years)	SPT-derived CRR [3] (t=200,000 years)	CPT-derived CRR [4] (t=5,000 years)	CPT-derived CRR [4] (t=200,000 years)
Fort Dorchester	8	2.4	-	141.9	18.6	67.6	-	0.35	-	-	0.41	0.42
	10	3	-	123.5	18.8	75.6	-	0.25	-	-	0.33	0.34
	12	3.7	-	118.6	14.8	77.4	-	0.24	-	-	0.31	0.32
	Average		-	128.0	17.4	73.5	-	0.27	-	-	0.35	0.36

			Field Data				Holocene CRR Values		Aged CRR Values			
	Depth (ft)	Depth (m)	$(N_1)_{60cs}$	(qc1N)cs	K_D	E_D (MPa)	SPT-derived CRR [1]	CPT-derived CRR [2]	SPT-derived CRR [3] (t=500 years)	SPT-derived CRR [3] (t=125,000 years)	CPT-derived CRR [4] (t=500 years)	CPT-derived CRR [4] (t=125,000 years)
Hollywood	9	2.7	-	122.8	9.8	38.1	-	0.25	-	-	0.32	0.34
	10	3.0	-	83.8	7.3	37.3	-	0.13	-	-	0.20	0.23
	11	3.4	8	105.6	5.4	25.3	0.1	0.19	0.18	0.21	0.26	0.28
	12	3.7	-	83.3	6.4	34.2	-	0.13	-	-	0.20	0.23
	13	4.0	10	69.7	5.7	30.8	0.12	0.11	0.19	0.23	0.18	0.21
	14	4.3	-	71.1	5.2	23.5	-	0.11	-	-	0.18	0.21
	Average		9	89.4	6.6	31.5	0.11	0.15	0.19	0.22	0.21	0.24

			Field Data				Holocene CRR Values		Aged CRR Values			
	Depth (ft)	Depth (m)	$(N_1)_{60cs}$	(qc1N)cs	K_D	E_D (MPa)	SPT-derived CRR [1]	CPT-derived CRR [2]	SPT-derived CRR [3] (t=1,660 years)	SPT-derived CRR [3] (t=1.5 million years)	CPT-derived CRR [4] (t=1,660 years)	CPT-derived CRR [4] (t=1.5 million years)
Four Hole Swamp	10	3	11	81.4	8.0	37.1	0.13	0.13	0.21	0.25	0.20	0.24
	12	3.7	4	47.0	2.8	6.1	0.08	0.09	0.15	0.18	0.16	0.19
	14	4.3	6	67.3	1.5	1.0	0.09	0.11	0.16	0.20	0.18	0.22
	Average		7	65.2	4.1	14.7	0.10	0.11	0.17	0.21	0.18	0.21

Note: Average CRR values calculated Using Average Field Data Values

[1] Equation 2.35

[2] Equation s 2.36-2.37

[3] CRR calculated using $(N_1)_{60,cs}$ and the Leon et al. (2006) methodology for SPT data

[4] CRR calculated using $(q_{c1N})_{cs}$ and the Leon et al. (2006) methodology for CPT data

Table 4.11 Age of Soil Deposits and Liquefaction Inducing Earthquakes

Site	Age of Soil Deposit (years)	Age of Earthquake (years)
Sampit	450,000 [1]	1,021 [5,6]
Gapway	450,000 [1]	5,038 [5,6]
Fort Dorchester	200,000 [1]	5,000 [7,1]
Hollywood	120,000-130,000 [2]	500 [7,8]
Four Hole Swamp	1.4-1.6 Million [4]	1,660 [9]

[1] Weems & Lemon, 1984; [2] Weems & Lemon, 1986; [3] Weems et al., 1986; [4] Weems et al., 1997; [5] Leon et al., 2006; [6] Talwani and Schaeffer, 2001; [7] Hasek et al. 2012; [8] Talwani and Cox, 1985; [9] Rajendran and Talwani, 1993

Figures 4.42 through 4.46 for SAM, GAP, FD, HWD, and FHS, respectively, show the range of CRR corrected for the effects of aging using the Leon et al. (2006) methodology. Part (a) of Figures 4.42, 4.43, 4.45, and 4.46 show the CRR-K_D data where the values of CRR were derived from the Leon et al. (2006) methodology using the SPT data from each site. The data is plotted with the transformed version of Leon et al.'s (2006) CRR-SPT relations as well as the existing CRR-DMT relations of Grasso and Maugerri (2006- Equation C), Monaco et al. (2005), Tsai et al. (2009), and the transformed version of the Idriss and Boulanger (2006) CRR-SPT relation.

Part (b) of Figures 4.42, 4.43, 4.45, and 4.46 and part (a) of Figure 4.44 also show CRR-K_D data but the CRR values in these subfigures were derived by incorporating each site's CPT data into the Leon et al. (2006) methodology. The Leon et al. (2006) curves shown in the (b) subfigures (and (a) subfigure of 4.44) have been transformed from the original Leon et al. (2006) CRR-CPT relations. The same existing CRR-DMT relations of Grasso and Maugerri (2006- Equation C), Monaco et al. (2005), and Tsai et al. (2009)

from the (a) subfigures are reproduced in the (b) subfigures, along with the transformed version of the Robertson and Wride (1998) CRR-CPT relation.

Part (c) of Figures 4.42, 4.43, 4.45, and 4.46 show the CRR-E_D data where the CRR values were obtained through the use of the Leon et al. (2006) methodology using SPT data. The transformed curves of Leon et al. (2006) were derived from the original CRR-SPT curves of Leon et al. (2006). The only existing CRR-E_D relation is by Tsai et al. (2009) and is also shown in the (c) subfigures. Part (d) of Figures 4.42, 4.43, 4.45, and 4.46 and part (b) of Figure 4.44 are similar to the (c) subfigures of Figures 4.42, 4.43, 4.45, and 4.46 but CRR was obtained using CPT data and the Leon et al. (2006) curves presented have been transformed from the original CRR-CPT curves of Leon et al. (2006).

Figures 4.47 and 4.48 present a summary of Figures 4.42 through 4.46 by plotting the average values from each site's source sand.

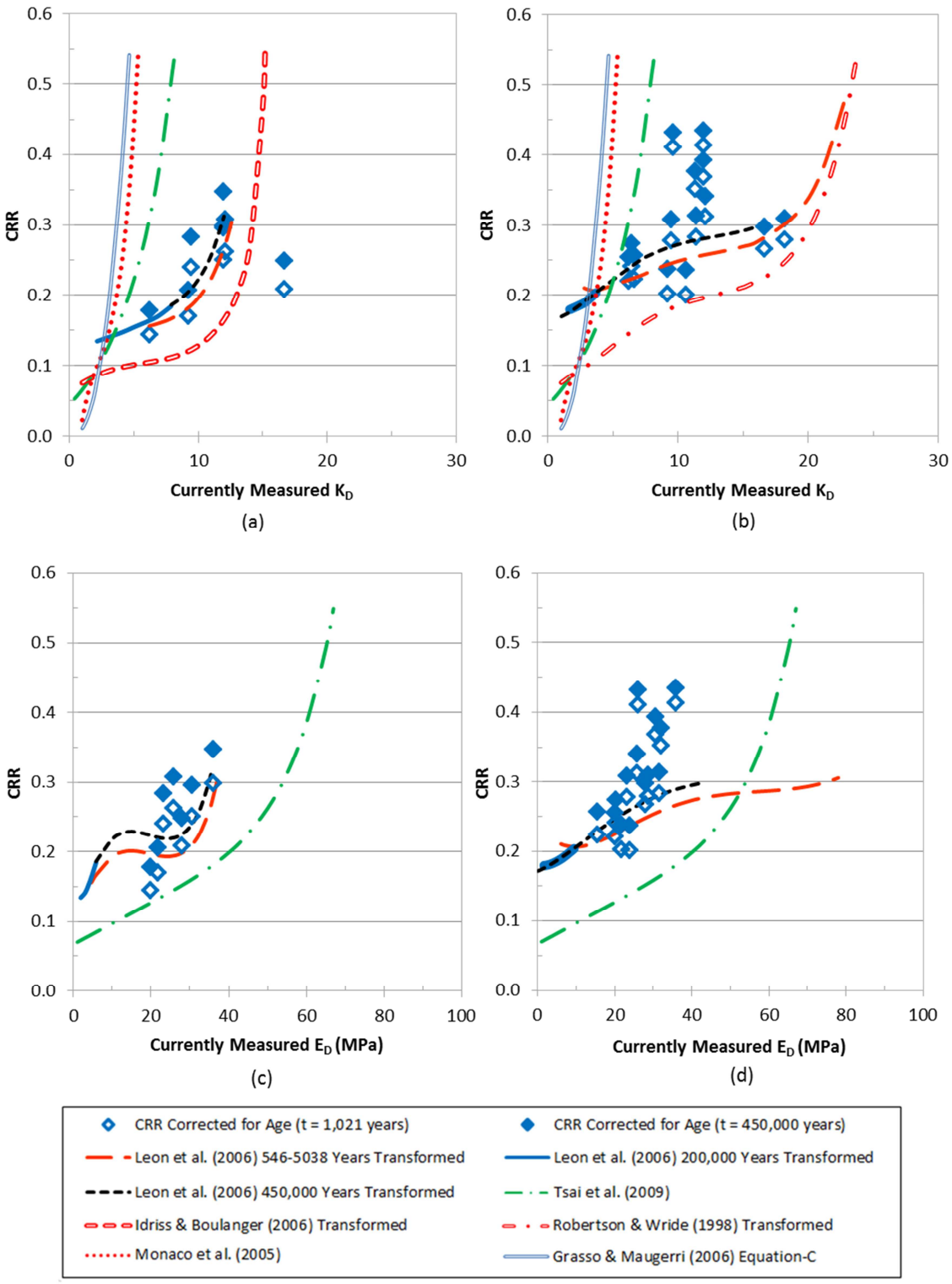

Figure 4.42 Range of CRR for the Sampit Source Sand: (a) SPT derived CRR-K_D relation; (b) CPT derived CRR-K_D relation; (c) SPT derived CRR-E_D relation; (d) CPT derived CRR-K_D relation

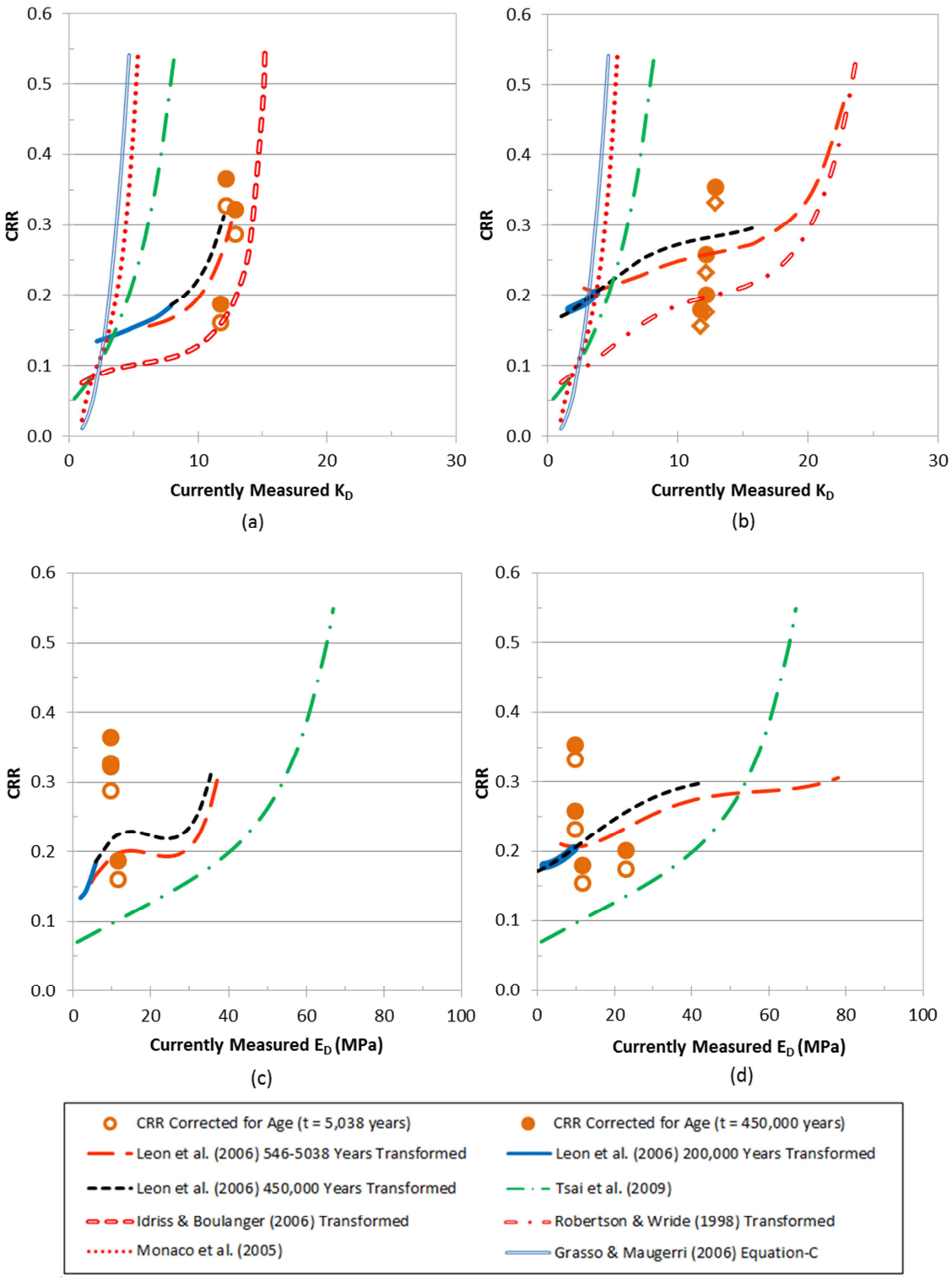

Figure 4.43 Range of CRR for the Gapway Source Sand: (a) SPT derived CRR-K_D relation; (b) CPT derived CRR-K_D relation; (c) SPT derived CRR-E_D relation; (d) CPT derived CRR-K_D relation

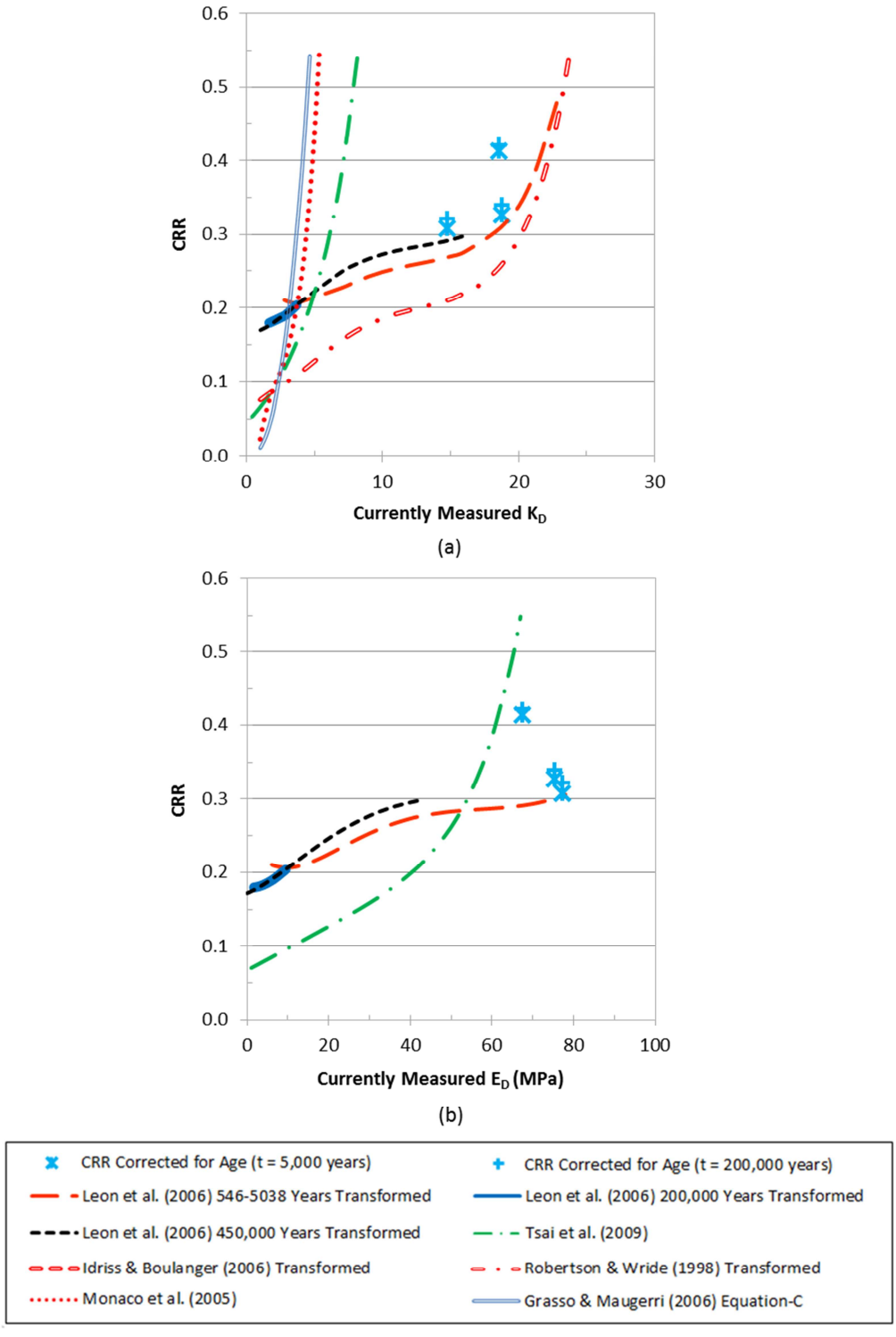

Figure 4.44 Range of CRR for the Fort Dorchester Source Sand: (a) CPT derived CRR-K_D relation; (b) CPT derived CRR-K_D relation

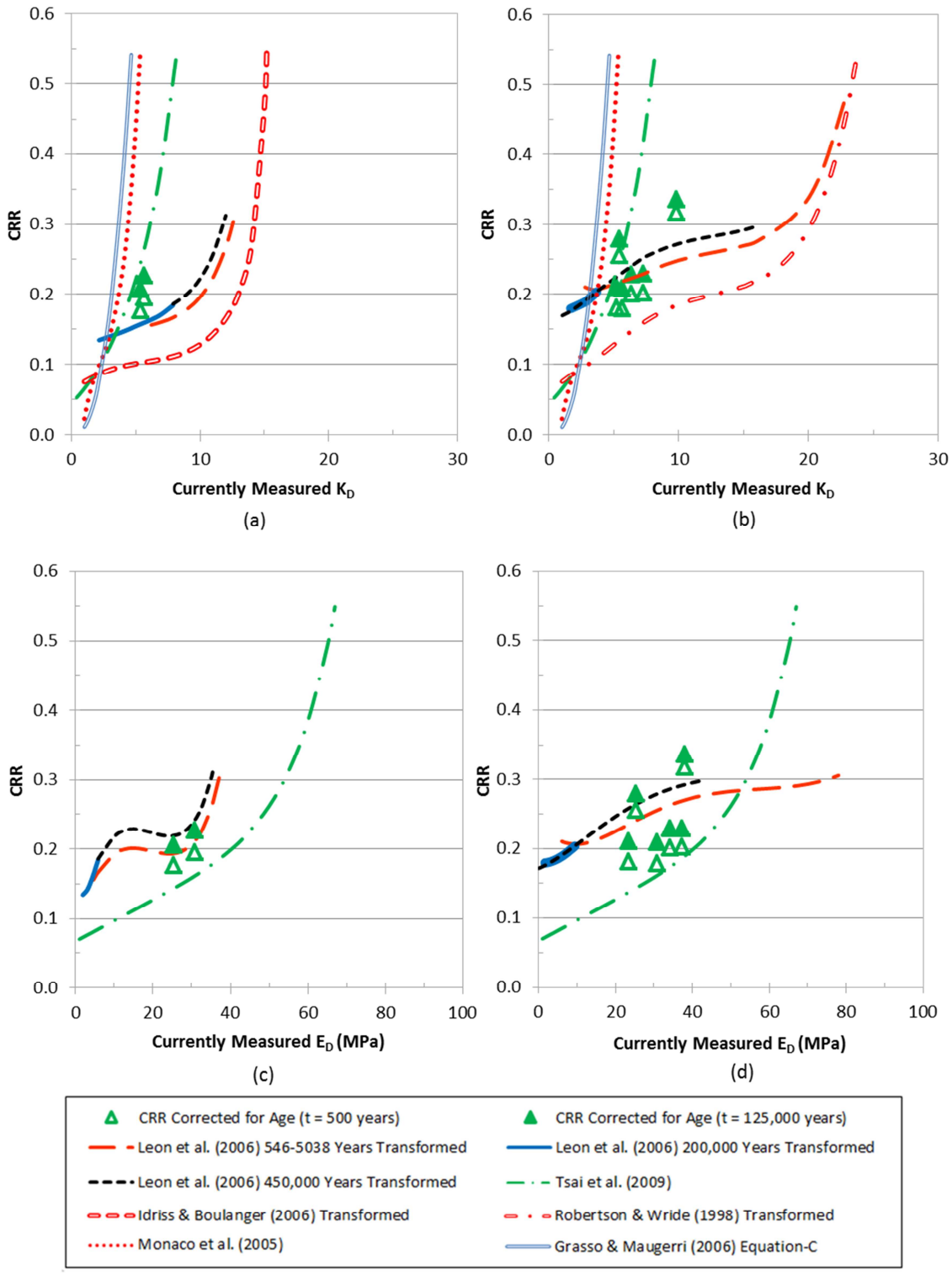

Figure 4.45 Range of CRR for the Hollywood Source Sand: (a) SPT derived CRR-K_D relation; (b) CPT derived CRR-K_D relation; (c) SPT derived CRR-E_D relation; (d) CPT derived CRR-K_D relation

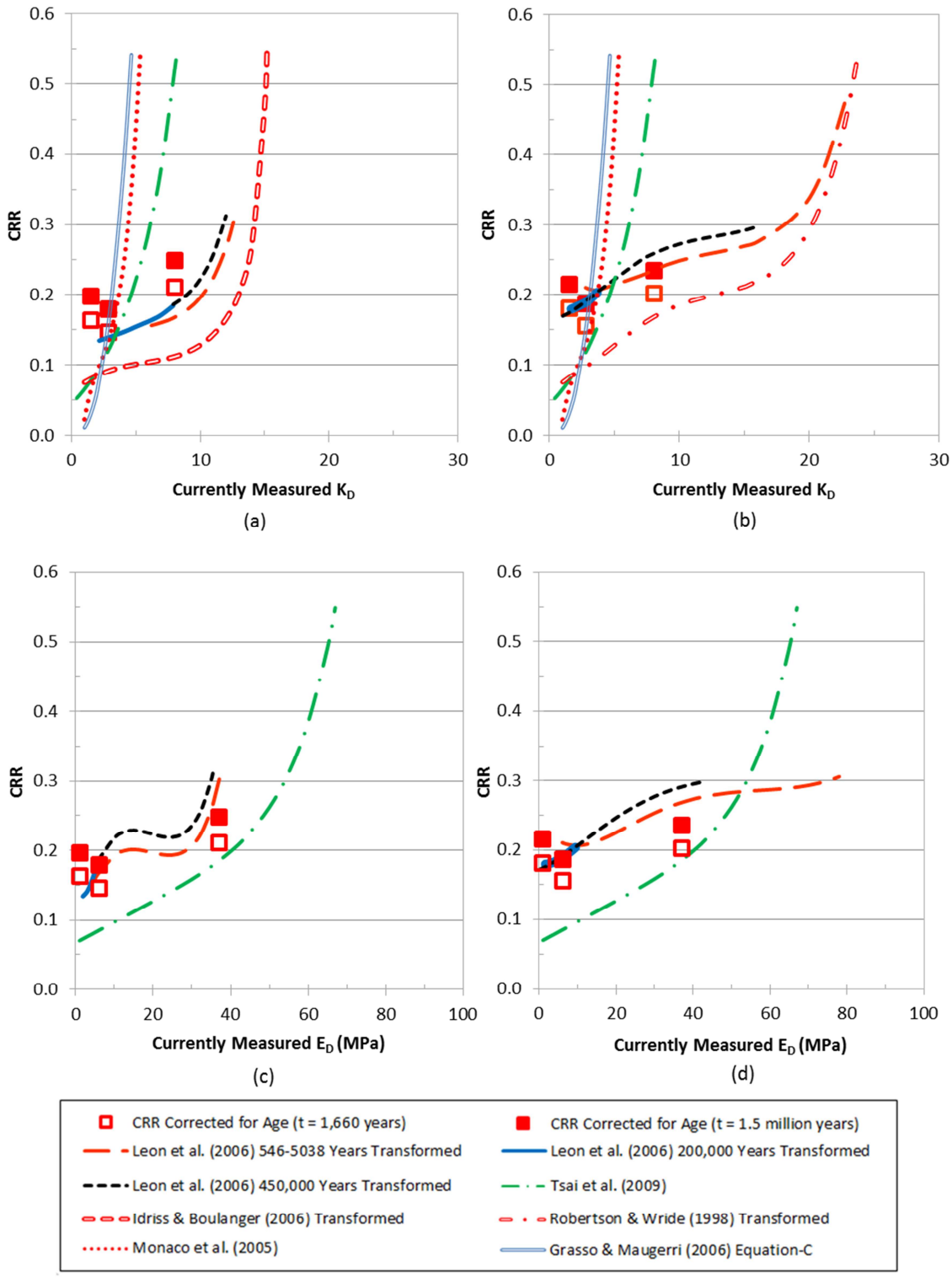

Figure 4.46 Range of CRR for the Four Hole Swamp Source Sand: (a) SPT derived CRR-K_D relation; (b) CPT derived CRR-K_D relation; (c) SPT derived CRR-E_D relation; (d) CPT derived CRR-K_D relation

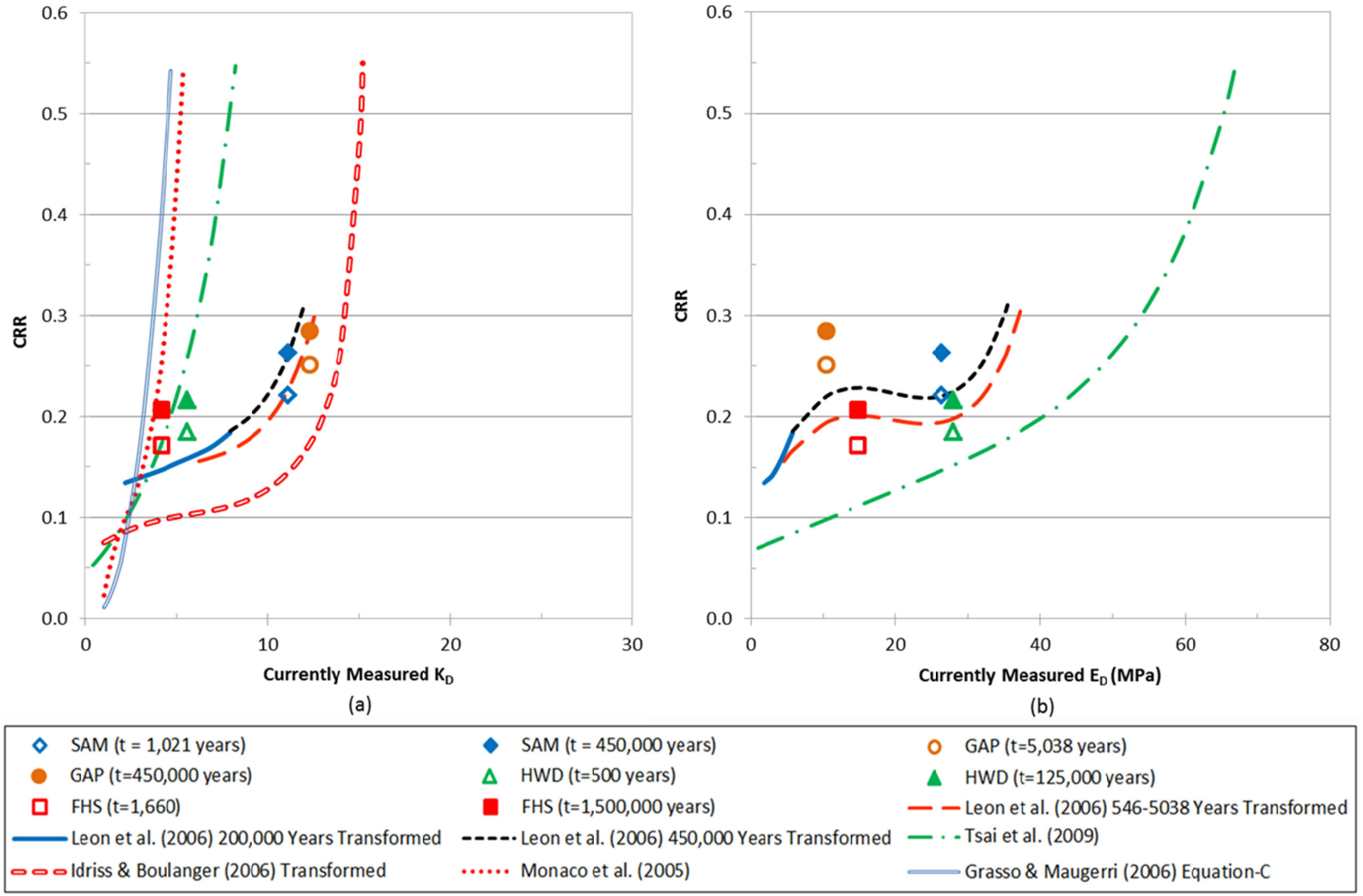

Figure 4.47 Average Values of CRR for the Source Sand Zones at Each Site Using SPT-Derived CRR-DMT Relations

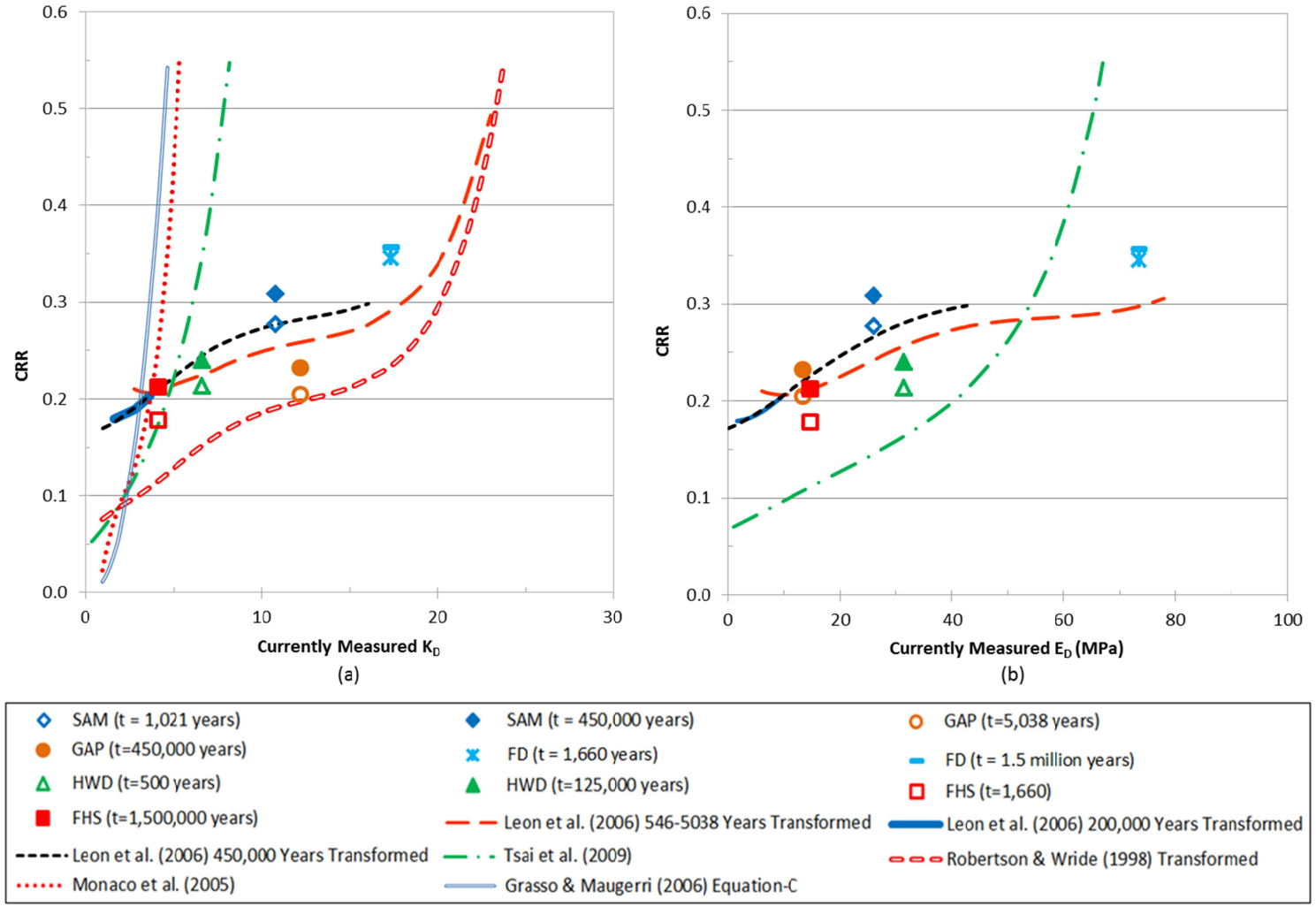

Figure 4.48 Average Values of CRR for the Source Sand Zones at Each Site Using CPT-Derived CRR-DMT Relations

4.3.3.1 Discussion

Recall from Figure 4.41 that before aging was considered, the majority of the data from the SCCP source sand zones plotted below and to the right of the existing CRR-K_D liquefaction boundary curves presented in the literature (Grasso & Maugeri (2006), Monaco et al. (2005), and Tsai et al. (2009)), deeming the soils unliquefiable. Figure 4.49 shows the CRR-K_D relationships of the SCCP data with a CRR that considers the effects of aging. Even with the new, higher CRR values, the majority of the SCCP data are still considered unliquefiable by the existing CRR-K_D liquefaction boundary curves; however Figures 4.42 through 4.48 show that nearly all of the data plots above and to the left of Leon's transformed CRR-DMT curves, which deem the soils as potentially liquefiable.

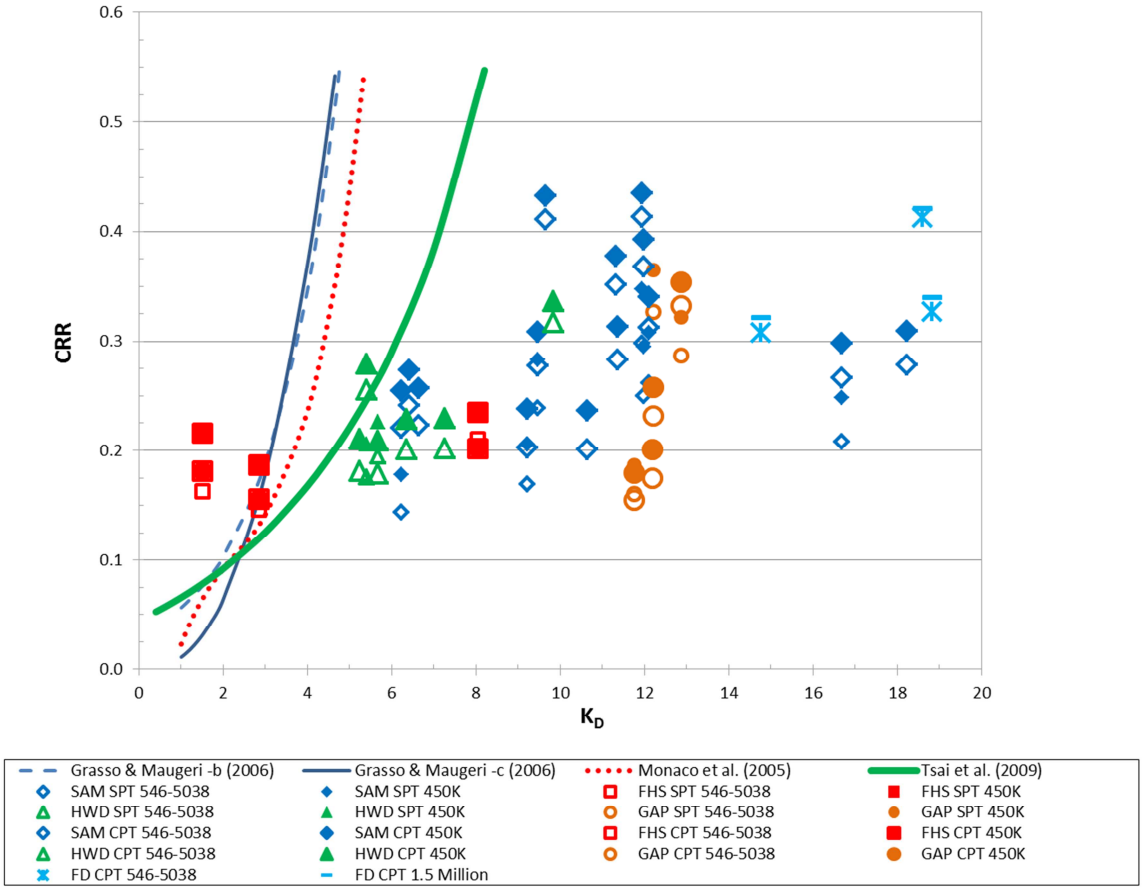

Figure 4.49 Comparison of Existing CRR-K_D Relations with SCCP Data Corrected for Age

Note: Small symbols denote CRR calculated through $N_{1,60cs}$,
Large symbols denote CRR calculated through $q_{c1N,cs}$
Open symbols denote CRR calculated with t = age of liquefaction inducing earthquake
Closed symbols denote CRR calculated with t = age of soil deposit

Consider Figure 4.42 (a) which shows that all of the SAM source sand data plots to the right of the existing CRR-K_D curves of Grasso & Maugeri (2006), Monaco et al. (2005), and Tsai et al. (2009). This illustrates that the existing curves consider the SAM source sand to be unliquefiable. With the exception of two outlying points, the entirety of the SAM source sand data plots very near to the transformed curves of the Leon et al. (2006) CRR-SPT relation. This data shows that the Leon et al. (2006) methodology

which accounts for aging considers the SAM source sand to be liquefiable. The transformed version of the Idriss and Boulanger (2006) CRR-SPT curve (an approach for Holocene soils that does not account for aging) plots below and to the right of the SAM source sand data (with the exception of the two outlying points). While the transformed Idriss and Boulanger (2006) curve considers the SAM source sand to be liquefiable, it underestimates CRR by as much as 95% when compared to the Leon et al. (2006) methodology, resulting in an overly conservative analysis. In short, Figure 4.42 (a) shows that the transformed CRR-SPT curves of Leon et al. (2006) agree with the CRR-DMT relations developed in this work for the SAM source sand. This relationship is to be expected because the Leon et al. (2006) methodology was developed using SCCP data.

Note that the two outlying points referenced above originate from a depth of 9 ft (2.7 m). Recall from Section 4.3.1.2.1 that these points lay on the boundary of the source sand zone (9-22 ft; 2.7-6.7 m), so their inclusion in the source sand is uncertain in the first place. As such, these points may be accurately portrayed as unliquefiable in Figure 4.42 (a).

Figure 4.42 (b) presents the CRR-K_D relations with the SAM source sand data that has been corrected to consider the effects of aging which was derived using CPT data. Like Figure 4.42 (a), Figure 4.42 (b) also shows that all of the SAM source sand data plots to the right of the existing CRR-K_D curves of Grasso & Maugeri (2006), Monaco et al. (2005), and Tsai et al. (2009). Again, this illustrates that the existing relations all consider the SAM source sand to be unliquefiable. The transformed version of the Robertson and Wride (1998) CRR-CPT relation (another approach for Holocene

soils that does not account for aging) plots below and to the right of the SAM source sand data, deeming the SAM source sand as liquefiable. This approach provides a reasonable estimation of CRR for four of the data points but underestimates CRR for the rest of the data within a broad range of 45-125% when compared to the CRR found from the Leon et al. (2006) methodology. The underestimation of CRR again results in an overly conservative analysis. The transformed CRR-CPT curves of Leon et al. (2006) provide a good estimation of CRR from the Leon et al (2006) methodology for approximately 70% of the SAM source sand data. CRR for the other 30% of the SAM source sand data is underestimated by the transformed CRR-CPT curves of Leon et al. (2006) within the range of 40-70%.

Figure 4.42 (c) presents the CRR-E_D data for the SAM source sand where CRR was calculated using SPT data. The existing relation of Tsai et al. (2009) does deem the SAM source sand as liquefiable; however, CRR is still underestimated for the majority of the data when compared to the CRR found from the Leon et al. (2009) methodology. While the Tsai et al. (2009) relation provides a good estimation for two of the data points, the CRR for the majority of the data is underestimated by 30-70%. The transformed versions of the Leon et al. (2006) CRR-SPT curves are shown to be in good agreement with the CRR-DMT relation developed in this work and provide a good estimation of CRR obtained from the Leon et al. (2006) methodology for all data points. Again, this relationship is to be expected due to the fact that the Leon et al. (2006) methodology was developed using SCCP data.

Figure 4.42 (d) presents the CRR-E_D data for the SAM source sand where CRR was calculated using CPT data. Again, the existing relation of Tsai et al. (2009) deems

the SAM source sand as liquefiable but underestimates the CRR of all data points when compared to the CRR obtained from the Leon et al. (2006) methodology. In this case, the underestimation ranges from 40-190%. Like Figure 4.42 (b), the transformed CRR-CPT curves of Leon et al. (2006) in Figure 4.42 (d) provide a good estimation of the CRR from the Leon et al. (2006) methodology for approximately 70% of the data, while the CRR of the other 30% of the data is underestimated within the range of 40-60%.

Figures 4.43 through 4.46 display similar results for GAP, FD, HWD, and FHS, respectively, as shown for SAM in Figure 4.42 where the CRR for SCCP data is:

- overestimated by the existing CRR-K_D relations of Grasso & Maugeri (2006), Monaco et al. (2005), and Tsai et al. (2009);
- underestimated by the transformed CRR-K_D versions of the Idriss and Boulanger (2006) CRR-SPT relation and the Robertson and Wride (1998) CRR-CRT relation;
- underestimated by the existing CRR-E_D relation of Tsai et al. (2009).

In all cases the CRR found from the Leon et al. (2006) methodology matches well with the transformed curves of Leon et al. (2006) as is expected considering that the Leon et al. (2006) methodology was developed using SCCP data.

A few minor exceptions exist at FD, FHS, and GAP. In Figure 4.44 (b) the FD source sand data is overestimated by the Tsai et al. (2009) CRR-E_D relation. This inconsistency may be credited to the fact that the soil was unsaturated at the time of field testing. Lutenegger (1988), Schmertmann (1982), and Lacasse and Lunne (1986) all identified that K_D and E_D both decrease as the degree of saturation increases. This phenomenon explains why K_D and E_D of the FD source sand are greater than K_D and E_D

of the other source sands (see Figure 4.34 and 4.36 for an illustration). It also suggests that if the FD soils were saturated at the time of field testing the resulting K_D and E_D would be less than what was measured and the resulting CRR corrected for age would be better estimated by the Tsai et al. (2009) and the transformed Leon et al. (2006) CRR-E_D relations in Figure 4.44 (b).

In Figures 4.46 (a) and (b) half of the FHS data points are considered liquefiable by all of the presented CRR-K_D relations, including the three existing relations of Grasso & Maugeri (2006), Monaco et al. (2005), and Tsai et al. (2009). This unanimous classification by all CRR-K_D relations is reserved for the extreme case of very loose sands that are most prone to liquefy.

In Figures 4.43 (a) and (b) three points from GAP have lower than average CRR values. As plotted, these points are estimated well by the transformed versions of the Idriss and Boulanger (2006) CRR-SPT curve (Figure 4.43 (a)) and the Robertson and Wride (1999) CRR-CPT curve (Figure 4.43 (b)). These points originate from a depth of 6-7 ft (1.8-2.1 m). Recall from Section 4.3.1.2.1 that because these points lie on the boundary of the source sand zone (4-7 ft; 1.2-2.1 m) their inclusion in the source sand is uncertain in the first place and may be accurately portrayed as unliquefiable in Figures 4.43 (a) and (b). While these points exhibit K_D values that are consistent with the rest of the source sand, their $(q_{c1N})_{cs}$ values are much lower than the upper half of the source sand (refer back to Figure 4.10). This disagreement between DMT and CPT data may be credited to the spatial difference between the two tests (272 ft, (82 m)). Because the CPT data was used to calculate CRR in Figure 4.43 (b) these points have seemingly low values of CRR. These outlying data points skew the calculation of the average values of CRR

for the GAP source sand. This is illustrated in Figure 4.48 (a) where it appears that the CRR of the GAP source sand is best estimated by the transformed version of the Idriss and Boulanger CRR-CPT relation. With these two errant points excluded from the calculation of the average values at GAP the average values of the GAP source sand become K_D=12.5, CRR=0.27 for *t*=5,038 years, and CRR=0.30 for *t*=450,000 years. As shown in Figure 4.50 (a), the change in these values moves the GAP data points in Figure 4.48 (a) above the transformed curve of Leon et al. (2006), which deems the soil as potentially liquefiable.

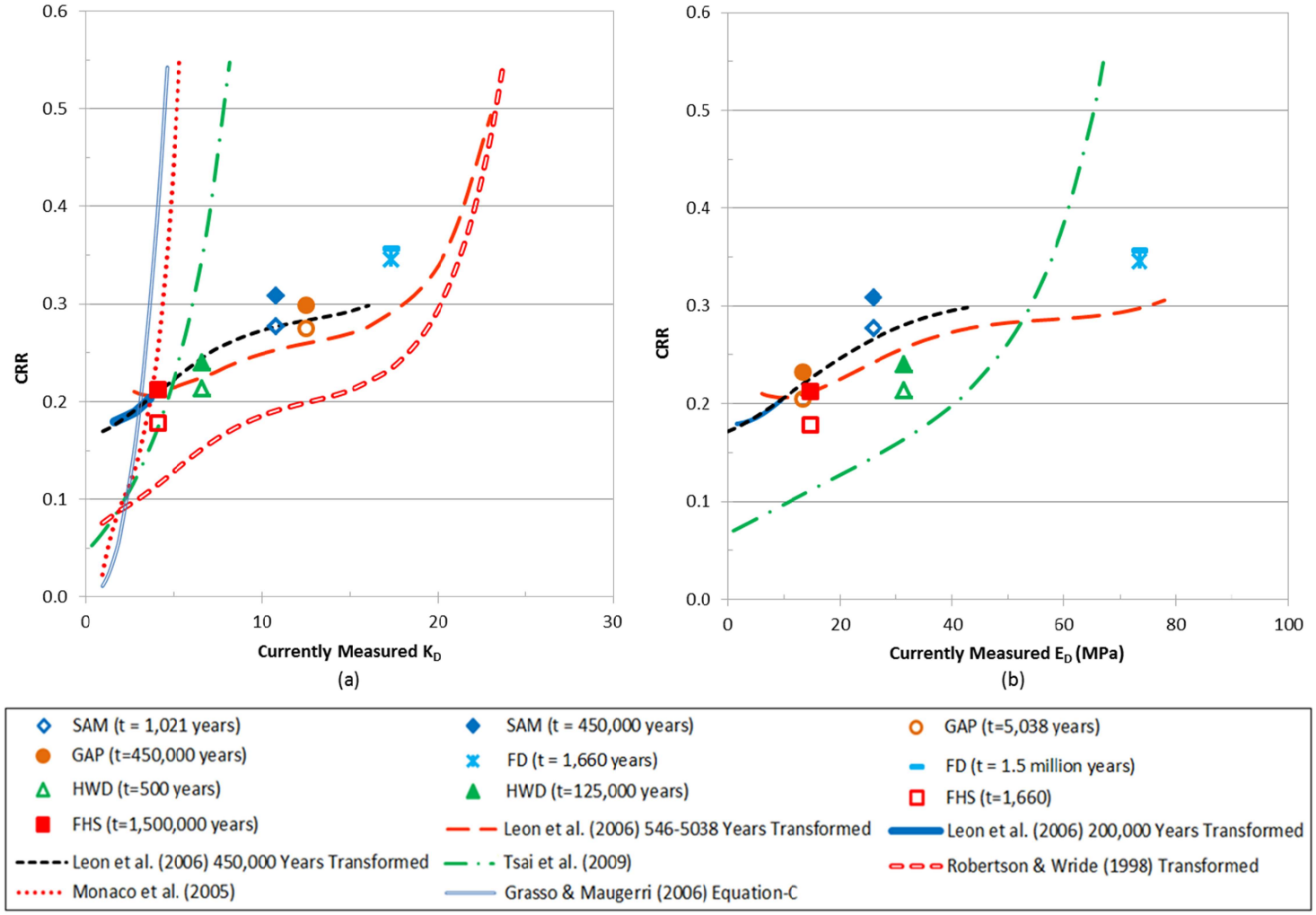

Figure 4.50 Average Values of CRR for the Source Sand Zones at Each Site Using CPT-Derived CRR-DMT Relations - Revised

Figures 4.47 and 4.50 present a summary of the SCCP data after it has been corrected to account for the effects of aging. All of the data in Figures 4.47 and 4.50 plot either above or very near to the transformed curves of Leon et al. (2006), showing agreement with the Leon et al. (2006) approach for estimating the liquefaction potential of SCCP soils.

In review of Figures 4.47 and 4.50 it appears that the CRR-K_D relations provided by the transformed curves of Leon et al. (2006) (Figures 4.47 (a) and 4.50 (a)) are slightly stronger than the CRR-E_D relations that are provided from the transformation of the Leon et al. (2006) curves (Figures 4.47 (b) and 4.50 (b)) as the data points (with CRR from the Leon et al. (2006) methodology) are more scattered about the CRR-E_D curves that result from the transformed curves of Leon et al. (2006) than are the points about the CRR-K_D curves that result from the transformation of the Leon et al. (2006) curves. There appears to be more confidence in the CRR-K_D relations provided by the transformed curves of Leon et al. (2006) than with the CRR-E_D relations that result from the transformed curves of Leon et al. (2006). The CRR-K_D curves that result from the transformation of the Leon et al. (2006) curves mirror, or have the same relative shape (similar curvature that constantly increases from left to right) as, other curves presented in the literature (Idriss and Boulanger (2006), Robertson and Wride (1998), Grasso & Maugeri (2006), Monaco et al. (2005), and Tsai et al. (2009): whereas this trend is not observed in the transformed CRR-E_D curves. The shape of the transformed curves of Leon et al. (2006) is a result of the regression correlations presented in Equations 4.1 through 4.4.

In regards to the differences in the CRR-K_D/E_D relations that result from the transformation of the Leon et al. (2006) curves derived from SPT versus CPT, both

options seem to be comparable in the degree of scatter that is exhibited by the data points plotted about the transformed CRR-K_D/E_D curves of Leon et al. (2006) (or the quality of the transformed CRR-K_D/E_D curves of Leon et al. (2006) as best-fit curves to the data points with CRR from the Leon et al. (2006) methodology) and in the quality and overall shape of the transformed curves. However, it is noted that the SPT derived relations (Figure 4.47) appear to be the more conservative case with both curves (CRR-K_D and CRR-E_D) appearing to have considerably lower integrals than the curves of the CPT derived relations (Figure 4.50) (i.e. less area under the curves yields a smaller unliquefiable region; i.e. the SPT derived relations consider more soils liquefiable).

4.3.3.2 Summary

In summary, it is shown that the Leon et al. (2006) approach can be used to develop CRR-K_D and CRR-E_D relations for liquefaction potential evaluation of SCCP soils. It appears that there is more confidence in the CRR-K_D relations than the CRR-E_D relations, and that the SPT-derived relations are generally more conservative than the CPT-derived relations. Normalizing E_D may improve the CRR-E_D relation.

4.3.4 Site-Specific CRR from Cyclic Triaxial Testing

Figure 4.51 relates $(N_1)_{60cs}$ for HWD, SAM and FHS to the CRR obtained from stress-controlled cyclic triaxial tests performed by Hasek (2013) on high-quality fixed-piston tube samples. The CRR corresponds to liquefaction at N=15 cycles of loading. Therefore, the results can be compared with the “generally accepted” M = 7.5 curves

since 15 significant stress cycles is considered equivalent to M = 7.5 (Seed and Idriss, 1982).

All of the data in Figure 4.51, with the exception of one point from Sampit, agrees with the Leon et al. (2006) boundary curves for estimating liquefaction potential of aged soils. The one Sampit data point that does not agree with the Leon et al. (2006) curves corresponds to a sample obtained from a depth of 9.8 ft (3.0 m). Recall from Section 4.3.1.2.1 that data from this depth should be excluded from the analysis, as this point lies on the boundary of the source sand zone. Also note that the Idriss and Boulanger (2006) curve for estimating the liquefaction resistance of Holocene soils underestimates the CRR of the SCCP soils.

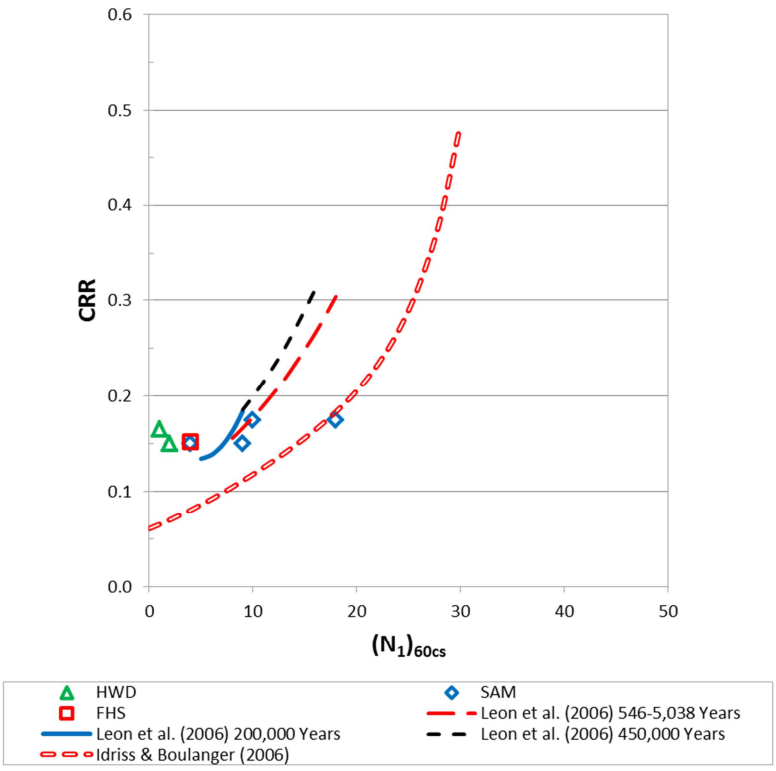

Figure 4.51 CRR from cyclic triaxial testing versus $(N_1)_{60cs}$

Figure 4.52 relates $(q_{c1N})_{cs}$ for HWD, SAM and FHS to the CRR obtained from cyclic triaxial tests performed by Hasek (2013). In this instance, CRR is overestimated by the Leon et al. (2006) aged approach while the Robertson and Wride (1998) Holocene approach provides a good estimation for the majority of the data. The Robertson and Wride (1998) curve provides a good estimate of the CRR for all three points from SAM and for one point from HWD, while it overestimates CRR for the one point from FHS and underestimates CRR for one point from HWD. It should be noted that the one outlying point from HWD is from a sample taken just outside of the boundary of the source sand. The source sand ranges from 9-14 ft (2.7-4.0 m) and the midpoint of the sample is 8.5 ft (2.6 m). The soil at 8.5 ft (2.6 m) exhibited a $(q_{c1N})_{cs} = 151$. According to Robertson and Wride (1998), soil with $(q_{c1N})_{cs} > 160$ is considered too dense to liquefy. With this sample being on the cusp of that boundary the Robertson and Wride (1998) curve accurately deems the soil as unliquefiable.

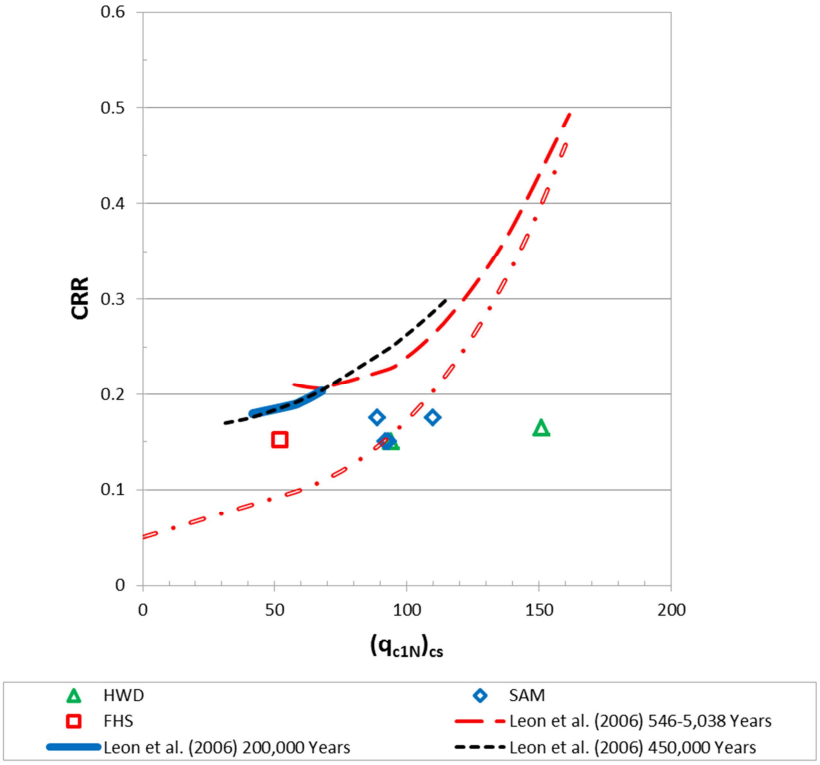

Figure 4.52 CRR from cyclic triaxial testing versus $(q_{c1N})_{cs}$

Figure 4.53 relates K_D for HWD, SAM and FHS to the CRR obtained from cyclic triaxial tests performed by Hasek (2013). This figure shows that all of the data, except for one outlying point from SAM, agrees with the transformed CRR-SPT curves of Leon et al. (2006). The outlying SAM point again comes from a depth of 9.8 ft (3.0 m) and should be excluded from the analysis, per Section 4.3.1.2.1. Figure 4.53 also shows that the transformed CRR-CPT curves of Leon et al. (2006) provide a reasonable estimation of CRR of SCCP soils as CRR is slightly overestimated; meanwhile the current methods for evaluating liquefaction potential (Tsai et al. (2009), Monaco et al. (2005), Grauso and Maugeri (2006)) overestimate CRR of SCCP soils by a factor of about 2 to 4..

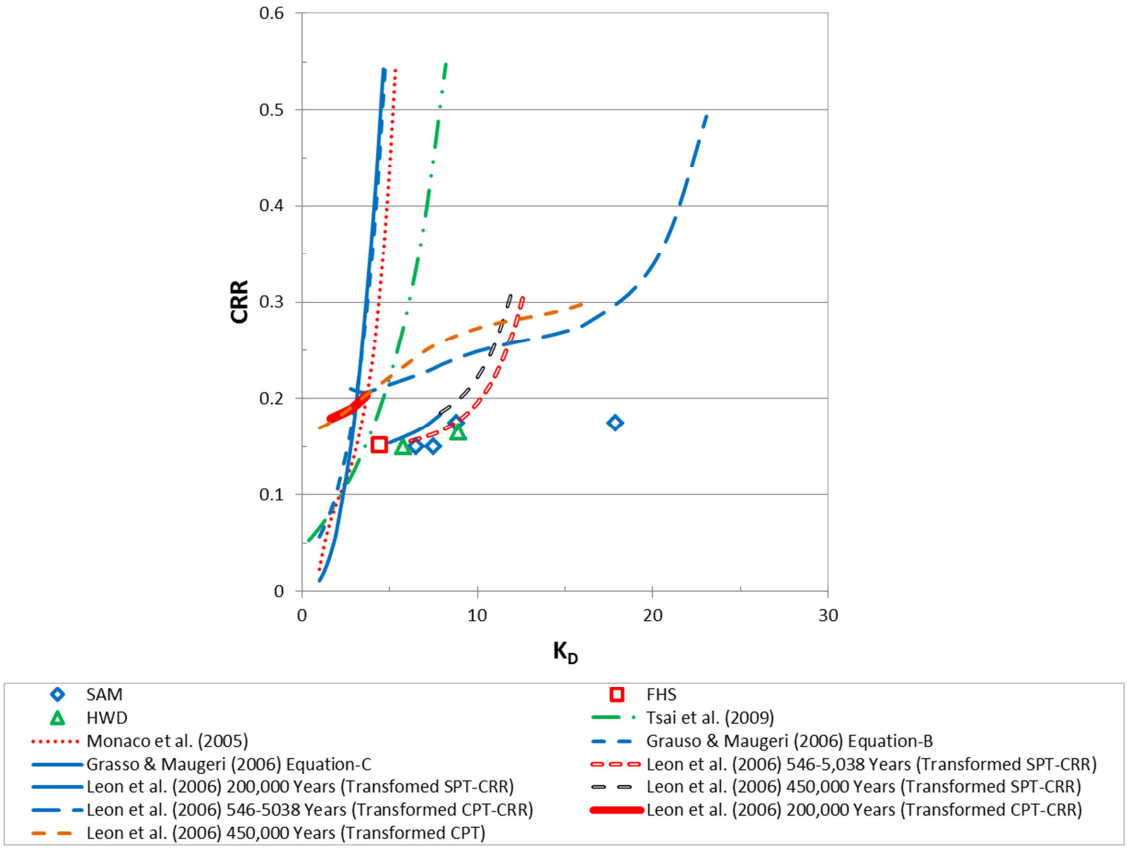

Figure 4.53 CRR from cyclic triaxial testing versus K_D

Figure 4.54 relates E_D for HWD, SAM and FHS to the CRR obtained from cyclic triaxial tests performed by Hasek (2013). In this case, the Tsai et al. (2009) curve has the best agreement to the CRR from cyclic triaxial tests of SCCP soils while the transformed curves of Leon et al. (2006) all slightly overestimate CRR. A summary of the data presented in Figures 4.51 through 4.54 is presented in Table 4.12.

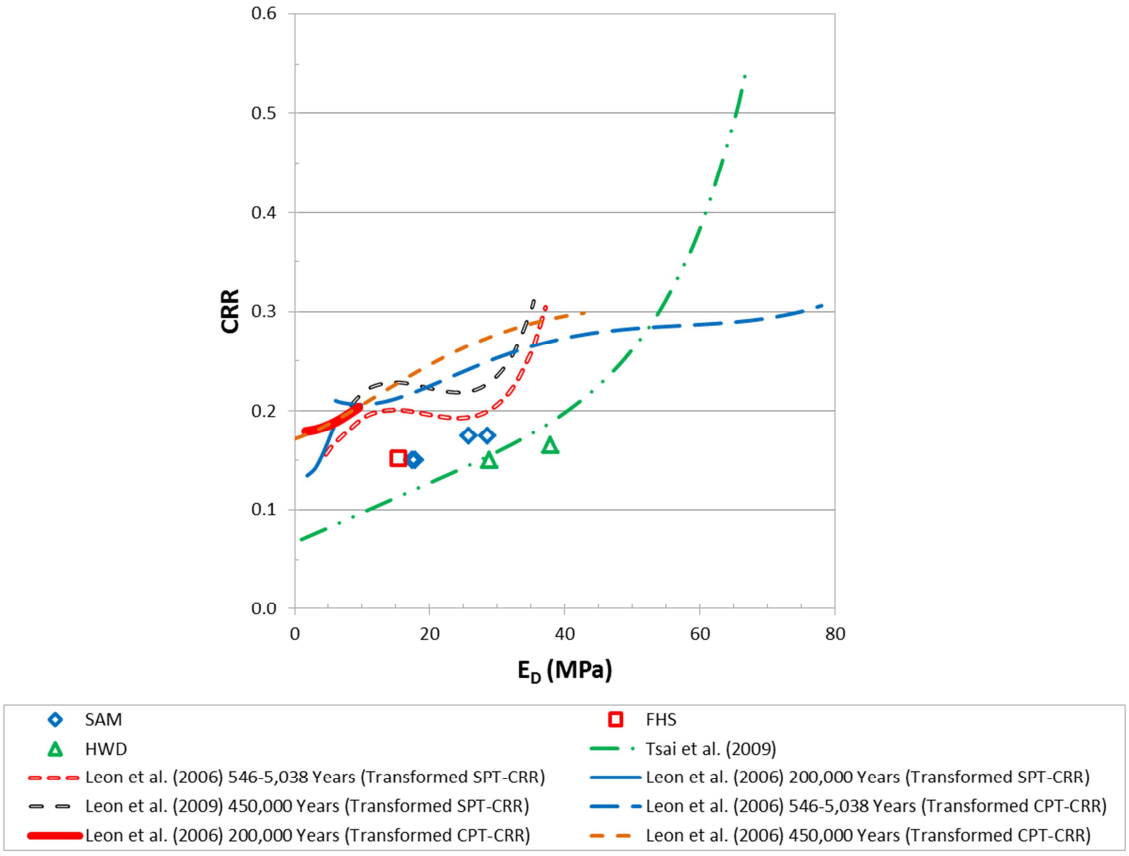

Figure 4.54 CRR from cyclic triaxial testing versus E_D

Table 4.12 Summary of Measured Field Data and CRR from Cyclic Triaxial Testing

Site	Depth (ft)	Depth (m)	$N_{(1)60cs}$	$(q_{c1N})_{cs}$	K_D	E_D (MPa)	CRR
HWD	8.5	2.6	8	151	8.9	37.9	0.165
	11.4	3.5	8	94	5.8	28.9	0.15
SAM	9.8	3.0	18	110	17.9	28.6	0.175
	15.7	4.8	9	92	7.5	17.5	0.15
	16.5	5.0	4	93	6.5	17.8	0.15
	17.5	5.3	10	89	8.8	25.8	0.175
FHS	11.4	3.5	4	52	4.4	15.4	0.152

In review of Figures 4.51 and 4.52 (CRR vs. SPT and CRR vs. CPT, respectively) it is clear that the Leon et al. (2006) methodology to account for aging provides a better estimate of CRR when incorporated with SPT data than with CPT data. Figure 4.53 (CRR vs. K_D) further supports this theory as all of the data in this figure falls very near to the Leon et al. (2006) transformed CRR-SPT curves while the transformed CRR-CPT curves considerably overestimate CRR of SCCP soils. Figure 4.54 (CRR vs. E_D) suggests that the transformed curves of both the SPT and CPT derived Leon et al. (2006) curves slightly overestimate CRR of SCCP soils.

4.4 Summary

This chapter presented the data from field and laboratory testing and presented correlations between DMT-SPT and DMT-CPT test parameters that are specific to SCCP soils. The results of the simplified procedure are also presented along with newly recommended CRR-K_D and CRR-E_D boundary curves for estimating the liquefaction potential of SCCP soils. The recommended curves are validated with site specific CRR-K_D and CRR-E_D relations where CRR is obtained from cyclic triaxial testing.

The field test data includes data from the DMT, SPT, and CPT tests. The laboratory index testing data includes fines content, C_u, C_c, Atterberg limits, specific gravity, USCS classification, and grain size distribution curves for each of the five sites studied in the SCCP.

DMT-SPT and DMT-CPT correlations that are specific to SCCP soils are also presented. These correlations were derived through the compilation of data from DMT, SPT, and CPT test that were performed side by side. The correlations between DMT-

SPT and DMT-CPT presented by Tsai et al. (2009) are plotted with the SCCP data and it is shown that K_D is underestimated by Tsai et al.'s (2009) $N_{1,60cs}$–K_D and $q_{c1N,cs}$–K_D relations, and E_D is underestimated by their $N_{1,60cs}$–E_D and overestimated by their $q_{c1N,cs}$–E_D relationship.

The simplified procedure for estimating liquefaction potential was implemented using the current methods presented by Idriss and Boulanger (2006) and Robertson and Wride (1998), both for Holocene soils, and also using the Leon et al. (2006) approach, which accounts for the effects of aging. The Idriss and Boulanger (2006) and Robertson and Wride (1998) methods overestimate CRR and imply that the SCCP soils are not liquefiable, but the Leon et al. (2006) method, which accounts for aging, is shown to provide a good estimation of CRR in SCCP soils.

The Leon et al. (2006) method for estimating CRR of SCCP soils was validated using site specific CRR relations which were developed using data from stress-controlled cyclic triaxial tests performed on high-quality fixed-piston tube samples. The site specific relations included CRR-$(N_1)_{60,cs}$, CRR-$(q_{c1N})_{cs}$, CRR-K_D, and CRR-E_D relations. The CRR-$(N_1)_{60,cs}$ and the CRR-K_D site specific relations where CRR was obtained from triaxial testing are in good agreement with the Leon et al. (2006) approach to estimate CRR in SCCP soils, while the CRR-$(q_{c1N})_{cs}$, and the CRR-E_D site specific relations show that the Leon et al. (2006) methodology overestimates the CRR of SCCP soils. The site specific CRR-$(q_{c1N})_{cs}$, relation where CRR was obtained from triaxial testing is in better agreement with the Robertson and Wride (1998) relation and the CRR-E_D relation is in better agreement with the Tsai et al. (2009) relation than they are with the Leon et al. (2006) approach to estimate CRR of SCCP soils.

The relations between CRR and currently recorded in situ indices (DMT, SPT, and CPT) of both the simplified procedure and the site specific CRR from cyclic triaxial testing suggest that the Leon et al. (2006) methodology of estimating CRR are in better agreement when found using the curves transformed from SPT rather than CPT. The SPT derived relations are also more conservative than the CPT derived relations. The results also suggest that the CRR-K_D relations provide a better estimation of CRR in SCCP soils than the CRR-E_D relations, which is in agreement with work by Monaco et al. (2005).

CHAPTER FIVE
CONCLUSIONS

The goal of this thesis was to aid in the development of new dilatometer (DMT) based methods of estimating the cyclic resistance ratio (CRR) of South Carolina Coastal Plain (SCCP) soils. The existing DMT-CRR database is limited and consists of data from varying soil types from around the world. This work enhances the existing database by adding data from five sites in the SCCP and presents new first approximation CRR-DMT relationships for evaluating the liquefaction potential of SCCP soils. Data from DMT, SPT, and CPT tests performed side by side were analyzed and correlations between DMT-SPT and DMT-CPT test parameters were derived. The correlations between the different test parameters were used to transform the existing methods of estimating CRR of Holocene (<10,000 year old) soil deposits (e.g. Idriss and Boulanger (2006) for SPT and Robertson and Wride (1998) for CPT) into new first approximation CRR-DMT relationships. The effects of aging were taken into account by implementing the Leon et al. (2006) methodology. The first approximation CRR-DMT relationships presented herein are supported by CRR-DMT relations developed using CRR obtained from cyclic triaxial testing of high quality undisturbed samples.

Based on the work presented herein, the following conclusions were drawn:

- For the five presented sites in the SCCP, it was found that when liquefiable soils were identified based on $(N_1)_{60,cs}<30$ (Seed et al., 1985) or $(q_{c1N})_{cs}<160$

(Robertson and Wride, 1998), both for Holocene soils, the corresponding limits from the DMT results were K_D<12 and E_D<40 Mpa. Using the upper limit of K_D<5, previously reported by Monaco et al (2005) for Holocene soils, would indicate that the majority of the SCCP soils are not liquefiable.

- K_D and E_D values of the SCCP soils were found to be higher than other published data (Grasso and Maugeri (2006), Monaco et al. (2005), and Tsai et al. (2009)) which were primarily obtained for Holocene soils.
- Correlations between DMT-SPT and DMT-CPT test parameters that are specific to SCCP soils were developed. Similar correlations presented by Tsai et al. (2009) were plotted with the SCCP data and were shown to underestimate K_D in both their DMT-SPT and DMT-CPT correlations, underestimate E_D in their DMT-SPT relation, and overestimate E_D in their DMT-CPT relation.
- The current CRR-DMT relations of Grasso and Maugeri (2006), Monaco et al. (2005), and Tsai et al. (2009) were shown to overestimate the CRR of the majority of the SCCP soils. The only case where the current CRR-DMT relations were in good agreement with the SCCP data was for the case of the very loose (N, q_c, K_D, and E_D all ≈ 0) sand layer at Four Hole Swamp, which is most prone to liquefy.
- The first approximation CRR-DMT curves found by transforming the CRR-SPT and CRR-CPT curves of Leon et al. (2006) were shown to be in good agreement with the SCCP data analyzed herein and serve as appropriate boundary curves between liquefiable and non-liquefiable soils for cases where aging effects need to be considered.

- The CRR-K_D relations presented herein appeared to be superior to the CRR-E_D relations. Normalizing E_D may improve the CRR-E_D relation. The CRR-DMT relationships were also found to be more conservative when derived using SPT-based methods than CPT-based methods.
- The CRR-DMT relationships developed with CRR from cyclic triaxial test data were in good agreement with the new first approximation CRR-DMT relations and also suggest that the CRR-K_D relationships are superior to the CRR-E_D relationships.

The proposed CRR-K_D and CRR-E_D boundary curves of this thesis are put forth to serve as first approximations with the aim of further evolving the dilatometer as a significant tool to evaluate the liquefaction resistance of soils and enhance the profession of geotechnical engineering.

REFERENCES

Amick, D.C. (1990). “Paleoliquefaction investigations along the Atlantic Seaboard with emphasis on the prehistoric earthquake chronology of coastal South Carolina.” Ph.D. thesis, University of South Carolina, Columbia.

Arango, I., Lewis, M.R., and Kramer, C. (2000). “Updated liquefaction potential analysis eliminates foundation retrofitting of two critical structures.” *Soil Dynamics and Earthquake Engineering*, 20, 17–25.

Arango, I., and Migues, R.E. (1996). “Investigation of the seismic liquefaction of old sand deposits.” *Report on Research, Bechtel Corporation, National Science Foundation Grant No. CMS-94-16169,* San Francisco.

Baligh, M.M. & Scott, R.F. (1975). "Quasi static deep penetration in clays". *Journal of Geotechnical Engineering*, ASCE, 101(GT11), 1119-1133.

Campanella, R.G. and Robertson, P.K. (1991). “Use and interpretation of a research dilatometer.” *Soil Mechanics Series No. 127,* University of British Columbia, Civil Engineering Department.

Doar, III, W.R. (2007). “Vibracore logs from the Fort Dorchester site”. South Carolina Department of Natural Resources, South Carolina Geological Survey (personal communication).

Dowding, C.H., and Hryciw, R.D. (1986). “A laboratory study of blast densification of saturated sand.” *Journal of Geotechnical Engineering*, ASCE, 112(2), 187–199.

Gibbs, H.J., Holtz, W.G. (1957). “Research on determining the density of sands by spoon penetration testing.” *Proceedings of the 4th ICSMFE*, 1, 35–39.

Grasso, S.,Maugeri,M. (2006). “Using K_D and V_s from seismic dilatometer (SDMT) for evaluating soil liquefaction.” *Proceedings of the 2nd International Flat Dilatometer Conference*, 281–288.

Hasek, M.J. (2013). “Liquefaction potential as a related to the aging of South Carolina outer coastal plain sands.” Ph.D. dissertation to be submitted to the University of South Carolina, Columbia, South Carolina.

Hu, K., Gassman, S.L., and Talwani, P. (2002a). “In-situ properties of soils at paleoliquefaction sites in the South Carolina Coastal Plain.” *Seismological Research Letters,* 73(6), 964-978.

Idriss, I.M. and Boulanger, R.W. (2006). “Semi-empirical procedures for evaluating liquefaction potential during earthquakes.” *Soil Dynamics and Earthquake Engineering*, 26, 115–130.

Jamiolkowski, M., Ladd, C.C., Germaine, J.T. & Lancellotta, R. (1985). “New developments in field and laboratory testing of soils.” *State of the Art Report, Proceeding of the XI ICSMFE,* San Francisco, 1, 57-153.

Joshi, R.C., Achari, G., Kaniraj, S.R., and Wijeweera, H. (1995). “Effect of aging on the penetration resistance of sands.” *Canadian Geotechnical Journal*, 32(5), 767–782.

Kayen, R.E., Mitchell, J.K., Seed, R.B., Lodge, A., Nishio, S., and Coutinho, R. (1992). ‘‘Evaluation of SPT-, CPT-, and shear wave-based methods for liquefaction potential assessment using Loma Prieta data.’’ *Proceedings of the 4th Japan-U.S. Workshop on Earthquake-Resistant Design of Lifeline Facilities and Countermeasures for Soil Liquefaction*, 1, 177–204.

Kulhawy, F. and Mayne, P. (1990). "Manual on estimating soil properties for foundation design". *Report No. EL-6800*, Electric Power Research Institute, Palo Alto, California, 306.

Lacasse, S. and Lunne, T. (1986). "Dilatometer tests in sand." *Proceedings of In Situ '86, ASCE Specialty Conference on "Use of In Situ Tests in Geotechnical Engineering"*, Virginia Tech, Blacksburg, Virginia, June, ASCE Geotechnical Special Publication, 6, 686-699.

Leon, E., Gassman, S.L., and Talwani, P. (2006). “Accounting for soil aging when assessing liquefaction potential.” *Journal of Geotechnical and Geoenvironmental Engineering*, ASCE, 132(3), 363-377.

Liao, S.S.C., and Whitman, R.V. (1986b). ‘‘Catalogue of liquefaction and non-liquefaction occurrences during earthquakes.’’ Research Report, Department of Civil Engineering, Massachusetts Institute of Technology, Cambridge, Massachusetts.

Lutenegger, A.J. (1988). "Current status of the Marchetti dilatometer test". Special Lecture, Proceedings of the ISOPT-1, Orlando, Florida, 1, 137-155.

Marchetti S. (1975) "A new in situ test for the measurement of horizontal soil deformability", *Proceedings Conference on "In Situ Measurement of Soil Properties", ASCE Specialty Conference*, Raleigh, North Carolina, 2, 255-259.

Marchetti, S. (1980). "In situ tests by flat dilatometer." *Journal of the Geotechnical Engineering Division*, ASCE, 106 (GT3), March, 299-321.

Marchetti, S., Monaco, P., Totani, G., and Calibrese, M. (2001). "The flat dilatometer (DMT) in soil investigations (ISSMGE TC16)." *Proceedings of the International Conference on In-Situ Measurement of Soil Properties and Case Histories*, Bali, Indonesia, 95–131.

Marchetti S. (2010) "Sensitivity of CPT and DMT to stress history and aging in sands for liquefaction assessment." *Proceedings of the CPT 2010 International Symposium*, Huntington Beach, California

Marchetti S. (2011) "Discussion of "CPT-DMT correlations" by Robertson P.K., *Journal of Geotechnical and Geoenvironmental Engineering*, ASCE, 137(4), April, 441-442.

Marchetti, S. (2013). "Photos DMT and SDMT." Retrieved April 14, 2013, from Flat Dilatometer (DMT) downloadable papers: http://www.marchetti-dmt.it/pagespictures/blade&case.htm.

Martin, J.R., and Clough, G.W. (1990). "Geotechnical setting for liquefaction events in the Charleston, South Carolina vicinity." *H. Bolton Seed Memorial Symposium*, 2, 313.

Mayne, P.W. (1995), "Profiling yield stress in clays by in-situ tests." *Transportation Research Record 1479*, National Academy Press, Washington, D.C., 43-50.

Mayne, P.W., and Liao, T. (2004). "CPT-DMT interrelationships in piedmont residuum." *Proceedings of the 2nd International Conference on Geophysical and Geotechnical Site Characterization, ISC-2*, Porto, Portugal, Millpress, Rotterdam, the Netherlands, 345–350.

Mesri, G., Feng, T.W., and Benak, J.M. (1990). "Post densification penetration resistance of clean sands." *Journal of Geotechnical Engineering*, ASCE, 116(7), 1095–1115.

Mitchel, J.K. (1986). "Practical problems from surprising soil behavior." *Journal of Geotechnical Engineering*, ASCE, 112(3), 259-289.

Mitchell, J.K., Lodge, A.L., Coutinho, R.Q., Kayen, R.E., Seed, R.B., Nishio, S. and Stokoe, K.H. (1994). "Insitu test results from four Loma Prieta earthquake liquefaction sites: SPT, CPT, DMT and shear wave velocity." *Report No. UCB/EERC-94/04*, Earthquake Engineering Research Center, University of California, Berkeley.

Mitchell, J.K., and Solymar, Z.V. (1984). “Time-dependent strength gain in freshly deposited or densified sand.” *Journal of Geotechnical Engineering*, ASCE, 110(11), 1559–1576.

Monaco and Marchetti (2007). "Evaluating liquefaction potential by seismic dilatometer (SDMT) accounting for aging." *Proceedings of the 4th International Conference on Earthquake Geotechnical Engineering*, Thessaloniki, Greece, June

Monaco and Schmertmann (2007). “Discussion of ‘Accounting for soil aging when assessing liquefaction potential’ by Leon, E. et al.” *Journal of Geotechnical and Geoenvironmental Engineering*, ASCE 133(9), 1177-1178.

Monaco, P., Marchetti, S., Totani, G., and Calabrese, M. (2005). “Sand liquefiability assessment by flat dilatometer test.” *Proceedings of the 16th ICSMGE*, 4, Osaka, Japan, 2693–2697.

Obermeier, S.F., Gohn, G.S., Weems, R.E., Gelinas, R.L., and Rubin, M. (1985). “Geologic evidence for recurrent moderate to large earthquakes near Charleston, South Carolina.” *Science*, 277, January, 408-411.

Obermeier, S.F., Jacobson, R.B., Powars, D.S., Weems, R.E., Hallbick, D.C., Gohn, G.S., and Markewich, H.W. (1986). “Holocene and late Pleistocene earthquake-induced sand blows in coastal South Carolina.” *Proceedings of the 3rd U.S. National Earthquake Engineering Conference*, 197-208.

Obermeier, S.F., Weems, R.E., and Jacobson, R.B. (1987), “Earthquake-induced liquefaction features in the coastal South Carolina region.” *US Geological Survey Open File Report*, 87, 504.

Rajendran, C.P. and Talwani, P. (1993), “Paleoseismic indicators near Bluffton, South Carolina: An appraisal of their tectonic implications.” *Geology*, 21,987-990.

Robertson P.K. (2009). "CPT-DMT correlations". *Journal of Geotechnical and Geoenvironmental Engineering*, ASCE, 135, 1762-1771.

Robertson, P.K., and Wride, C.E. (1998). ‘‘Evaluating cyclic liquefaction potential using the cone penetration test.’’ *Canadian Geotechnical Journal*, Ottawa, 35(3), 442–459.

Schmertmann, J.H. (1981). “A general time-related soil friction increase phenomenon.” *Laboratory Shear Strength of Soil*, ASTM Standard Test Procedure 740, R.N. Yong and F.C. Townsend, Eds., American Society for Testing and Materials, 456-484.

Schmertmann, J.H. (1987). “Discussion of ‘Time-dependent strength gain in freshly deposited sand,’ by James K. Mitchell and Zoltan V. Solymar.” *Journal of Geotechnical Engineering,* ASCE, 113(2), 173-175.

Seed, H.B., and Idriss, I.M. (1971). “Simplified procedure for evaluating soil liquefaction potential.” *Journal of the Soil Mechanics and Foundation Division,* 97(9), 1249-1273.

Seed, H.B., Tokimatsu, K., Harder, L.F., and Chung, R.M. (1985). ‘‘The influence of SPT procedures in soil liquefaction resistance evaluations.’’ *Journal of Geotechnical Engineering,* ASCE, 111(12), 1425–1445.

Skempton, A.W. (1986). “Standard penetration test procedures and the effects in sands of overburden pressure, relative density, particle size, aging, and overconsolidation.” *Geotechnique,* 36(3), 426-447.

Talwani, P., Amick, D.C. and Schaeffer, W.T. (1999). “Paleoliquefaction studies in the South Carolina Coastal Plain.” *Technical Report NUREG/CR-6619,* Nuclear Regulatory Commission, Washington, D.C., 109.

Talwani, P., and Cox, J. (1985). "Paleoseismic evidence for recurrence of earthquakes near Charleston, South Carolina." *Science,* 229 (4711), 379-381.

Talwani, P., Hasek, M., Gassman, S.L,. Doar, III, W.R. and Chapman, A. (2011). “Discovery of a sand blow and associated fault in the epicentral area of the 1886 Charleston earthquake,” *Seismological Research Letters,* 82(4), July/August, 561-570.

Talwani, P., and Schaeffer, W.T. (2001). “Recurrence rates of large earthquakes in the South Carolina Coastal Plain based on paleoliquefaction data.” *Journal of Geophysical Research,* 106(B4), 6621–6642.

Tsai P., Lee D., Kung G.T., and Juang C.H. (2009) "Simplified DMT-based methods for evaluating liquefaction resistance of soils", *Engineering Geology,* 103,13-22.

Tanaka, H. and Tanaka, M. (1998). "Characterization of sandy soils using CPT and DMT". *Soils and Foundations,* Japanese Geotechnical Society, 38(3), 55-65.

Weems, R.E., and Lemon, Jr., E.M. (1984). “Geologic map of the Mount Holly Quadrangle, Berkeley and Charleston Counties, South Carolina.” *US Geological Survey Geologic Quadrangle Map.” GQ-1579, scale, 1*(24), 000.

Weems, R.E. and Lemon, Jr., E.M. (1986). “Geology of the Bethera, Cordesville, Huger, and Kitteredge Quadrangles, Berkeley County, South Carolina.” *US Geological Survey, Miscellaneous Investigation Series, Map I-1854,* 2 sheets.

Weems, R.E., Obermeier, S.F., Pavich, M.J., Gohn, G.S. and Rubin, M. (1986). "Evidence for three moderate to large prehistoric Holocene earthquakes near Charleston, South Carolina." *Proceedings of the 3rd U.S. National Conference on Earthquake Engineering, Charleston, South Carolina*, Earthquake Engineering Research Institute, Oakland, California, 1, 3-13.

Weems, R.E., Lemon, E.M., and Nelson, M.S. (1997). "Geology of the Pringletown, Ridgeville, Summerville, and Summerville Northwest Quadrangles, Berkeley, Charleston, and Dorchester Counties, South Carolina." *US Geological Survey, Miscellaneous Investigation Series, Map I-2502*, 2 sheets.

Youd, T.L., and Idriss, I.M. (1997). "Summary report." *Proceedings of the NCEER Workshop on Evaluation of Liquefaction Resistance of Soils, Technical Report NCEER-97-0022*, National Center for Earthquake Engineering Research, State University of New York, Buffalo, 1–40.

Youd, T.L., Idriss, I.M., Andrus, R.D., Arango, I., Castro, G., Christian, J.T., Dobry, R., Finn,W.D.L., Harder, L.F., Hynes, M.E., Ishihara, K., Koester, J.P., Liao, S.C., Marcuson III,W.F., Martin, G.R., Mitchell, J.K., Moriwaki, Y., Power, M.S., Robertson, P.K., Seed, R.B., Stokoe II, K.H (2001). "Liquefaction Resistane of Soils: Summary Report from the 1996 NCEER and 1998 NCEER/NSF Workshops on Evaluation of Liquefaction Resistance of Soils." *Journal of Geotechnical and Geoenvironmental Engineering*, ASCE, 127(10), October, 817-833.